AD-A096 376 HAWAII UNIV HONOLULU DEPT OF PHYSICS AND ASTRONOMY F/G 20/8
DEVELOPMENT AND APPLICATION OF LOW ENERGY X-RAY AND ELECTRON PH--ETC(U)
JAN 81 B L HENKE AFOSR-79-0027
UNCLASSIFIED AFOSR-TR-81-0147 NL

1 OF 2
AD A096376

AFOSR-TR-81-0147

LEVEL II

(4)

Interim Scientific Report

Grant AFOSR-79-0027

DEVELOPMENT AND APPLICATION OF LOW ENERGY X-RAY AND ELECTRON PHYSICS

01 October 1979 through 30 September 1980

This interim scientific report for the AFOSR Grant period 1979-80 includes the following:

A. A Brief Description of the Principal Research Efforts Including Four Research Reports (Published or to be Published):

1. "X-Ray Spectrometry in the 100-1000 eV Region,"
2. "The Characterization of X-Ray Photocathodes in the 0.1-10 keV Photon Energy Region;"
3. "Description of a Fixed, Elliptical Analyzer Spectrograph for Pulsed Source Analysis."
4. "Low Energy X-Ray Interaction Coefficients: Photoionization, Scattering and Reflection."

B. APPENDICES

I. A General Description of this AFOSR Program.

II-A. Research Publications by the Principal Investigator and Co-Workers.

II-B. Invited Research Papers Presented by the Principal Investigator on this Research Program - 1979-1980.

III. First-Page Abstracts of Selected Examples of Some Research Publications.

IV. The Low Energy X-Ray and Electron Spectrograhic Systems Developed under this Program.

BURTON L. HENKE
Principal Investigator

Department of Physics and Astronomy
University of Hawaii
Honolulu, Hawaii 96822

January 1981

A BRIEF DESCRIPTION OF PRINCIPAL RESEARCH EFFORTS--1979-80

A. Development of the Spectrometry for Intense, Pulsed X-Ray Sources

The quantitative diagnostics of the intense, laser and particle beam driven sources is of considerable importance at this time. For many of such sources, the associated x-ray pulse to be analyzed is of duration in the nanosecond to the picosecond range. The associated plasma temperatures that are generated are in the million degree range and greater as, for example, in the inertially confined fusion experiments. The low energy x-ray spectroscopy of these sources can yield important temperature and density information. With streak camera detection, the characteristics of such short duration plasma states can be time-resolved into the picosecond region.

A program was initiated this past year by this AFOSR program on the development of a specially designed spectrograph for pulsed x-ray spectroscopy. An essential objective of this new spectrograph design is the presentation of spectra in the difficult region of 100-1000 eV which is relatively free of background and which may be quantitatively characterized. A calibration facility has been completed in this laboratory this past year for the new spectrographs. Collaborative arrangements have been made for introducing these spectrographs as calibrated in this laboratory at the large, pulsed x-ray sources which are under development at the national laboratories.

A detailed description of this new spectrograph system with that for the calibration facility is presented in this Section. The spectrograph system consists of a stacked set of three elliptical analyzer spectrograph modules utilizing two molecular multilayer analyzers, lead behenate and lead laurate, and a naturally grown crystal analyzer, potassium acid phthalate of 2d values equal to 120, 70 and 26.6 angstroms, respectively, which present spectra in three bands for the 100-1000 eV region. During this past year, we have been able to essentially complete the development of methods for making these elliptical analyzers.

[illegible] -12 (7c).

A. [illegible]

[illegible] Officer

B. The Continued Development and Characterization of Multilayer Analyzers for the Low Energy X-Ray Spectroscopy

On this AFOSR program a highly successful on-going program has been conducted on the development of multilayer analyzers for low energy x-ray analysis that are constructed of molecular layers of lead salts of straight-chain fatty acids and with 2d-values of 70 to 160 A. We describe this type of multilayer as the *molecular multilayer*. We have applied these analyzers to valence band and molecular orbital analysis in this laboratory, demonstrating their high efficiency and energy resolution of better than 1 eV. We have shown that the multilayer spectrograph complements very well the higher resolution grazing incidence grating spectrograph by providing a multilayer spectroscopy that is simpler, more amenable to accurate calibration for quantitative analysis and allows large aperture (high sensitivity) measurement.

During the past year, we have had the opportunity to evaluate another type of multilayer which is constructed by either sputtering or evaporating successive layers of high and low atomic number materials in order to generate a "crystal" suitable for Bragg reflection spectroscopy in the low energy x-ray region. These that we have studied have been developed by Dr. Troy Barbee of Stanford University (sputtered type) and by Dr. Eberhart Spiller of IBM-Yorktown (evaporated type). We have been comparing their reflection characteristics with those of our molecular multilayers using the calibration facilities of this AFOSR laboratory. The *sputtered/evaporated multilayers* (typically tungsten/carbon or rhenium-tungsten/carbon) have higher integrated reflectivities and comparable peak reflectivities, when optimized, as compared with the molecular multilayers. The molecular multilayers are of higher resolution and are more stable than the present sputtered/evaporated multilayers. The molecular multilayers have the advantage of permitting their construction on any substrate curvature. The sputtered/evaporated multilayers can be designed for narrow-band (low resolution) monochromator applications.

Our work on the theory and practice of multilayer spectroscopy is not only of importance in spectroscopy, but also may be of considerable value in the development of new and highly efficient techniques for x-ray microscopy and x-ray telescopy. We have demonstrated that the reflectivity at near normal incidence for a given wavelength for a multilayer-coated mirror can be increased to values between ten and thirty percent. We plan to continue to collaboratively work on the development of such coated x-ray optical mirror systems.

C. The Continued Development and Characterization of Photocathode Systems for Pulsed X-Ray Source Measurements

Time-resolved x-ray diagnostics of pulsed sources can be achieved in the subnanosecond and picosecond region by coupling an appropriate photocathode system to a high speed oscilloscope or to a streak camera. The x-ray burst is converted into mostly a corresponding secondary electron emission current pulse that is then measured. The attainable time resolution is ultimately set by the sensitivity of the photocathode (quantum yield as electrons/incident photon) and by the width of the secondary electron energy distribution which causes the arrival time difference at the output end of an x-ray diode or streak camera.

During the past three years, facilities have been designed and constructed in this laboratory for the high resolution measurement of the secondary electron distribution curves and for the measurement of the total and secondary electron yields of photocathode systems in the 0.1-10 keV photon energy region. These instruments are shown in Appendix IV. Two major papers have been presented on the experimental measurements and theoretical models for x-ray photoemission of 1) metals and 2) semiconductors and insulators (which is presented here in Appendix III-B). A third work on a detailed characterization of the gold and the cesium iodide photocathode for both front surface and transmission systems has been presented at the Twenty-third Annual Meeting of the American Physical Society, Division of Plasma Physics, Boston, 12-16 November 1979, and is now in preparation for publication. We have also collaborated with Dr. E. Saloman of the National Bureau of Standards on the extension of these measurements of the yield of copper iodide and cesium iodide into the extreme ultraviolet region using their synchrotron radiation source (SURF). (See Appendix III.)

There is, at present, a great interest and need for practical, optimized photocathode systems that are accurately calibrated and which can be applied to the diagnostics of the new laser/particle beam driven sources that are under development. Also, there is the important and promising new application of some of these pulsed sources to the excitation of chemical, optical and electronic systems on which time-resolved spectral analysis in the picosecond region may be achievable and for which special, optimized photocathodes will be required. For these reasons, it is considered to be of importance that this AFOSR effort on the development and characterization of x-ray photocathodes be extended.

D. The Continued Development of the Theoretical and Computational Aspects of the Application of the Low Energy X-Ray Physics

In the development of optimized x-ray spectrometry, crystal and multilayer analyzers, and of photocathode systems, it is essential that the low energy x-ray interaction coefficients be accurately known and well applied. It is for this reason that an appreciable continuing effort has been made by this AFOSR project on the compilation and fitting of the best available measured and theoretical photoionization cross section data (including those measured in this laboratory). In 1975, a detailed set of tables of these cross sections were publised by this project for all elements and for the 100-1500 eV region (see Appendix III.) We are now completing our *1980* tables, which are for all elements and also for the extended photon energy region of 30 to 10,000 eV. With these best available basic photoionization cross section data, we have applied the quantum mechanical dispersion relations to determine the oscillator densities and then the complex atomic scattering factors, $f_1 + if_2$, for all elements and for the low energy x-ray region of 100-2000 eV which include the relatively strong anomalous dispersion features. Sample pages from these new "state-of-the-art" tables are presented in I-D. Also presented here are examples of our application of the atomic scattering factors to the calculation of the integrated reflection efficiencies of the molecular multilayers and of the acid phthalate analyzers. In our modeling of the x-ray photocathodes, we have shown that the quantum yield has a photon energy dependence given by that of the imaginary part of the atomic scattering factors, f_2, as summed for the constituent atoms of the photocathode material.

In our calibration and characterization of the multilayer analyzers for low energy x-ray spectroscopy, we are able to accurately determine their rocking-curves (diffraction broadened profiles). It follows that these may then be unfolded from measured spectra in order to enhance the spectral resolution. We have developed very efficient deconvolution procedures for our flat crystal spectrometry. It is planned that a similar deconvolution program be developed for the proposed elliptical analyzer spectrographs for pulsed source spectrometry.

Finally, we plan to add to the computational efforts of this AFOSR research program this next year the x-α program that will be specially modified for the calculation of the valence band and molecular orbital energy levels and symmetries that are of considerable value in the interpretation of low energy spectra in materials analysis.

Presented here are four reports (published or to be published) which describe in detail some of the efforts of this 1979-80 AFOSR program:

1. "X-Ray Spectrometry in the 100-1000 eV Region," *Nucl. Instrum. Methods 177*, 161 (1980). An invited paper presented for an international seminar at the University of Hawaii, November 5-9, 1979. This review paper by the principal investigator discusses the current research in low energy x-ray and electron physics of this program.

2. "The Characterization of X-Ray Photocathodes in the 0.1-10 keV Photon Energy Region," *J. Appl. Phys.* (March 1981).

3. "Description of a Fixed, Elliptical Analyzer Spectrograph for Pulsed Source Analysis."

4. "Low Energy X-Ray Interaction Coefficients: Photoionization, Scattering and Reflection." Outline and example of applications to be published.

Nuclear Instruments and Methods 000 (1980) 000–000

X-RAY SPECTROSCOPY IN THE 100–1000 eV REGION

Burton L. HENKE
University of Hawaii, Department of Physics and Astronomy, 2505 Correa Road, Watanabe Hall, Honolulu, Hawaii 96822, USA

Some current methods for achieving low energy X-ray spectroscopy in the 10–100 A region are reviewed. Gratings, crystals and multilayers can be used as monochromators or dispersive analyzers. Some of the important characteristics are noted here which can help to determine their applicability to a given spectroscopic analysis situation. The "trade-off" between resolution and spectrographic speed (gratings versus multilayers) may be an important consideration when the number of photons available for measurement is limited, as, for example, by the excitation dosage allowed for a given sample. For pulsed X-ray sources and for time-resolved spectroscopy, special fixed-crystal spectrographs have been developed. These may be applied with X-ray diodes and fast oscilloscopes or with X-ray streak cameras for detection. The optimum design and characterization of the photocathode systems for such detection have been studied in detail and some of the results of this work are briefly reviewed.

1. Introduction

The new synchrotron radiation and laser-produced plasma sources can provide pulsed, broad-band radiation in the UV and X-ray region of such high intensity as to present a new dimension for spectroscopic analysis. This may be of particular importance for low energy X-ray spectroscopy in the 10–100 Å region for which high intensity, selective excitation has generally not been available.

X-ray absorption and emission spectroscopy in this low energy region is of considerable interest for the measurement of the spectra that originate from transitions between the outermost electronic levels and the relatively sharp, first core levels. Such valence band spectroscopy can sensitively reflect the chemical, optical and electronic properties of matter.

The importance of having continuous selectivity of the excitation for absorption spectrometry is well known, particularly for extended absorption fine structure measurements. Selective, narrow-band excitation can also present a critical advantage in emission spectrometry by providing "clean" meaningful spectra with a minimum of background radiation, and by minimizing possible effects of radiation-induced changes in the sample.

An illustration of the critical role of radiation damage in molecular orbital spectroscopy is presented in fig. 1. The chlorine-LII,III spectra in the 150–250 eV region were measured in order to determine the relative molecular orbital strengths of s and d symmetries for various oxidation states in chlorine

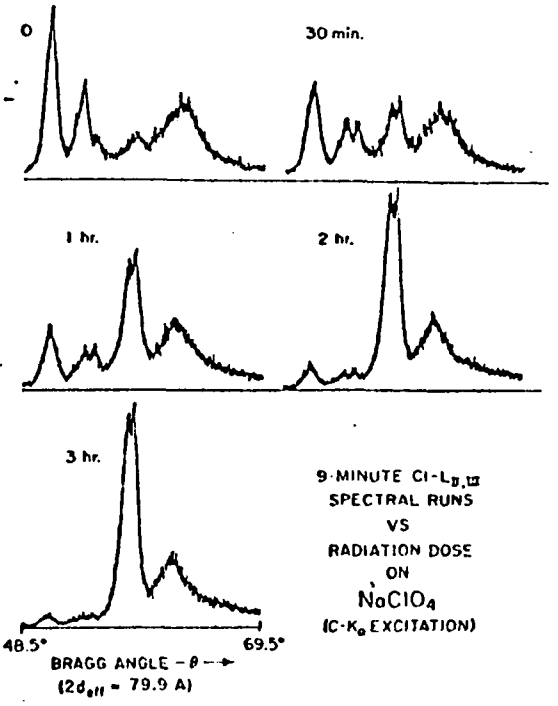

Fig. 1. Radiation-induced decomposition of polycrystalline $NaClO_4$. The excitation intensity was similar to that employed for the Cl-$L_{II,III}$ spectroscopy [1.75×10^{13} C-Kα (277 eV) photons/s cm^2 at the sample surface]. The quick scans reveal spectral changes corresponding to the appearance of reduction products such as $NaClO_3$ and $NaClO_2$. After three hours, the spectra correspond to that for NaCl.

compounds [1]. In the design of such measurements it is necessary to know how much radiation dosage can be tolerated without significantly affecting the spectrum characteristic of the system under study. Shown here are "fast" spectral scans that were taken while a polycrystalline sample of $NaClO_4$ was irradiated under a typical excitation line source of C-Kα (277 eV) of 1.75×10^{13} photons/cm^2 intensity at the sample surface. We demonstrate here, using an analysis of the successive spectra, a radiation-induced reduction of $NaClO_4$ through the various oxidation states to that for the NaCl state. The allowable radiation exposure for a proposed spectral analysis measurement can be determined from such data and the required "speed" for an appropriate spectrograph is fixed, as is usually the spectral resolution that may be expected. For high resolution spectroscopy of many materials, it is very important to selectively excite the spectra with only those photons of such energy as to be most efficient in creating the desired "hole" states. Then a minimum of excitation energy is deposited for the given measurement and the radiation damage is correspondingly minimized.

An example is shown in fig. 2 that illustrates the importance of narrow-band selective excitation in emission spectroscopy. Argon-$L_{II,III}$ spectra were studied in order to determine the possible differences in the outer electronic level structure for the gas and solid states [2]. Shown here is the Ar-$L_{II,III}$ spectrum of solid argon selectively excited by a C-Kα (277 eV) line source and resulting from predominantly single ionizations of either the $2p_{1/2}$ or $2p_{3/2}$ levels. The allowed transition from the M_I level results in the expected doublet with the statistical weights of 2 : 1 in the spin–orbit splitting of 2.2 eV. Also shown here is the spectrum measured under similar conditions but with Cu-Lα (932 eV) line source excitation. This excitation results in the obliteration of the single-electron transition spectrum by the superposition of slightly higher energy satellite, multiple ionization structure. The ionization energies of the L_I and the $L_{II,III}$ levels are 320 and 250 eV, respectively. With the Cu-Lα (932 eV) excitation the L_I level is also ionized. The L_I hole decays by a Coster–Kronig process, for example as $L_IL_{II,III}M_I$, resulting in a double vacancy and consequently the high energy satellite of the $L_{II,III}$ spectrum. The selective excitation of only the $L_{II,III}$ levels results primarily in a single-electron transition spectrum that is immediately amenable to relatively simple theoretical modelling. A nonselective excitation typically results in a multiple ionization structure (and often high-order dispersed background) that seriously compromises the spectral analysis. ✓compromises

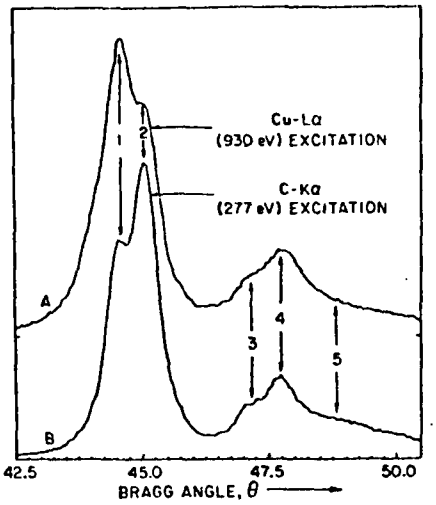

Fig. 2. An example of selective excitation. The $L_{II,III}$ spectra for solid argon as excited by C-Kα (277 eV) and Cu-Lα (932 eV) line sources. With the C-Kα excitation, L_{II} and L_{III} levels are predominantly excited (~250 eV ionization energy) and the single-electron transition, $L_{II,III}$–M_I, results, revealing the spin–orbit splitting of 2.2 eV of the $2p_{1/2}$ and $2p_{3/2}$ states (peaks 1 and 2). The Cu-Lα excitation can also excite the L_I level (~320 eV ionization energy) which decays through a Coster–Kronig process to create, for example, the double vacancy in $L_{II,III}$ and in M_I. As illustrates here, this multiple ionization obliterates the single-electron transition spectrum by a superposition of the higher energy satellite. satellite (The molecular multilayer, lead myristate, was the analyzer employed for this study.)

With synchrotron radiation sources, the excitation line source is replaced very effectively by a narrow band selected by a suitable primary monochromator Such a monochromator for the low energy region is described in section 2 on multilayer analyzers.

Another important capability of the new synchrotron and laser-produced plasma sources is that the high intensity radiation can be presented in pulses of duration in the subnanosecond region. With a proper choice of the photocathode, X-ray streak cameras can be used to characterize the structure of these pulses in the picosecond resolution range and to apply them for time-resolved spectroscopy. The characterization of X-ray photocathodes for photoelectric detection systems is described in section 3. In section 4 a fixed-analyzer crystal spectrometer for pulsed X-ray spectroscopy and for time-resolved spectroscopy is briefly described.

2. Low energy X-ray analyzers

2.1. Diffraction gratings

The advantage of the grating over the crystal spectrograph in the low energy X-ray region of 10–100 Å is its higher resolution capability [3]. Typically we can obtain about 0.1 eV resolution with gratings and about 1 eV resolution with appropriate crystals. The disadvantage of grating systems is that the grazing incidence geometry that is required is more tedious and the "speed" or effective aperture is usually considerably smaller than that of the crystal spectrograph.

As suggested above, it is *not* necessarily the intensity of the excitation source that determines the requirement for spectrographic speed but rather, very often, it is the excitation radiation dose permitted by the sample to be analyzed. It is of considerable importance that the design of grating spectrographic measurements be optimized as to geometry, excitation and detection in order to achieve maximum speed without a loss of the high resolution capability. In the past two decades there has been a large improvement in the overall efficiency of X-ray grating spectrographs [4]. Nevertheless, high resolution grating spectroscopy is not practicable or even possible for a large number of materials analysis applications because of insufficient speed and/or flexibility. For such applications, we must consider the possible advantages of low energy X-ray crystal or multilayer spectroscopy.

2.2. Crystal analyzers

For an optimization of a crystal spectrographic measurement, it is usually important to choose a crystal of $2d$-value that approaches that of the wavelengths to be measured in order to have large Bragg angle diffractions [5,6]. Although the integrated reflectivity of the crystal analyzer is usually maximized for both small and large Bragg angles, the large angle operation allows the very crucial maximization of resolution. The higher angular dispersion for the large Bragg angles allow a more efficient utilization of collimation or, alternatively, of focusing geometry for high resolution and thus a minimum loss of aperture or speed. At the small Bragg angle operation for the low energy X-rays, the tail of the specular reflection distribution from the crystal may contribute an appreciable background relative to the Bragg reflected spectrum [7].

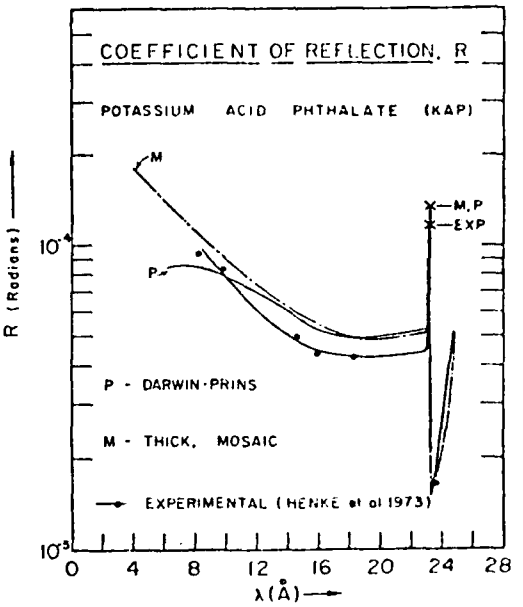

Fig. 3. The measured integrated reflectivity, R, for the KAP analyzer and shown for comparison the calculated curve established using the Darwin–Prins perfect crystal theory and the thick mosaic crystal theory. The O-K absorption edge structure and the strong, resonance reflection at 23.3 Å limits its application for spectral analysis to wavelengths below 20 Å. It is an outstanding analyzer for the 10–20 Å region.

For spectroscopy in the 10–20 Å range, the most effective analyzers that are available at this time are the organic acid phthalates of $2d$-values of 25–27 Å *. These include potassium acid phthalate (KAP), rubidium acid phthalate (RAP) and thallium acid phthalate (TAP). These crystals have rocking curve widths (fwhm) of about 1 eV and relatively high, monotonic integrated reflection coefficients for the 10–20 Å band as shown in figs. 3 and 4. Generally these analyzers cannot be used for analysis above 20 Å because of the marked reflectivity changes near the oxygen-K absorption edge [8]. It is also important to note the existence of a very sharp and large enhancement of reflectivity at 23.3 Å. The KAP analyzer can be cleaved to sufficiently thin (~200

* The integrated reflectivities for the acid phthalate series have been recently measured in detail for the 2–25 Å region (to be published). It is experimentally verified that for the cations thallium, rubidium, potassium, sodium and ammonium (NH_4), the integrated reflectivity, R, and the energy resolution, W, decrease with the atomic number of the cation (ref. [8]).

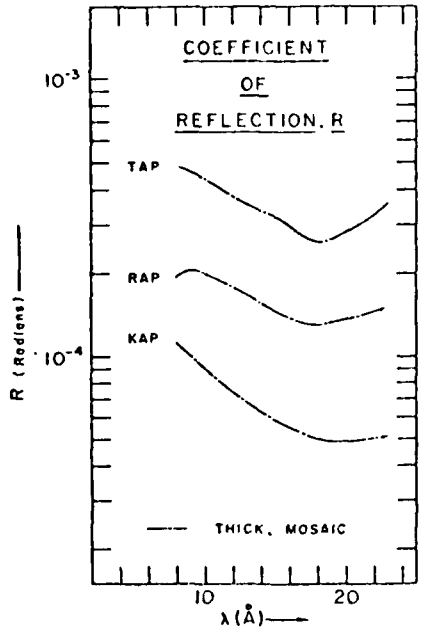

Fig. 4. The relative integrated reflectivities for thallium acid phthalate, rubidium acid phthalate and potassium acid phthalate are presented here. (The rocking-curve width also increases, however, with the atomic number of the cation.)

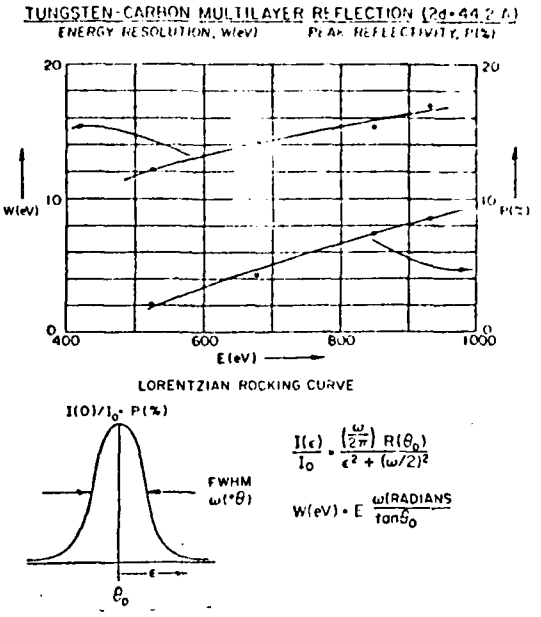

Fig. 5. Reflection characteristics of a tungsten–carbon, sputtered multilayer of 62 d-spacings (11 Å of W and 11 Å of C) and an effective $2d$-value of 44.2 Å. Reflectivity curves were obtained by the deconvolution of a series of low energy X-ray line spectra and found to be essentially Lorentzian. Presented here are the peak reflectivities and the fwhm equivalent energy widths.

μm) and flexible, large area sections which allows it to be bent to curvatures suitable for focusing crystal optics.

2.3. Sputtered and evaporated multilayers

There are, at present, no naturally grown crystals of $2d$-values in the 40-50 Å range that are suitable as analyzers for spectroscopy in the 20–50 Å wavelength region. However, it has been recently demonstrated that relatively high quality multilayer analyzers can be constructed with these $2d$ values by the successive vacuum deposition (sputtering or evaporation) of heavy and light element of alloy layers *†. Preliminary evaluations of such multilayer systems for low energy X-ray spectroscopy have recently been made at this laboratory and at others [10,11]. Shown here in figs. 5 and 6 are the reflection characteristics of a sputtered multilayer constructed with 62 d-spacings of 11 Å tungsten and 11 Å of carbon. The multilayer was mounted in a flat-crystal vacuum spectrograph and a series of profiles of characteristic line sources in the low energy region were recorded using a collimator of 0.34° Gaussian full width. Upon deconvoluting the collimation broadening and that caused by the respective emission line widths, the intrinsic reflectivity curves for the multilayer were determined and found to be essentially Lorentzian. Shown here are the areas under the I/I_0 versus θ deconvoluted curves (the integrated reflectivity, R, in milliradians), the fwhm, W, in equivalent eV units, and the peak value of I/I_0, P (%).

As noted in fig. 6, this multilayer had *no* measurable even or odd high-order reflections, indicating that the layered structure must consist of a graded tungsten carbide. By modelling this structure with sinusoidally varying optical constants, δ and β, as

* The sputtered multilayer of graded tungsten carbide that is described here was constructed by Professor Troy W. Barbee, Material Sciences, Stanford University, for the Diagnostics Development Group, Y Division, Lawrence Livermore Laboratories.

† Evaporated multilayers have been constructed at the IBM T.J. Watson Research Center, Yorktown Heights, New York, and the Deutsches Elektronen – Synchrotron DESY, Institut fur Experimentalphysik, Universitat Hamburg, Hamburg, FRG. We have recently measured the reflection characteristics of their Re-W/B analyzers and found them to be of comparable reflectivity as the sputtered W/C multilayer described here but with normally strong high-order reflections present.

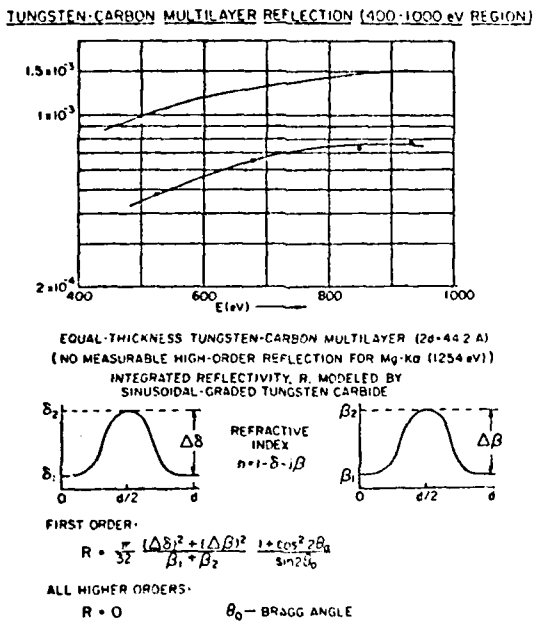

Fig. 6. The measured integrated reflectivities for the W/C multilayer described for fig. 5. This multilayer has *no* high order reflectivity indicating that the structure is probably a graded tungsten carbide with an effectively sinusoidal variation in the optical constants δ and β. A theoretical expression derived for the integrated reflectivity for this multilayer with such a variation in the refractive index is also presented here.

shown, a theoretical expression for R was derived and is plotted here. R is finite for first-order reflection and becomes equal to zero for all high order reflections [12].

This W/C multilayer analyzer as compared with KAP has an order of magnitude larger integrated reflectivity, but also an order of magnitude larger energy width (pass band). In the 20–50 Å region with a $2d$-value of 44.2 Å, it has very similar reflection properties to that of the molecular multilayer, lead myristate, of 80 Å $2d$-value. At this stage in the development of the sputtered, evaporated and molecular multilayers, non have achieved the energy resolution of 1 eV for the 20–50 Å wavelength region.

It is important to note, however, that unlike the organic analyzers, this W/C sputtered multilayer can be operated under high total radiation intensities and at relatively high temperatures and therefore can be applied as a very efficient primary monochromator for narrow-band, selective excitation with a complete rejection of high order reflected components.

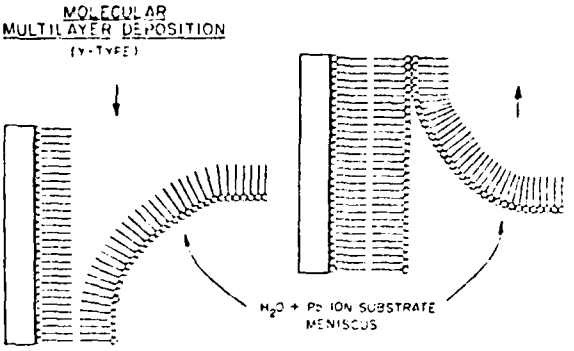

Fig. 7. Illustrated here is the deposition of a Langmuir–Blodgett, Y-type monomolecular layer system of a salt of a straight-chain fatty acid. For the construction of molecular multilayers for X-ray analysis, the cations are usually heavy metal atoms such as lead (circles).

2.4. Molecular multilayers

Molecular multilayers have been developed with $2d$-values in the 70–160 Å range. For the 50–100 Å wavelength region, these multilayers have high reflec-

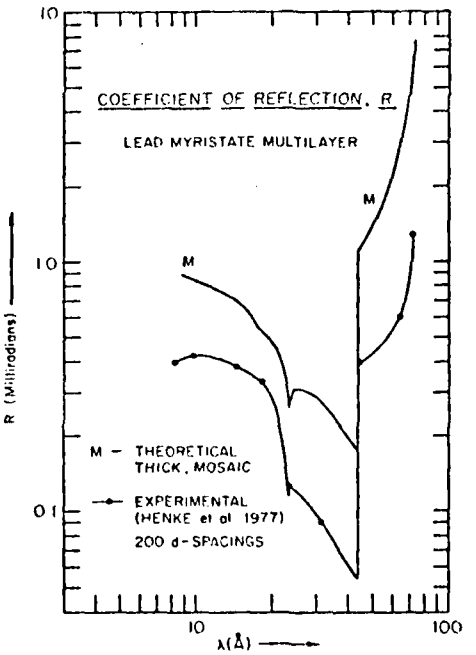

Fig. 8. The measured reflectivity for the lead myristate, molecular multilayer and shown for comparison the calculated curve according to the mosaic crystal theory. The $2d$-value is 80 A. The reflection characteristics for this type of molecular multilayer analyzer is outstanding for wavelengths above the C-K edge of 44 A.

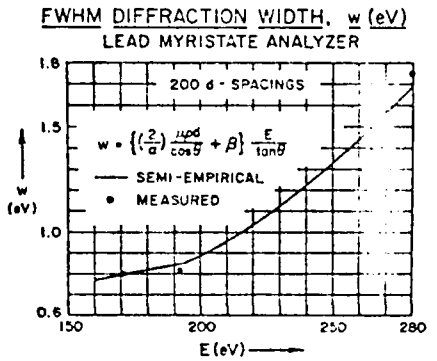

Fig. 9. The measured fwhm-energy widths for a lead myristate analyzer of ~~several~~ d-spacings at several line source wavelengths and shown for comparison an energy resolution curve predicted by a semi-empirical expression derived for the molecular multilayer energy resolution.

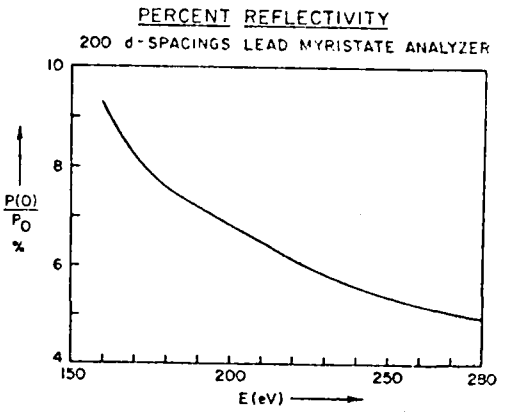

Fig. 10. The peak reflectivity (%) corresponding to the area, R, and the fwhm values for lead myristate analyzer described in figs. 8 and 9.

tion efficiency and an energy resolution of about 1 eV. They may be constructed on relatively large areas and upon surface of any curvature. As depicted in fig. 7, the molecular multilayer is built up by the successive dipping of a substrate into a water surface on which is deposited an insoluble monomolecular layer (usually a lead salt of a straight-chain fatty acid – the length of the chain determines the d-spacing of the multilayer). The multilayers that have been developed in this laboratory for application as analyzers for the low energy X-ray region have been lead laurate, lead myristate, lead stearate, lead lignocerate and lead melissate with $2d$-values equal to about 70, 80, 100, 130 and 160 Å, respectively. Their construction and reflection characteristics have been reported elsewhere [5,6,7,13] and, as an example, the characteristics of the lead myristate multilayer are presented here. In fig. 8 are shown the theoretical and the experimental integrated reflectivity curves. They show that for the long wavelength region of 50–100 Å (at the large Bragg angles and high dispersion), the inegrated reflectivity, R, is maximized. However, below the carbon absorption edge, in the 20–50 Å region, these multilayers have relatively low reflection efficiency. The monotonic region of high integrated reflection above 50 Å is associated with a high percentage of reflectivity and good energy resolution as described in figs. 9 and 10. As may be noted from the semi-empirical relation presented in fig. 9 which has been derived for the fwhm energy width, W, of these multilayers [5,6], the highest resolution is obtained by choosing a multilayer of $2d$-value that is close to that of the wavelengths that are to be measured. In fig. 11, the effect of the $2d$-value upon the integrated reflectivity is predicted by the mosaic crystal model. Also presented here is the specific dependence, according to the mosaic crystal model, of the integrated reflectivity, R, upon the molecular density, ϕ, the real and imaginary components of the molecular structure factor, F_1 and F_2, the mass absorption coefficient, μ, the mass density, ρ, and the Bragg angle, θ_0.

It was noted earlier that the energy resolution of typical grating spectrographic measurements is about 0.1 eV and that of crystal or molecular multilayer measurements at large Bragg angles is about 1 eV. It should be noted here, however, that it has been demonstrated that for the crystal and multilayer spectrographic measurements in the low energy X-ray region, a very simple and efficient deconvolution procedure can be applied to bring this energy resolution into the subelectron-volt region [6]. This is because it is possible to determine precisely by direct measurement the two broadening functions, that for the collimation and other spectrographic geometric effects and that for the diffraction broadening of the analyzer. (The corresponding instrument functions are not so easily determined for the grazing incidence grating spectrographs.)

3. X-ray photocathodes

Typically, for synchrotron radiation and laser-produced plasma sources, X-ray sensitive photomul-

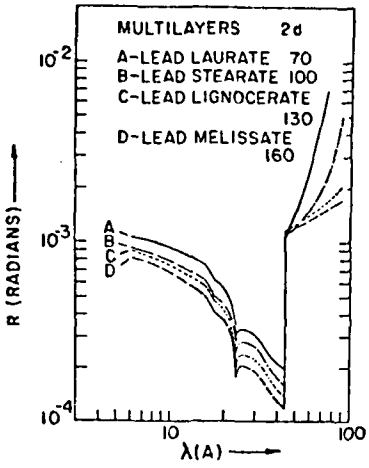

COEFFICIENT OF REFLECTION, R
(THICK, MOSAIC CRYSTAL MODEL)

$$R = \frac{r_0^2 \phi^2 \lambda^3 (F_1^2 + F_2^2)}{4\mu\rho} \left(\frac{1+\cos^2 2\theta_0}{\sin 2\theta_0} \right) \text{radian}$$

Fig. 11. The relative values of the integrated reflectivity, R, according to the mosaic crystal theory for molecular multilayers of several $2d$-values. Also expressed here is the dependence of R upon the molecular number density, ϕ, the real and imaginary components of the molecular structure factor, F_1 and F_2, the multilayer mass absorption coefficient, μ, its mass density, ρ, and the Bragg angle, θ_0.

tipliers, X-ray diodes and X-ray streak cameras are used for detection depending upon the time resolution that is needed. The application of these detectors for quantitative spectroscopy requires that the photocathodes, which convert the photon flux to electron current, be well characterized. The electronic signal consists of a spectrum of primary electrons (photoelectrons and Auger electrons) along with a considerably larger number of secondary electrons of energies below 30 eV. In fig. 12 is depicted such an electron energy spectrum from a photocathode. When the photocathode is excited by photons in the 0.1–10 keV region, the fraction of the number of electrons of energy above 30 eV increases from about 1 to 20% as the photon energy increases for relatively

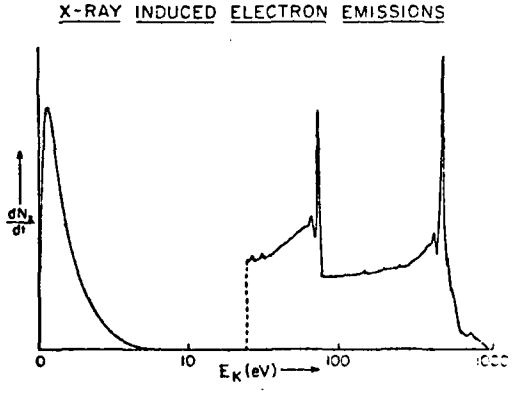

Fig. 12. Depicting the electron emission spectrum as excited by X-rays. Most of the electron current is in secondary emission, usually below 10 eV electron energy. The remaining primary electron emission is associated with that of the photoelectrons and Auger electrons excited by the initial photon absorption.

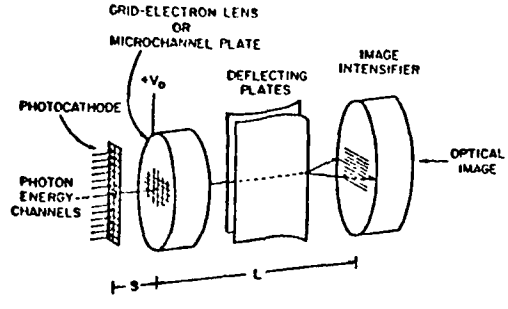

TEMPORAL RESOLUTION LIMIT, τ

$$\tau = 3.37 \frac{(\Delta)^{1/2}}{\epsilon_0} \left\{ 1 + \frac{1}{4} \left(\frac{L}{S} - 2 \right) \left(\frac{\Delta}{eV_0} \right)^{1/2} \ldots \right\} \text{ PICOSECONDS}$$

Δ = SECONDARY ELECTRON ENERGY SPREAD IN eV

ϵ_0 = EXTRACTION FIELD, V_0/S IN kV/mm

Fig. 13. For fast, time-resolved X-ray spectroscopy, the electron image of the spectrum that excites the slit transmission photocathode is deflected across an image intensifier section presenting a time base in the sub-nanosecond range. The quantum yield of the photocathode must be high and the energy width, Δ, of its secondary electron distribution must be small. The spread in the arrival time at the image intensifier, τ, is given here as a function of Δ and of the extraction field at the photocathode surface, ϵ_0.

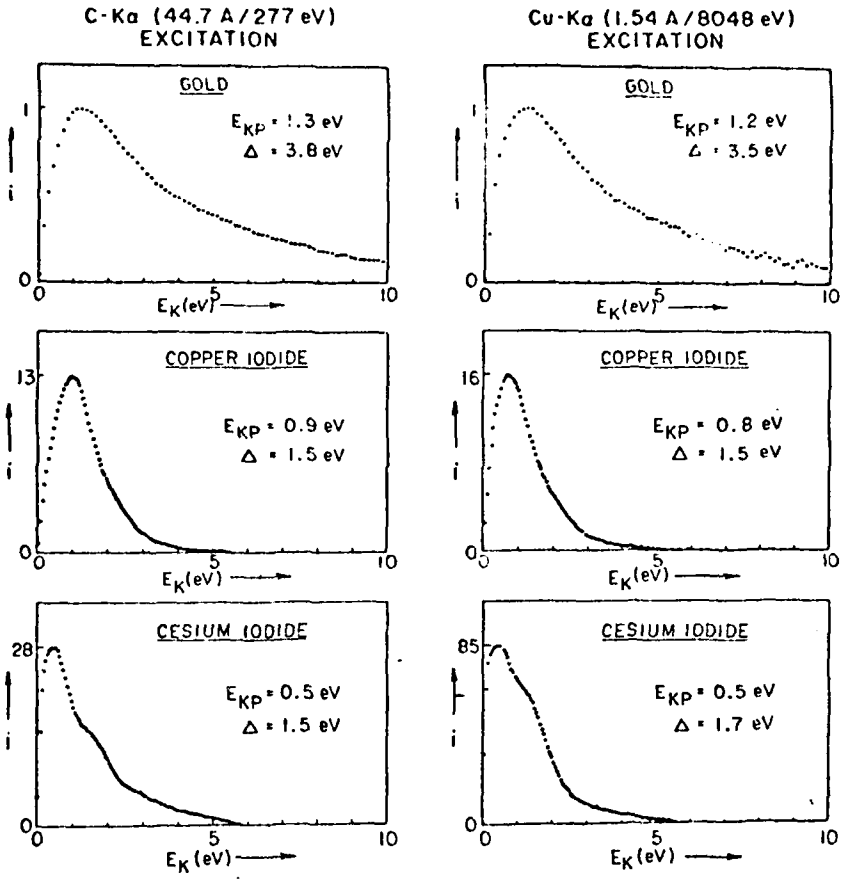

Fig. 14. The measured secondary electron energy distributions for the photocathode layers of gold, copper iodide and cesium iodide, as excited by C-Kα (277 eV) and Cu-Kα (8050 eV) photons. p and γ are the peak currents and the secondary electron yield relative to these values for gold under identical excitation and measurement conditions. The shapes of the electron energy distribution curves are essentially invariant for photon energies in the 0.1–10 keV region.

insensitive photocathodes such as gold and aluminum. This fraction is typically less than 1% for photocathodes of relatively high yield as cesium iodide [14].

In the X-ray streak camera, only the secondary electrons are utilized and the energy width of their distribution ultimately determines the spread in arrival time at the image intensifier end of the tube and hence the temporal resolution [16]. This dependence upon the width of the secondary distribution, Δ, is described in Fig. 13. For an energy distribution width of 2 eV and an extraction field at the photocathode of 5000 V/mm, the leading term in the expression for the time resolution, τ, becomes equal to 1 ps. It is therefore feasible that a streak camera could resolve the shapes of the subnanosecond pulses characteristic of the new storage rings and of the laser-produced plasma sources for their diagnostics, calibration and application to time-resolved spectroscopy.

Shown in fig. 14 are the measured secondary electron distributions for the photocathodes consisting of thick films of gold, of the semiconductor, copper iodide, and of the insulator, cesium iodide, as excited by C-Kα (277 eV) and Cu-Kα (8050 eV) photons [16,17]. The distribution peak height, p, and the area under the distribution or yield, γ, are given here relative to the corresponding values for the gold photocathode. It is important to note that the CuI and the CsI photocathodes have appreciably smaller distribution widths and higher quantum yields than does the gold photocathode. It has also been recently deter-

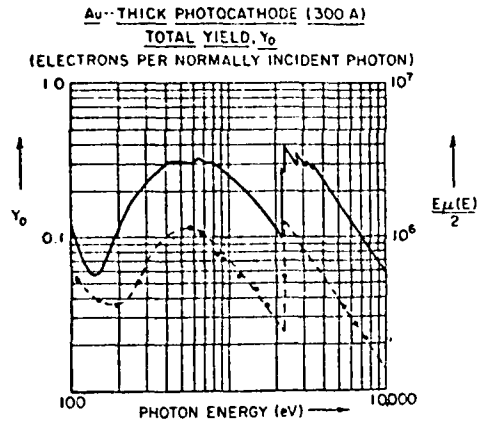

Fig. 15. The total yield from the surface of a 300 A vacuum-evaporated film of gold on a chromium substrate. As predicted, the response in this 0.1–10 keV region follows approximately as the product of the photon energy and the photocathode mass absorption coefficient, $E\mu(E)$.

mined that the time response of these nonmetal, thin film photocathodes is essentially the same as that for gold in the subnanosecond region [18].

Based upon measurements such as these which indicate that the shape of the secondary electron distribution in the 0.1 to 10 keV photon energy region is essentially invariant, a relatively simple theoretical model for X-ray photoemission has been derived which predicts that the total yield (electrons per normally incident photon) should follow a form

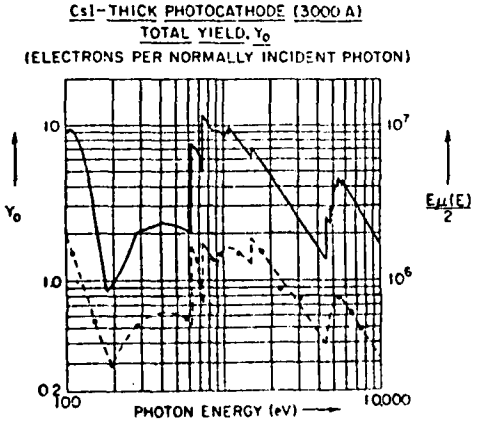

Fig. 16. The total yield from the surface of a 3000 A vacuum-evaporated cesium iodide film on a chromium substrate. As also indicated in fig. 5, the yield is approximately proportional to $E\mu(E)$ in its photon energy dependence.

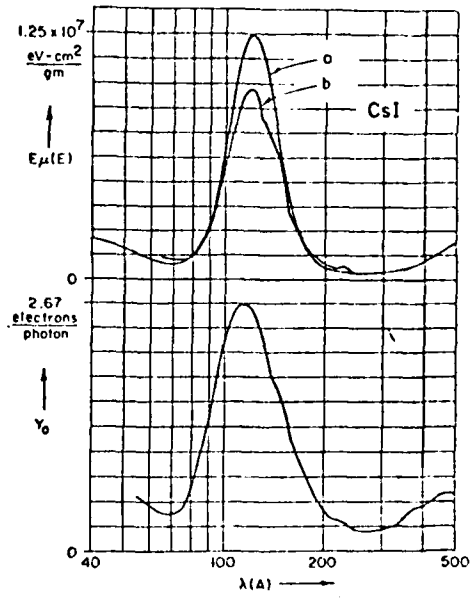

Fig. 17. The total yield of the cesium iodide photocathode in the eUV region. (Measurements were made using the SURF II Facility at the National Bureau of Standards – Saloman et al. 1979.) Shown here for comparison are the $E\mu(E)$ plots, (a) using data for xenon (Cs and I in the ionic crystal CsI are xenonlike) and (b) using directly measured absorption data for CsI films. The strong absorption and yield at about 100 eV is the result of the atomic-like 4d–4f transitions in both cesium and iodine ions.

approximately as the product of the photon energy and the photocathode mass absorption coefficient, $E\mu(E)$ [16,17]. This prediction is borne out as illustrated in the log–log plots of the measured total quantum yields alongside the $E\mu(E)$ curves for the gold and cesium iodide photocathodes in figs. 15 and 16. This relationship seems also to obtain for the eUV photon energy region as shown in fig. 17 [19]. Methods for precisely measuring such photocathode response curves have been recently developed at this and other laboratories in order to support the quantitative application of low energy X-ray spectroscopy with pulsed X-ray excitation sources [14,20,21,22].

4. Single pulse and time-resolved spectroscopy

The high intensity and short duration pulse characteristics of the synchrotron radiation and laser-produced plasma sources allow fixed-analyzer, single-pulse spectroscopy with time resolutions in the sub-

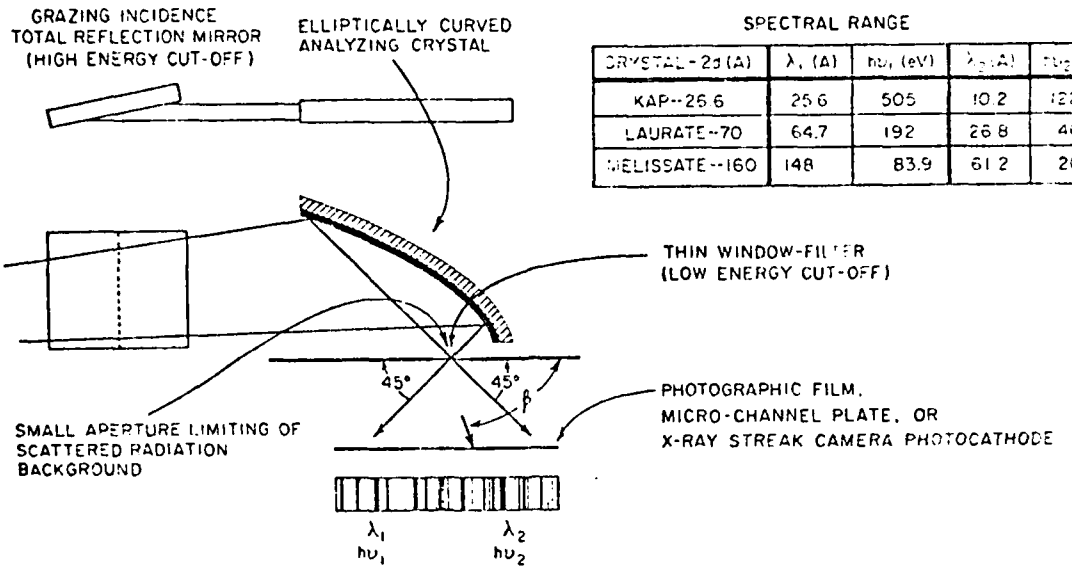

SPECTRAL RANGE

CRYSTAL-2d (A)	λ1 (A)	hυ1 (eV)	λ2 (A)	hυ2 (eV)
KAP--26.6	25.6	505	10.2	1220
LAURATE--70	64.7	192	26.8	463
MELISSATE--160	148	83.9	61.2	203

Fig. 18. A spectrograph for pulsed X-ray spectroscopy utilizing a fixed crystal or multilayer analyzer. All wavelengths from a point source at one of the foci of an elliptically curved analyzer will focus at the other focal point and through a small scatter aperture into the detector module. For nearly parallel incident radiation, the analyzer is parabolic and the wavelength for first-order diffraction is given by $2d \sin(\beta/2)$. A grazing incidence mirror reflection of the incident beam provides a high-energy cut-off. A low energy cut-off is effected by an appropriate filter at the scatter entrance aperture.

nanosecond and picosecond range. Focusing grating spectrometers can be most efficient for pulsed, low energy X-ray spectroscopy provided that the constraints of grazing incidence optics do not seriously limit the application of appropriate detection and recording systems. Fixed crystal or multilayer analyzers may also be used, and usually with a considerably simpler and more flexible geometry. Such a spectrometer is described in fig. 18 [29]. For this spectrometer, an ellipsoidal or a cylindrically elliptical analyzer is utilized. Molecular multilayers are easily constructed upon doubly curved surfaces. Thin cleaved crystals and sputtered or evaporated multilayers on thin flexible substrates can be pressed into cylindrical curvatures. All wavelengths from a point source at one of the foci of the elliptical arc will reflect and focus through the other focal point at which is located a small scatter aperture at the entrance of a detector module. For synchrotron radiation sources, the incoming radiation in this plane is essentially parallel and the focusing surface becomes effectively parabolic. For this case the exit angle, β, is simply equal to twice the Bragg reflection angle off the analyzer and the associated wavelength for a first-order diffraction is $2d \sin(\beta/2)$. Examples of wavelength bands that are accomodated for β-values between 45° and 135° for nearly parallel source radiation and for several analyzer d-spacings are indicated here. Such spectrometer systems are of thin geometry and may be "stacked" for multiple-band coverage. A grazing incidence mirror reflection is applied to the incident beam as shown in order to effect a high energy cut-off, and appropriate low energy cut-off filters can be applied at the scatter aperture and as selected filter segments along the detection plane. Detection may be photographic, by microchannel, charge collecting arrays or the spectrum can be placed upon the entrance slit of an X-ray streak camera for time resolved spectroscopy.

The author gratefully acknowledges the invaluable assistance of the students and staff of the Low Energy X-Ray Physics Group, University of Hawaii. This program is supported by a grant from the Air Force Office of Scientific Research, Grant No. 79-0027B, and by a supplemental contract from the Department of Energy, DOE DE-AS03-76SF00235.

References

[1] B.L. Henke, R.C.C. Perera and D.S. Urch, J. Chem. Phys. 68 (1978) 3692.

[2] R.C.C. Perera and B.L. Henke, X-ray Spectrometry, ~~to be published~~. 9 (1980) 51.
[3] R.J. Speer, Culham Laboratory Report 843 (Jan., 1973).
[4] G. Andermann, L. Bergknut, M. Karras and G. Griesenhaber, Rev. Sci. Instr., to be published; B. Gilberg, M.J. Hanus and B. Foltz, Jap. J. Appl. Phys. 17 Suppl. 17-2 (1978) 101, J. Nordgren, H. Agren, C. Nordling and K. Siegbahn, Ann. Acad. Reg. Sci. Uppsaliensis 21 (1978); J. Nordgren, H. Agren, L. Petterson, L. Selander, S. Griep, C. Nordling and K. Siegbahn, UUIP-1002 (April, 1979); R.J. Speer, Space Sci. Instr. 2 (1976) 463; R.J. Speer and D. Turner, Culham Laboratory Report 843 (Nov., 1971).
[5] B.L. Henke and K. Taniguchi, J. Appl. Phys. 47 (1976) 1027.
[6] B.L. Henke, R.C.C. Perera, E.M. Gullikson and M.L. Schattenburg, J. Appl. Phys. 49 (1978) 480.
[7] B.L. Henke and M.A. Tester, Advances in X-ray Analysis, Vol. 18 (Plenum, New York, 1975).
[8] R. Blake, Los Alamos Scientific Laboratory, Los Alamos, New Mexico, private communication.
[9] A. Burek, Space Sci. Instr. 2 (1976) 53.
[10] E. Spiller, A. Segmüller and R.P. Haelbich, IBM Research Report, RC 7710, No. 33292 (1979).
[11] L.N. Koppel, T.W. Barbee and D.T. Attwood, 21st Ann. Meeting of the Division of Plasma Physics of the American Physical Society, Boston, Massachusetts (Nov., 1979) to be published.
[12] B.L. Henke, P. Lee, T.J. Tanaka and R.L. Shimabukuro, to be published.
[13] B.L. Henke, F.G. Fujiwara and B.K.F. Young, to be published.
[14] B.L. Henke, J.P. Knauer and K. Premaratne, 21st Ann. Meeting of the Division of Plasma Physics of the American Physical Society, Boston, Massachusetts (Nov. 1979) to be published.
[15] B.L. Henke and K. Premaratne, Proc. Int. Conf. on X-ray and XUV Spectroscopy, Sendai, Japan (August, 1978); Jap. J. Appl. Phys. 17 Suppl. 17-2 (1978) 23.
[16] B.L. Henke, J.A. Smith and D.T. Attwood, J. Appl. Phys. 48 (1977) 1852.
[17] B.L. Henke, J. Liesegang and S.D. Smith, Phys. Rev. B19 (1979) 3004.
[18] G.L. Stradling, H. Medecki, D.T. Attwood, R. Kauffman and B.L. Henke, 21st Ann. Meeting of the Division of Plasma Physics of the American Physical Society, Boston, Massachusetts (Nov., 1979); Bull. Am. Phys. Soc. 24 (1979) 1099.
[19] E.B. Saloman, J.S. Pearlman and B.L. Henke, ~~to be published~~. Appl. Opt. 19 (1980) 749.
[20] R.H. Day, 21st Ann. Meeting of the Division of Plasma Physics of the American Physical Society, Boston, Massachusetts (Nov. 1979); Bull. Am. Phys. Soc. 24 (1979) 1098.
[21] R.L. Kauffman, H. Medecki and E.L. Pierce, 21st Ann. Meeting of the Division of Plasma Physics of the American Physical Society, Boston, Massachusetts (Nov. 1979); Bull. Am. Phys. Soc. 24 (1979) 1099.
[22] M.J. Bernstein and J.A. Smith, IEEE Trans. Nucl. Sci. NS-26 (1979) 1.
[23] B.L. Henke, to be published.

To be Published
in the
JOURNAL OF APPLIED PHYSICS
(March 1981 issue)

The Characterization of X-Ray Photocathodes in the 0.1-10 keV Photon Energy Region

B. L. Henke, J. P. Knauer* and
K. Premaratne

University of Hawaii
Honolulu, Hawaii 96822

ABSTRACT

A method and instrument are described for the measurement of the absolute quantum yield for front-surface and transmission photocathodes in the 0.1 to 10 keV photon energy region. The total and the secondary electron photoemission yields have been measured for the Al, Au, CuI and CsI photocathodes as required for the absolute calibration of the x-ray diode detectors and for the x-ray streak cameras. The

relative secondary electron yields have also been measured for the same photocathodes by high resolution electron spectroscopy of the secondary electron energy distributions which are in good agreement with the absolute yield measurements. The secondary electron yield of CsI is ten to one-hundred times higher than that for Au in the 0.1 to 10 keV region and with a secondary energy distribution that is appreciably sharper. For these reasons, CsI should be an effective photocathode for sensitive, time-resolved spectroscopy into the picosecond region. It is verified experimentally that the secondary electron quantum yield varies approximately as $E\mu(E)$, with E as the photon energy and $\mu(E)$ as the photoionization cross section, and that the primary (fast) electron quantum yield is a small fraction of the total yield and varies approximately as $E^2\mu(E)$. A simple model for x-ray photoemission is described which leads to semiempirical equations for front and back surface secondary electron photoemission as based upon an escape depth parameter that may be obtained from yield-vs-photocathode thickness data. The model predictions are in good agreement with experiment.

I. INTRODUCTION

Time-resolved x-ray spectroscopy has become of considerable importance in the temperature-density-composition diagnostics of high temperature plasmas involved in controlled thermonuclear fusion studies which utilize laser, particle beam or magnetic compression-confinement production. The time duration of the associated x-ray emissions ranges from picoseconds to seconds. Time-resolved x-ray spectroscopy is also important in the development of super-radiant, pulsed x-ray sources and in their application to studies of the radiation effects of x-ray bursts upon materials and to the x-ray analysis of atomic, molecular and solid state time-resolved processes into the picosecond region.

The electron currents that are emitted by photo-cathodes under x-ray excitation can be a very effective basis for time-resolved spectroscopic measurement using x-ray diode or streak camera detection.[1-5] In the latter, an x-ray spectrum can be established along a slit-defined transmission photocathode of the streak camera by using focussing filter-total-reflection monochromator or crystal/multilayer arrays, or by using nonfocussing, Bragg reflecting crystal/multilayer analyzer systems.

In time-resolved x-ray spectroscopy, the ultimate limit on the achieveable time resolution is the quantum conversion efficiency of the photocathode (which determines

signal statistics) and the energy spread of the emitted electrons as is noted in Fig. 1 (which determines the time resolution).[6] The relatively small fraction of fast electrons that is photoemitted is effectively blocked by the electron optical apertures of the typical streak camera. In Fig. 2 the difference in the arrival time at the output end of the streak camera is given as a function of the energy width, Δ, of the secondary electron energy distribution, the extraction field, ε_o, and of the geometry of the camera. In addition to the absolute yield-vs-photon energy and the shape of the secondary electron distribution curves, other important characteristics of the x-ray photocathode are its stability, reproducibility, simplicity of spectral response and the linearity of its time response.

Described here is a method and instrument for the measurement of the absolute total and secondary electron yields (electrons emitted per normally incident photon) for both front-surface and transmission photocathodes in the 0.1 to 10 keV photon energy region and the application to the characterization of photocathode materials of current practical importance such as gold and cesium iodide. In addition to the measurements of the total electron emission in the secondary and the primary electron components, high resolution electron spectroscopic measurements of the secondary electron energy distributions

for these photocathodes are also presented. A simple model for the quantum yield of x-ray photoemission is outlined here that includes the effect of photocathode thickness upon the front and back surface emissions.

II. THE MEASUREMENT OF X-RAY PHOTOEMISSION

The facility that has been developed for making absolute yield measurements in the photon energy region of 0.1 to 10 keV is shown in Fig. 3. Six filtered, fluorescent sources of essentially monochromatic characteristic x-radiations may be excited by a closely coupled, 2-4 kilowatt demountable x-ray source of strong characteristic line radiation of photon energy just above that of the fluorescent line being used.[7] The photocathodes are also brought in as closely as possible to the fluorescent source in order to maximize the photoemission currents to be measured. The absolute x-ray flux per stearadian at the same take-off angle from a 3 cm fluorescent source disk is measured by a calibrated flow proportional counter at the end of an extended vacuum path and with an accurately defined pinhole aperture (to limit the counting rates to less than ~5000 c/s for negligible coincidence loss).

An eight-position, front-surface photocathode Teflon sample holder (four positions for transmission photocathodes) has been accomodated in order to allow precise

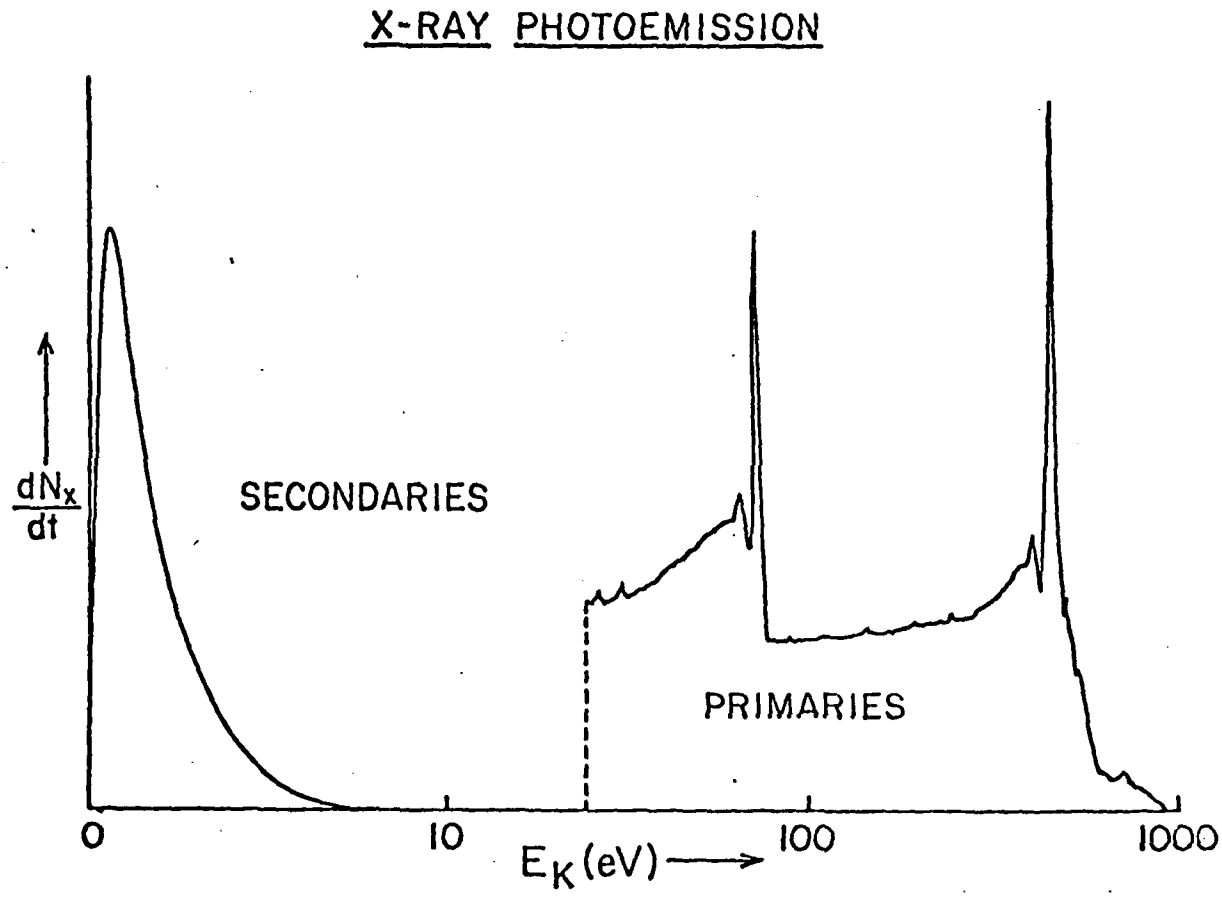

Figure 1. In the 0.1-10 keV photon energy region the larger fraction of the electrons that are emitted are the secondary electrons, typically as a narrow distribution below 10 eV. The higher energy, fast electron photoemission consists of relatively sharp elastically scattered photoelectrons and Auger electron "lines" along with a much larger number of inelastically scattered electrons in their low energy tail region.

TIME RESOLVED X-RAY SPECTROSCOPY

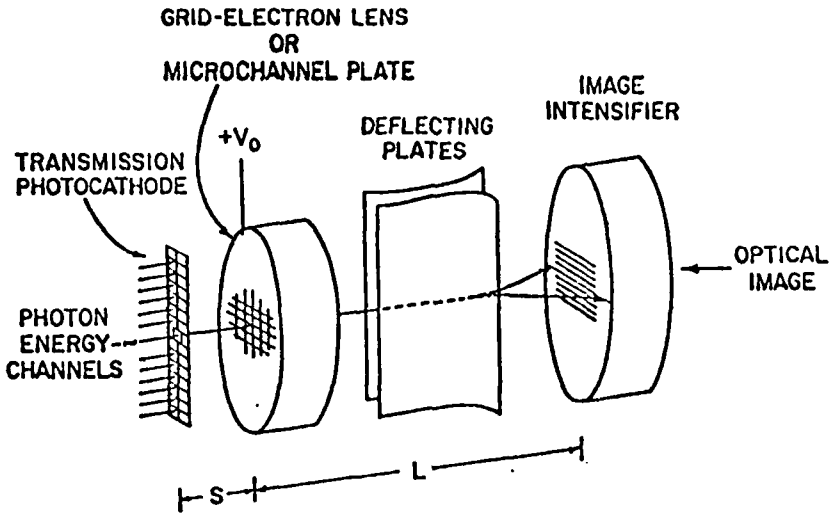

TEMPORAL RESOLUTION LIMIT, τ

$$\tau = 3.37 \frac{(\Delta)^{1/2}}{\epsilon_0} \left\{ 1 + \frac{1}{4} \left(\frac{L}{S} - 2 \right) \left(\frac{\Delta}{eV_0} \right)^{1/2} \ldots \right\} \text{ PICOSECONDS}$$

Δ = SECONDARY ELECTRON ENERGY SPREAD IN eV.

ϵ_0 = EXTRACTION FIELD, V_0/S IN kV/mm

Figure 2. A schematic of an x-ray streak camera for time-resolved x-ray spectroscopy. Its ultimate time resolution is determined by the difference in arrival time, τ, at the output end of the camera associated with the energy width, Δ, of the secondary electron distribution emitted from the transmission photocathode. For a secondary electron energy spread, Δ, of 2 eV and an extraction field, ϵ_0, of 5 kV/mm, the time resolution, τ, is approximately one picosecond. (The fast electron photoemission is essentially blocked electron optically in the streak camera.)

relative measurement, for example, of a series of different photocathode materials, or of different photocathode thicknesses.

A cylindrical "grid" technique has been developed for the retarding of the secondary electron emission currents in the determination of the primary or fast electron components. This cylindrical grid system is so designed that no direct x-radiation can reach surfaces that can contribute background emission currents which might return to the photocathode when it is at a relatively positive, retarding potential. High transparency mesh surfaces are placed in front of surfaces which are at appreciably higher positive potential thereby trapping the large angle photoemitted electrons which might otherwise excite secondary electron background. This cylindrical grid method for separating the secondary from the total photoemission current is illustrated as applied to both front-surfaces and to transmission photocathode characterization in Figs. 4, 5, 6 and 7. As illustrated here, detailed equipotential maps of the accelerating and retarding fields have been compared along with photoemitted electron ray traces[8] in order to determine the potential "hill" characteristics of the cylindrical grids.

The filter-window material on the proportional counter aperture is identical to that on the entrance aperture to

FRONT AND BACK SURFACE PHOTOEMISSION MEASUREMENT (0.1-10 keV)

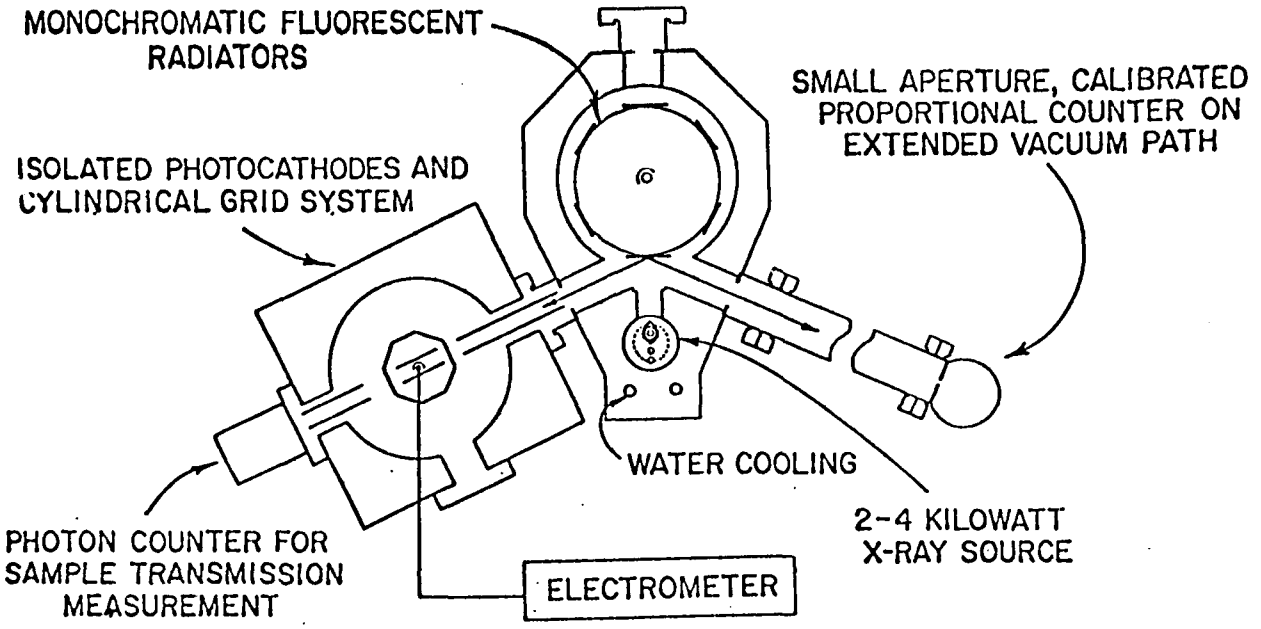

Figure 3. An instrument for the relative and absolute measurement of the quantum yields for front-surface and transmission photocathodes in the 0.1-10 keV photon energy region. Characteristic fluorescent line sources are excited by a closely-coupled x-ray source of strong line radiation of photon energy just above that of the fluorescent lines. The fluorescent line intensities are measured by a calibrated proportional counter which views the source at the same take-off angle as does the photocathode. The filter material between the source and the photocathode is identical to that on the proportional counter aperture. The monochromaticity of the fluorescent sources under similar excitation and filtering are evaluated spectroscopically and are monitored by a multichannel pulse height analyzer during the measurements. The electrometer current output is converted proportionally to a frequency from zero to 25 kilohertz for rapid and precise digital signal averaging.

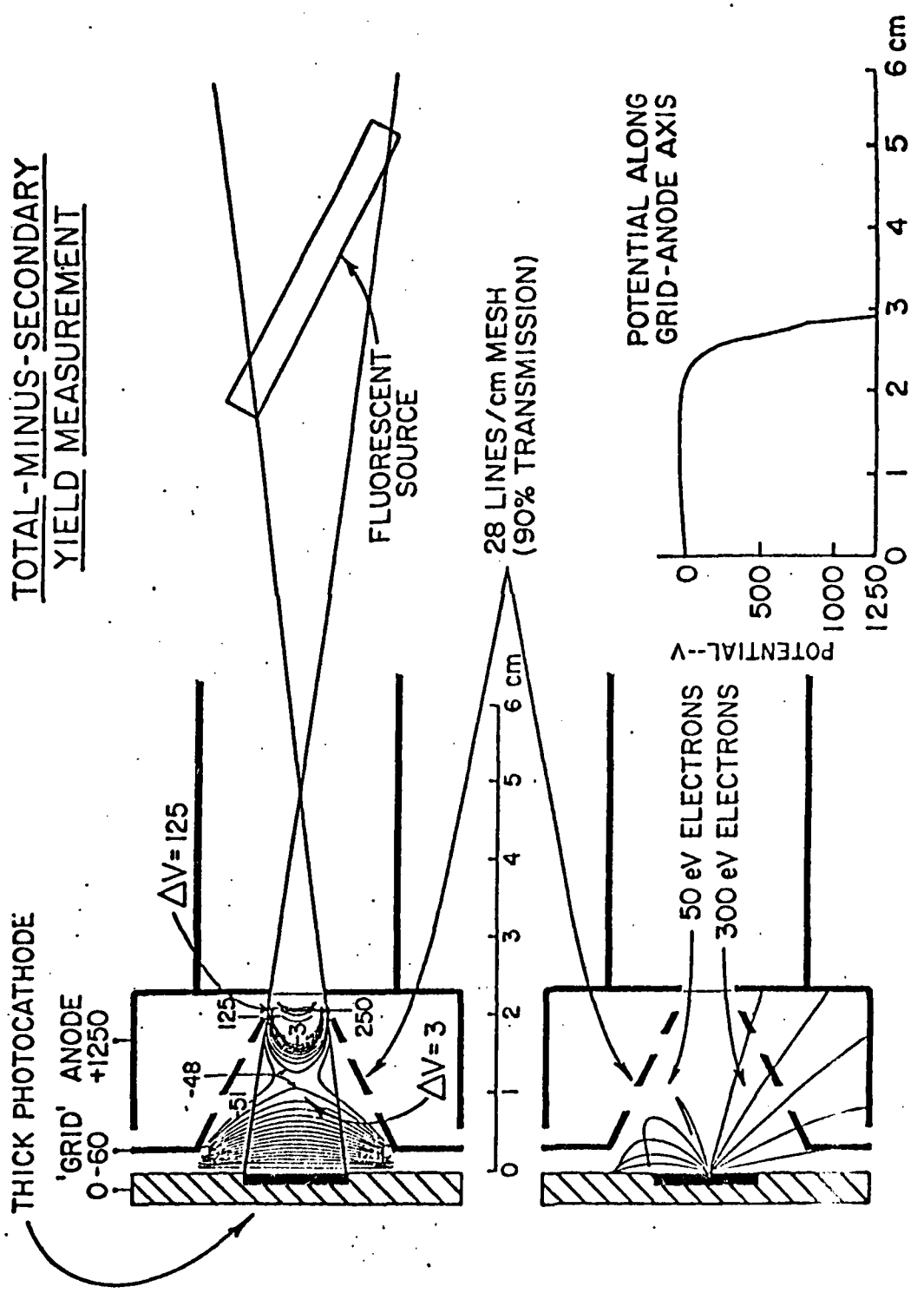

Figure 4. Cylindrical grid geometry for front-surface photoemission measurement. Illustrating the retarding field, potential "hill" characteristics and electron ray traces for the measurement of the fast electron photoemission component.

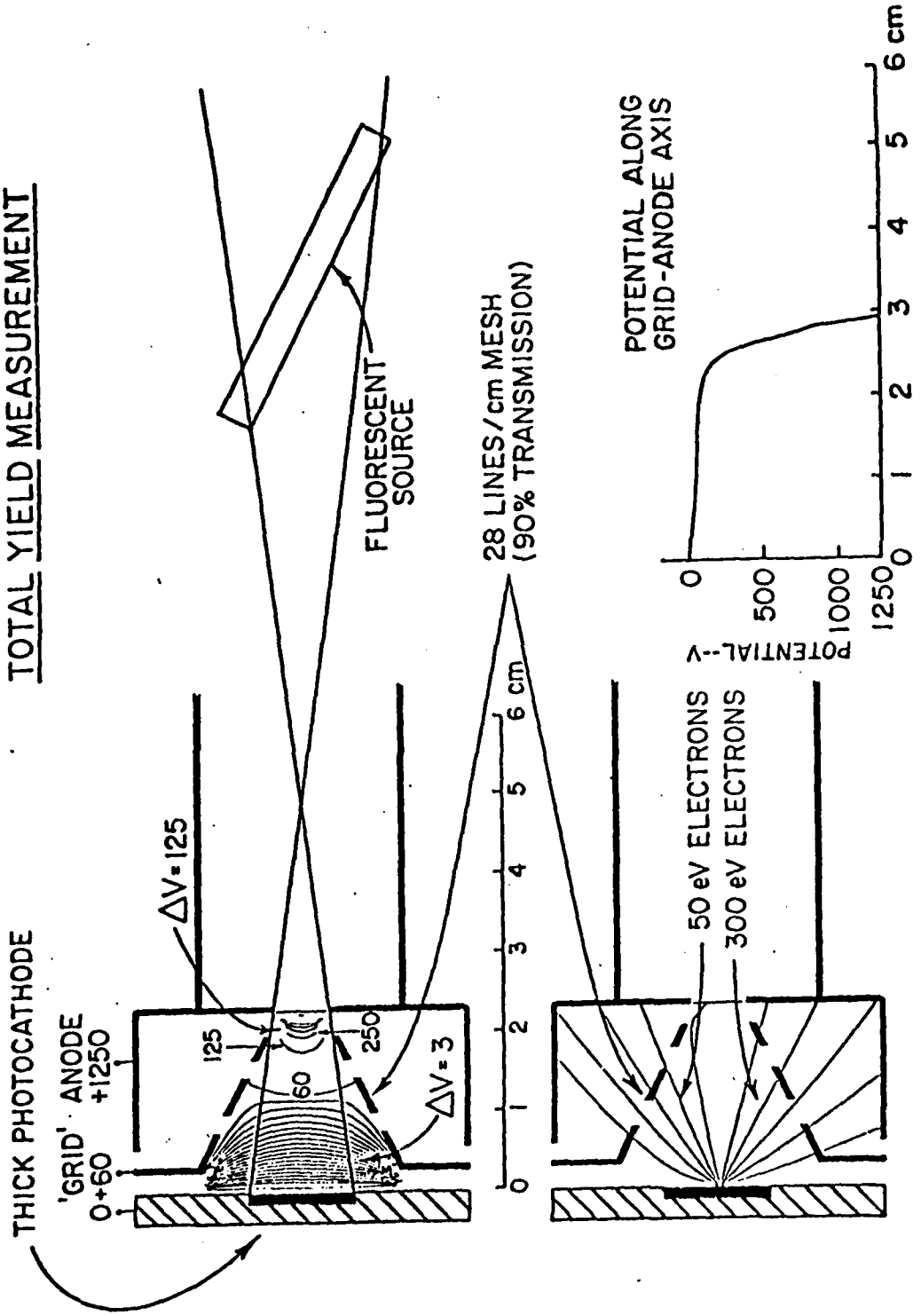

Figure 5. Total yield measurement of front-surface photoemission.

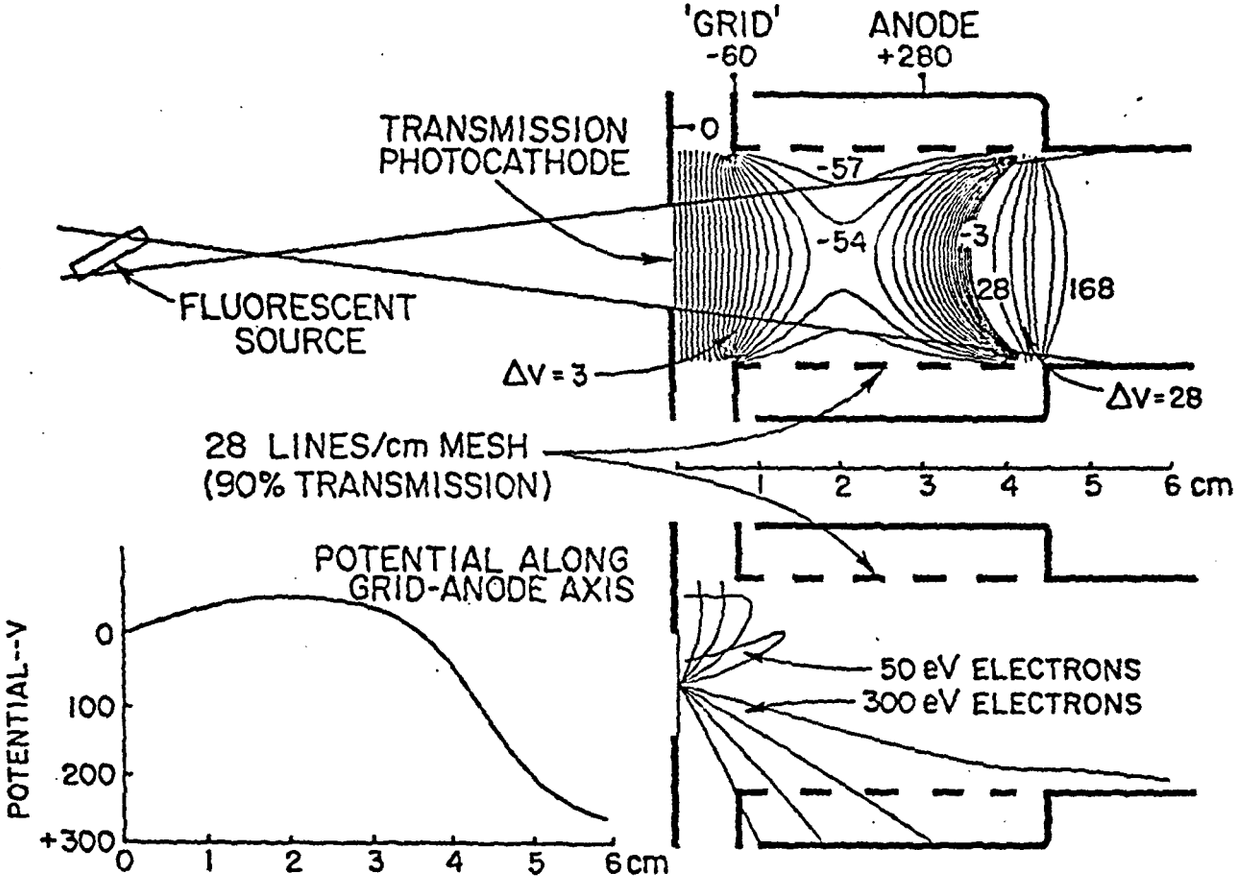

Figure 6. Cylindrical grid geometry for back-surface photoemission measurement. Illustrating the retarding field, potential "hill" characteristics and electron ray traces for the measurement of the fast electron photoemission component.

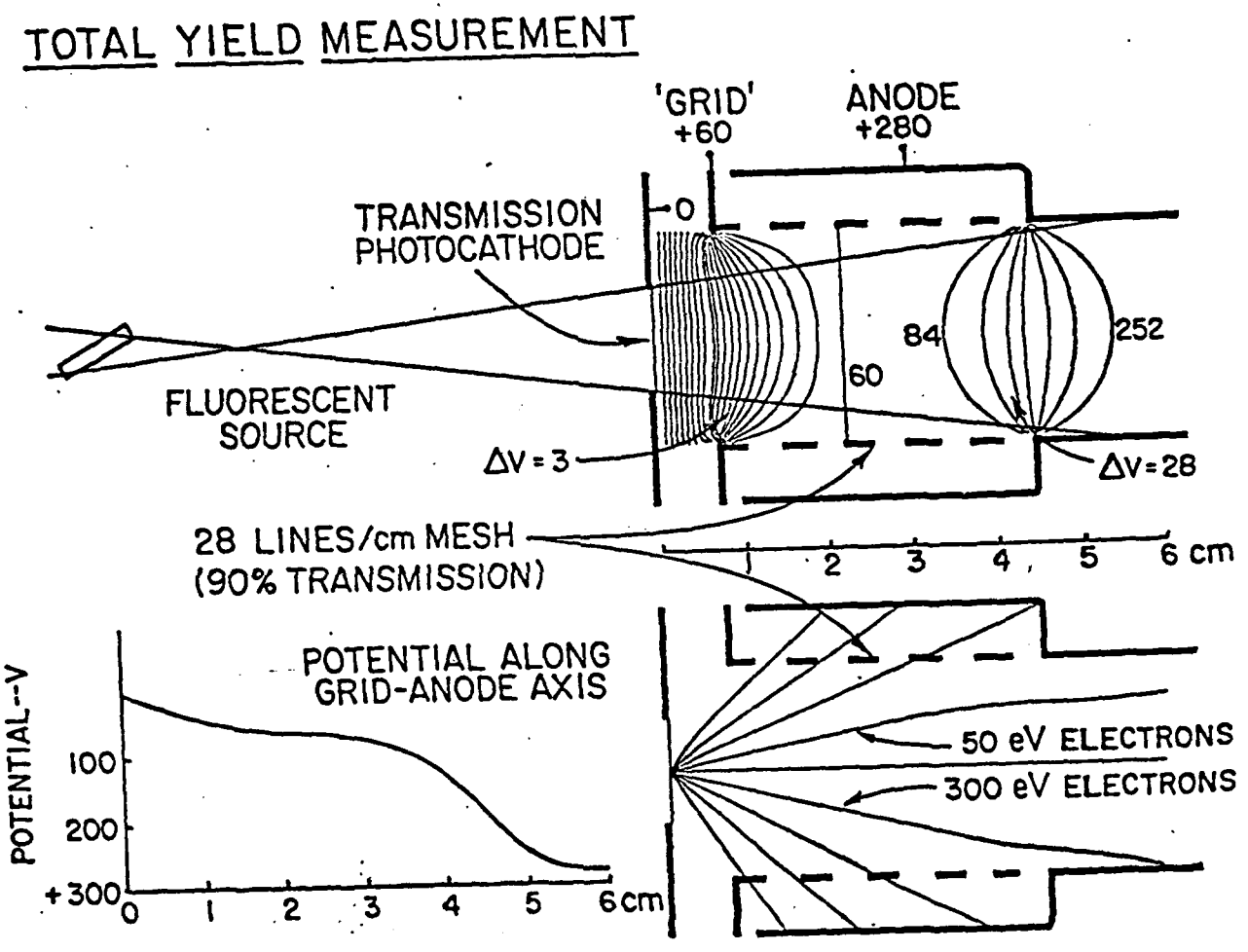

Figure 7. Total yield measurement of back-surface photoemission.

the photocathode section so that their transmission cancel in the absolute yield measurements. By using a similar material on the back, substrate surface of the transmission photocathodes, the back-surface photoemission current is effectively cancelled by that from the adjacent entrance window surface thereby improving the measurement statistics in the difference measurements.

The x-radiation that passes through the side-window proportional counter is limited by the entrance pinhole window to a narrow beam that just misses the central anode wire and, if not absorbed, proceeds through an exit hole in the opposite side and into a positive potential electron trap region. The effective absorption path, between the two apertures, is 3.51 cm. The anode wire diameter is 50 microns. When possible, the photon absorption efficiency is set between 85 and 95 percent for a given photon energy by the choice of the counter gas and its pressure. This "pressure tuning" minimizes ionization change loss at the entrance window and photon loss through the exit aperture and provides minimum-width pulse height distributions.[7] A multichannel pulse height analyzer is used to monitor the output pulses of the proportional counter in order to verify that a given fluorescent line source is optimally excited and filtered for minimum background x-radiation.

In Table 1 are presented a list of the fluorescent

TABLE 1. Parameters for the calibrated fluorescent line excitation sources.

λ(A)	E(eV)	FLUORESCENT SOURCE	EXCITING SOURCE	FILTER	FILTER THICKNESS	FILTER TRANSMISSION(%)	PROPORTIONAL COUNTER		
							GAS	PRESSURE	EFFICIENCY(%)
1.79	7469	Ni-Kα	Cu-K	Ni	12 μ	47	P-10	760	53
1.94	6397	Fe-Kα	Cu-K	Ni	12 μ	38	P-10	760	69
2.29	5411	Cr-Kα	Cu-K	Ni	12 μ	20	P-10	760	84
4.16	2981	Ag-Lα	Cr-K	Ag	0.5 μ	77	P-10	760	85
5.41	2292	Mo-Lα	Cr-K	Ag	0.5 μ	59	P-10	760	85
7.13	1739	Si-Kα	Cr-K	Ag	0.5 μ	35	P-10	760	98
8.34	1486	Al-Kα	Cr-K	Ag	0.5 μ	22	P-10	760	100
9.89	1254	Mg-Kα	Al-K	Mg	6.6 μ	57	Propane	200	80
13.3	930	Cu-Lα	Al-K	Mg	6.6 μ	28	Propane	200	98
14.6	852	Ni-Lα	Al-K	Mg	6.6 μ	20	Propane	200	99
17.6	705	Fe-Lα	Ni-L	Fe	0.6 μ	36	Propane	75	95
18.3	677	F-Kα	Ni-L	Fe	0.6 μ	33	Propane	75	96
23.6	525	O-Kα	Ni-L	Formvar	52 μg/cm²	66	Propane	50	99
31.6	392	N-Kα	Cu-L, O-K*	Formvar	52 μg/cm²	43	Propane	50	100
44.7	277	C-Kα	Cu-L, O-K*	Formvar	52 μg/cm²	84	Propane	100	82
64.4	193	Mo-Mζ	C-K	Formvar	52 μg/cm²	65	Propane	50	88
82.1	151	Zr-Mζ	C-K	Formvar	52 μg/cm²	46	Propane	50	98
114	109	Be-Kα	C-K	Formvar	52 μg/cm	20	Propane	50	100

*Oxidized copper anode

line sources that were employed in the measurements that are reported here along with a description of the excitation, filtering and flow proportional counter parameters that were chosen to obtain the calibrated photon excitation of the photocathodes.

The photocathode materials were vacuum evaporated upon chromium coated microscope slide substrates and were mounted upon a rotatable, insulating Teflon structure. The vibrating reed preamplifier head of a Carey 401 Electrometer was connected through a rigid co-axial section to a low-loss feedthrough and to a spring contact upon a polished button which fastens each photocathode to the holder. Typical measurement current levels for these studies were between 10^{-12} and 10^{-15} amperes. A mechanical shutter for the x-ray beam was provided between the source and the photocathode to permit a determination of the effective background current ($\sim 10^{-17}$ amperes).

For rapid and convenient signal averaging, the electrometer output current was converted by a variable frequency oscillator circuit (IC-Raytheon 4151) to a frequency that is precisely proportional to the current and in the 0 to 25 kiloHertz region. The quantum yield (as the charge collected per photon incident upon the photocathode) is measured by counting the number of cycles within a time interval that is determined by that required

to collect a set number of photons at the proportional counter (typically 10,000 counts).

III. EXPERIMENTAL RESULTS

A. Front-Surface Photoemission--Thick Photocathodes

For x-ray diode detectors, effective front-surface emission photocathodes have been aluminum, gold, the semiconductor copper iodide and the insulator cesium iodide. These have been included in this study. The materials, vacuum evaporated as thick photocathode systems upon chromium-coated microscope slide substrates, were handled in a dry-nitrogen atmosphere outside the vacuum systems. The total yields and the fast, primary electron yields (secondary electrons retarded by a -50 volt potential "hill") were measured for eighteen photon energies in the 0.1 to 10 keV region. The total yield data are presented in Figs. 8, 9, 10 and 11. In Fig. 12 are presented the associated curves for the measured ratios of the primary yield (fast electron component) to the total yield, Y_P/Y_T. From these data it may be noted that the dominant photoemission current is that of the secondary electrons, and that for the several photocathodes characterized here, the primary yields are very similar and the insulator and semiconductor photocathodes, CsI and CuI, have considerably higher secondary electron

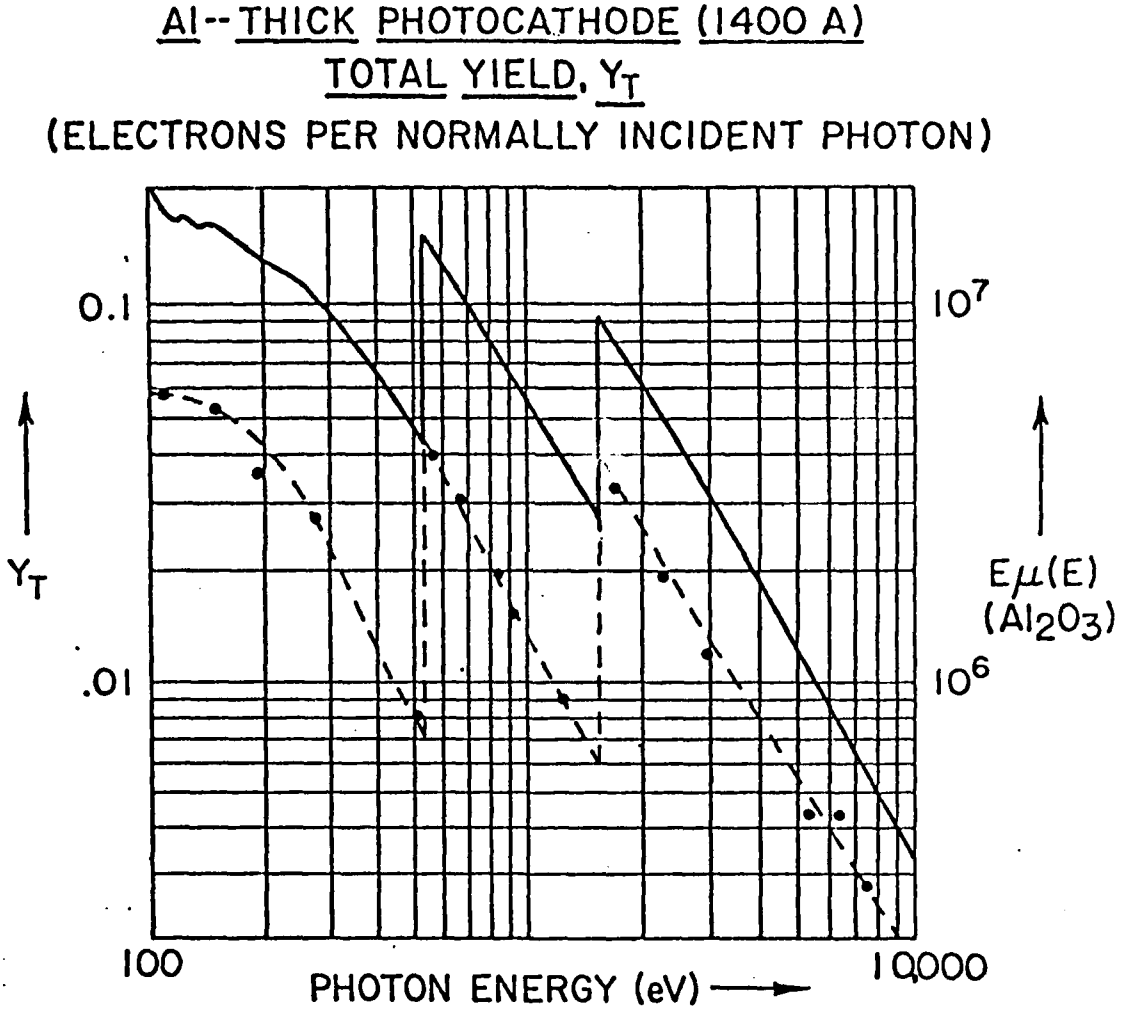

Figure 8. Front-surface, total quantum yield for a 1400 A evaporated aluminum photocathode. (Compared to $E\mu(E)$ for Al_2O_3.)

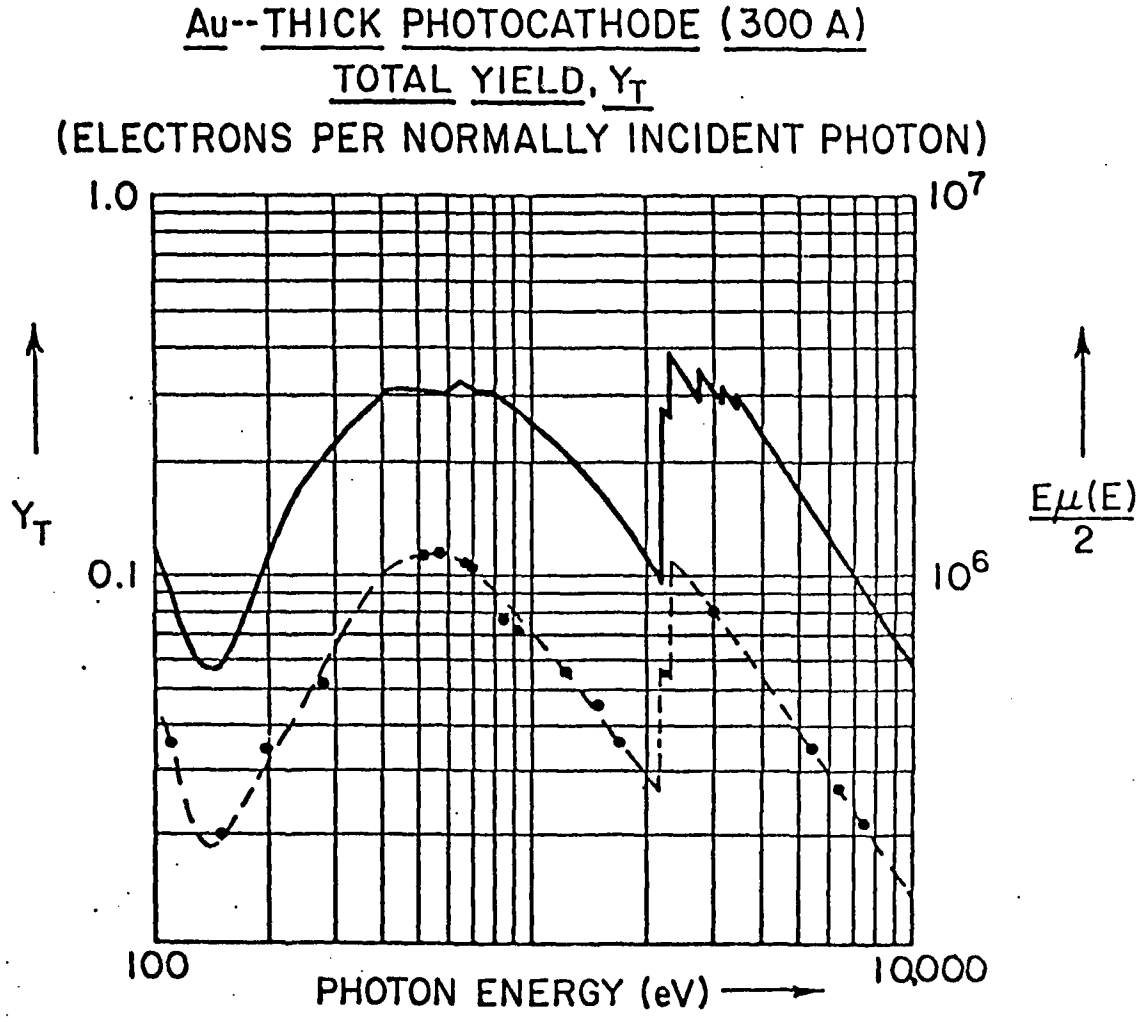

Figure 9. Front-surface total quantum yield for a 300 A evaporated gold photocathode. (Compared to $E\mu(E)$ for Au.)

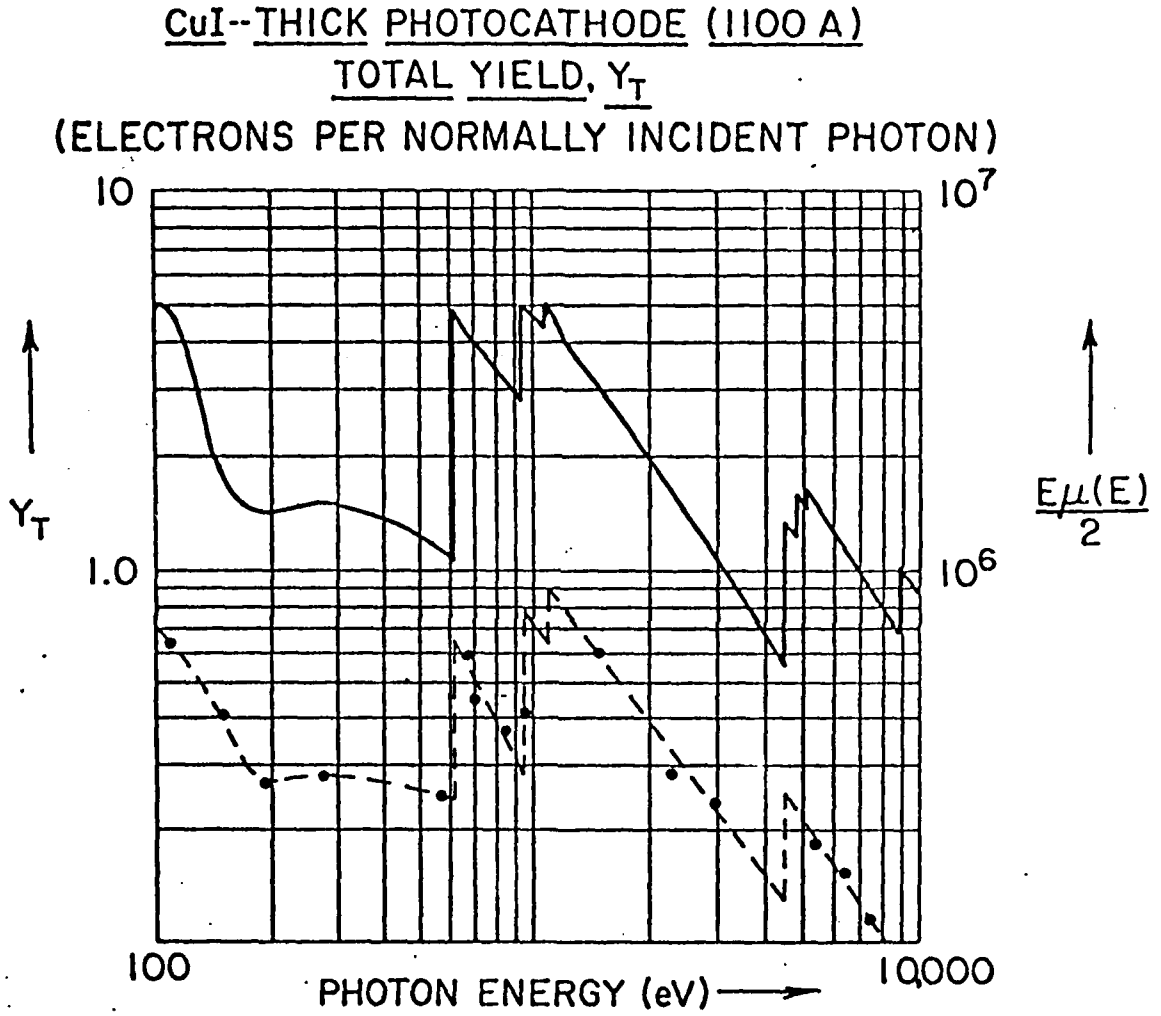

Figure 10. Front-surface total quantum yield for a 1100 A evaporated copper iodide photocathode. (Compared to $E\mu(E)$ for CuI.)

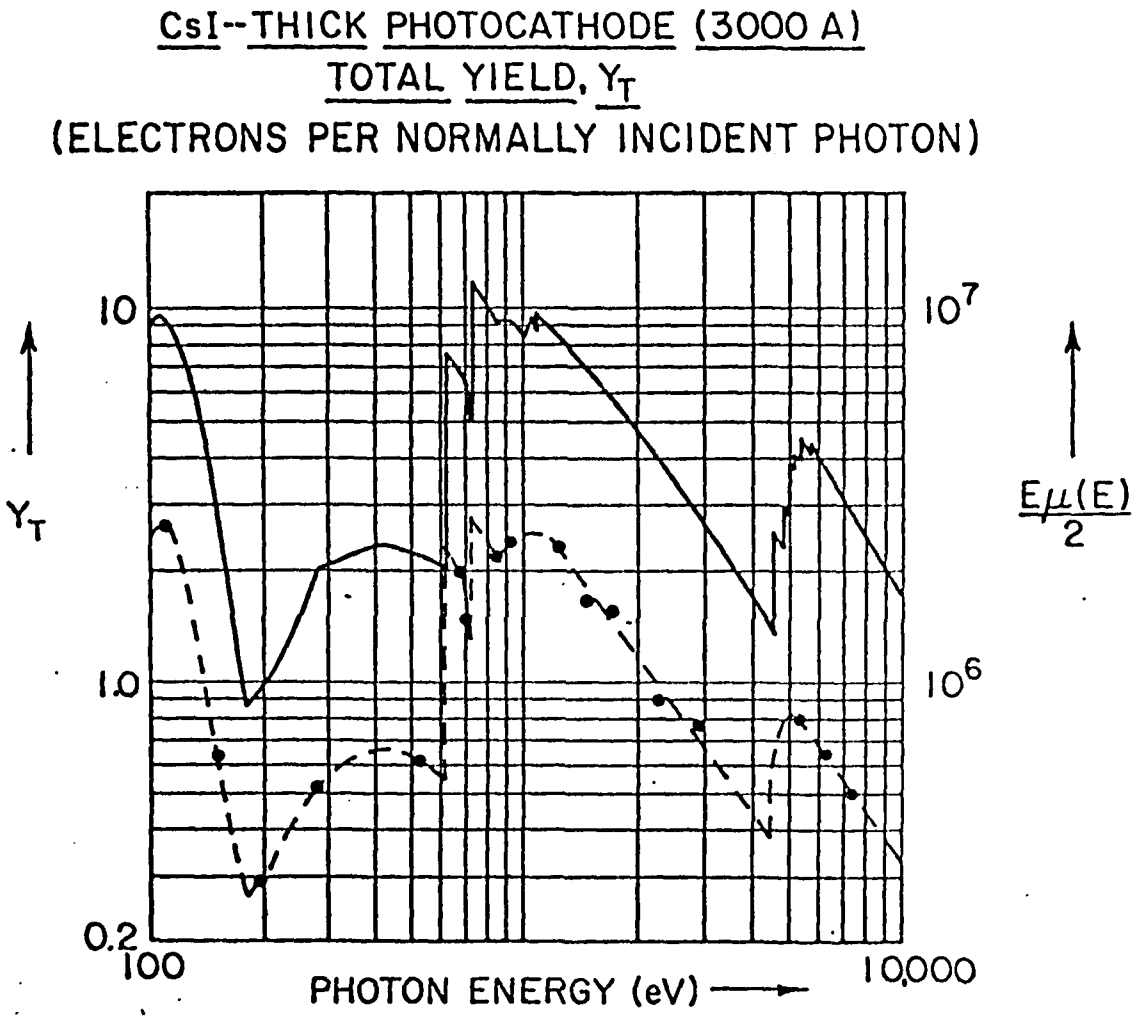

Figure 11. Front-surface total quantum yield for a 3000 A evaporated cesium iodide photocathode. (Compared to $E\mu(E)$ for CsI.)

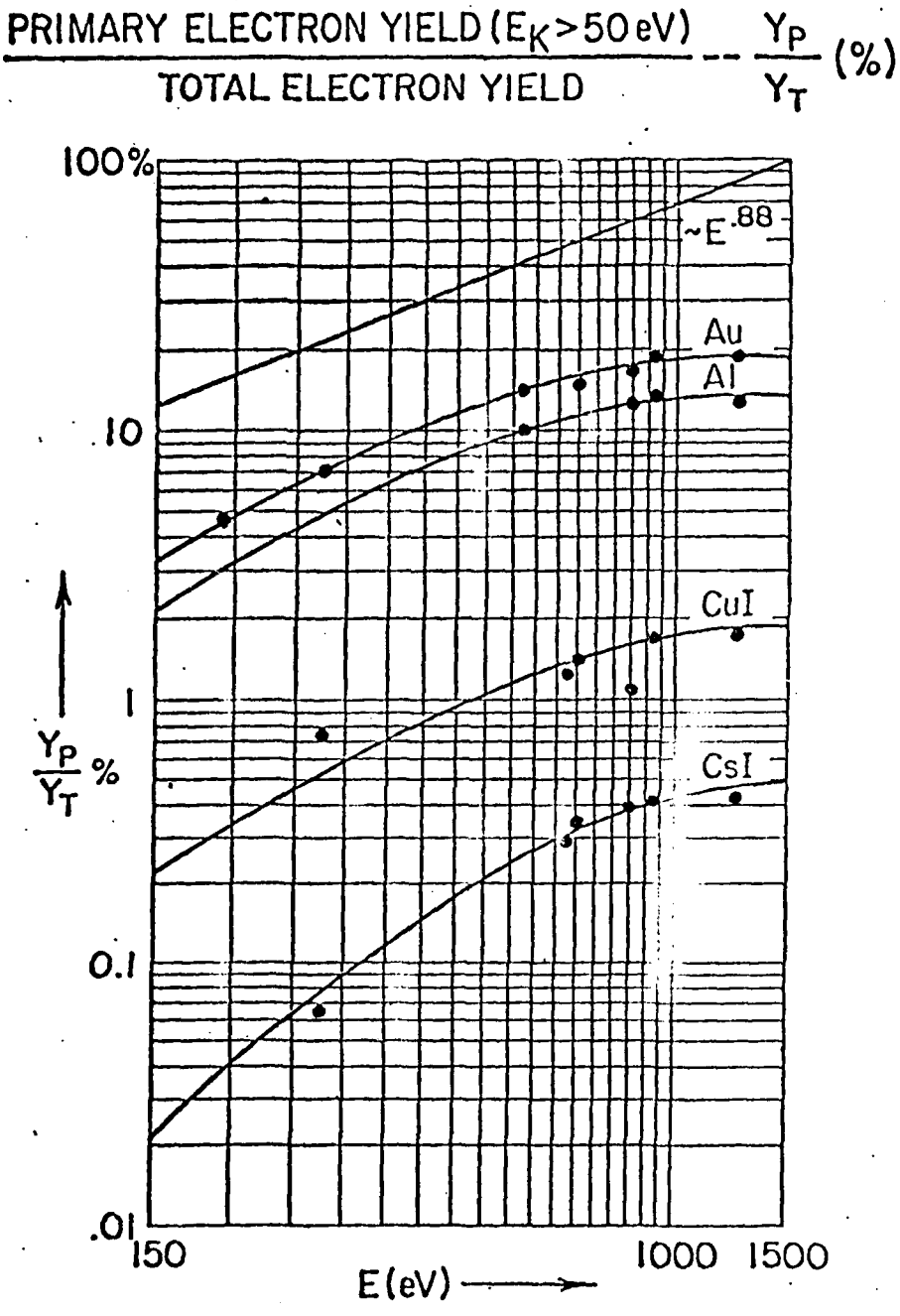

Figure 12. Ratio of the primary (fast) electron yield to the total electron yield for Au, Al, CuI and CsI. According to the x-ray photoemission model presented here and based upon an effective escape depth for the primary electron photoemission that is proportional to the range given by the Bethe-Bloch continuous-slowing-down-approximation, the ratio Y_P/Y_T, is predicted to vary as $E^{\cdot 88}$ for these photocathodes.

yields than do the metal photocathodes, Al and Au.

It is of interest to compare here the secondary electron energy distributions for these same photocathodes. To measure these, the photocathodes were transferred to an electron spectrograph and analyzed with about .01 eV resolution as has been described previously.[9,10] Presented in Figs. 13 and 14 are spectra for the four photocathodes as photoexcited by C-Kα (277 eV) and by Cu-Kα (8080 eV). The peak intensities of the distributions are given relative to that for the gold photocathode. Also noted here are the peak positions, E_{KP}, and the full-width-at-half-maximum, Δ, for each secondary electron energy distribution.

It is important to note that, as is illustrated here, there is no significant change in the shape of the secondary electron energy distributions for a given photocathode in the 0.1 to 10 keV excitation region. It is also of considerable practical importance that the CuI and CsI photocathodes do have the narrow secondary electron energy distributions and high quantum efficiency that is required for sensitive time-resolved spectroscopy in the picosecond range[11] (see Fig. 2).

By measuring the area under the secondary electron energy distribution curves, as those presented in Figs. 13 and 14, we have obtained the relative secondary electron yields for photocathodes as excited and analyzed under

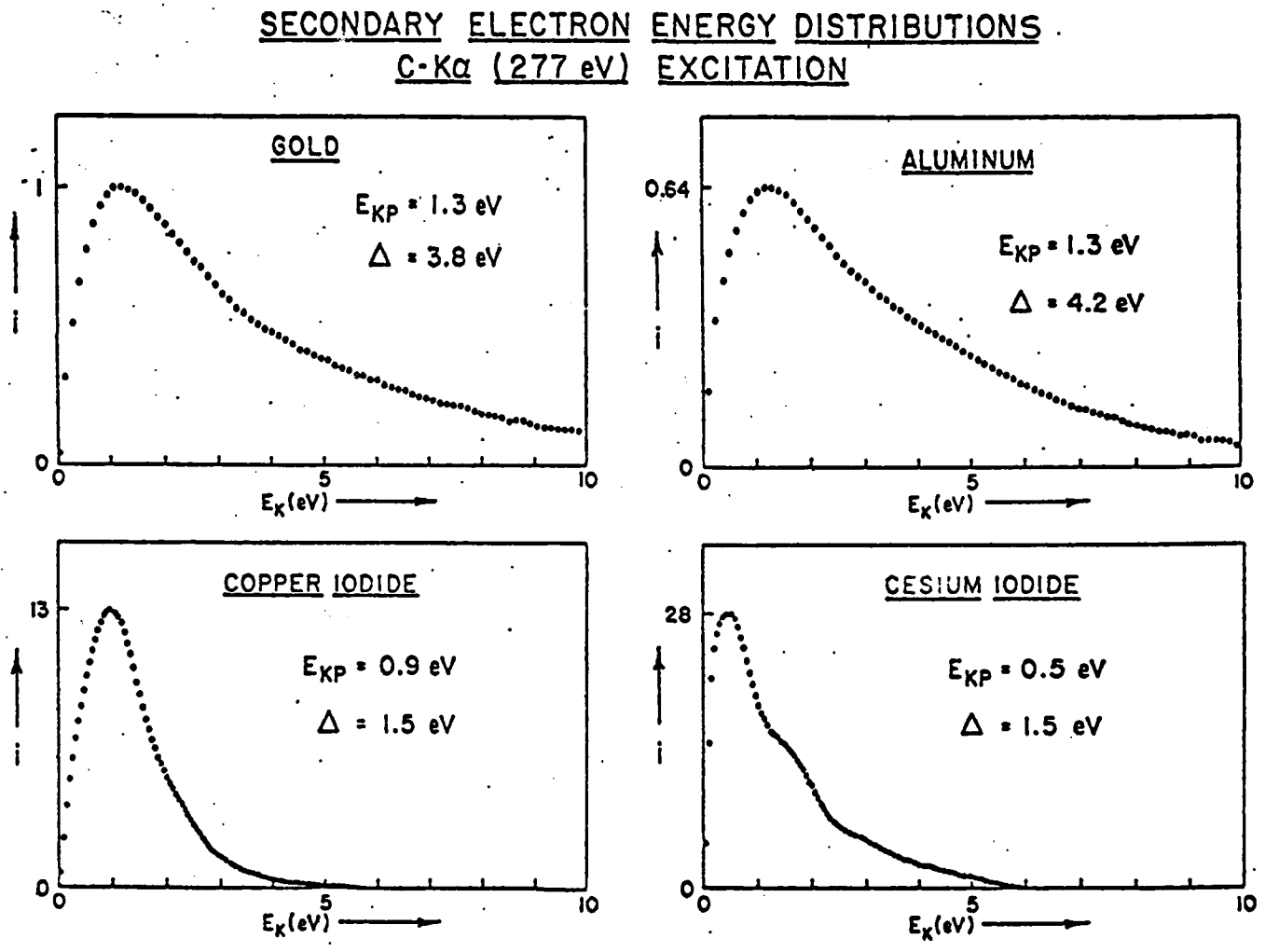

Figure 13. Secondary electron energy distributions for Au, Al, CuI and CsI photocathodes (as measured in Figs. 8-11). Excited by C-Kα (277 eV) x-radiation.

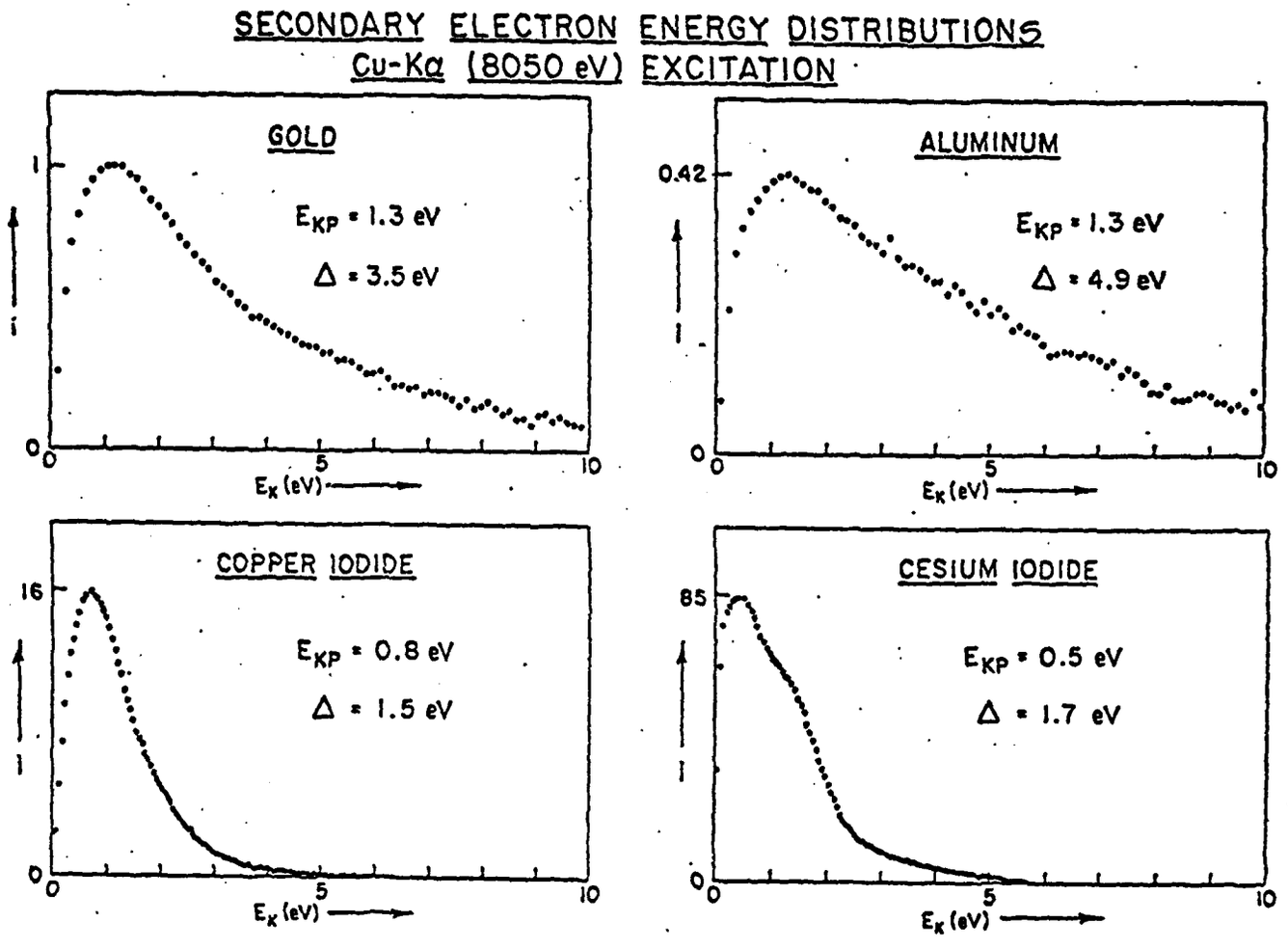

Figure 14. Secondary electron energy distributions of Au, Al, CuI and CsI photocathodes (as measured in Figs. 8-11). Excited by Cu-Kα (8080 eV) x-radiation. Note that the shapes of these distribution curves are essentially the same as those excited by the C-Kα (277 eV) x-radiation.

identical conditions. In Table 2 are presented the secondary electron yield of cesium iodide relative to that for gold as determined by the total-and-retarded absolute yield measurements described above and by the electron spectroscopy[10] of the secondary distributions. As shown here, the agreement between these independent methods is very good.

In order to define an appropriate thickness for the "thick", front-surface photocathodes and to measure the effective escape depth of the secondary electron emission for a given photocathode, the secondary electron yields have been measured as a function of film thicknesses. An example of these determinations is presented in the yield-vs-thickness data of Fig. 15 for the cesium iodide photocathode. (A Chromium substrate was used for CsI films because its very low photoemission yield relative to that for CsI allows only a negligible contribution to the measured yields.) The film thicknesses greater than a few hundred angstroms were measured by multiple-beam interferometry; smaller thicknesses were determined by extrapolation using the thickness dependence upon an inverse-square of the distance of the sample from an effective point evaporation source. These data suggested our use of 3000 A CsI films for the thick photocathode measurements that are described here and which would be appropriate for x-ray diode detector applications.

TABLE 2. $Y_S(CsI)/Y_S(Au)$ for thick photocathode secondary electron yields.

Relative Yields--$Y_S(CsI)/Y_S(Au)$

PHOTON ENERGY eV	FROM ABSOLUTE YIELDS	FROM SECONDARY ELECTRON ENERGY DISTRIBUTIONS
277	11	10
1487	44	42
8080	34	34

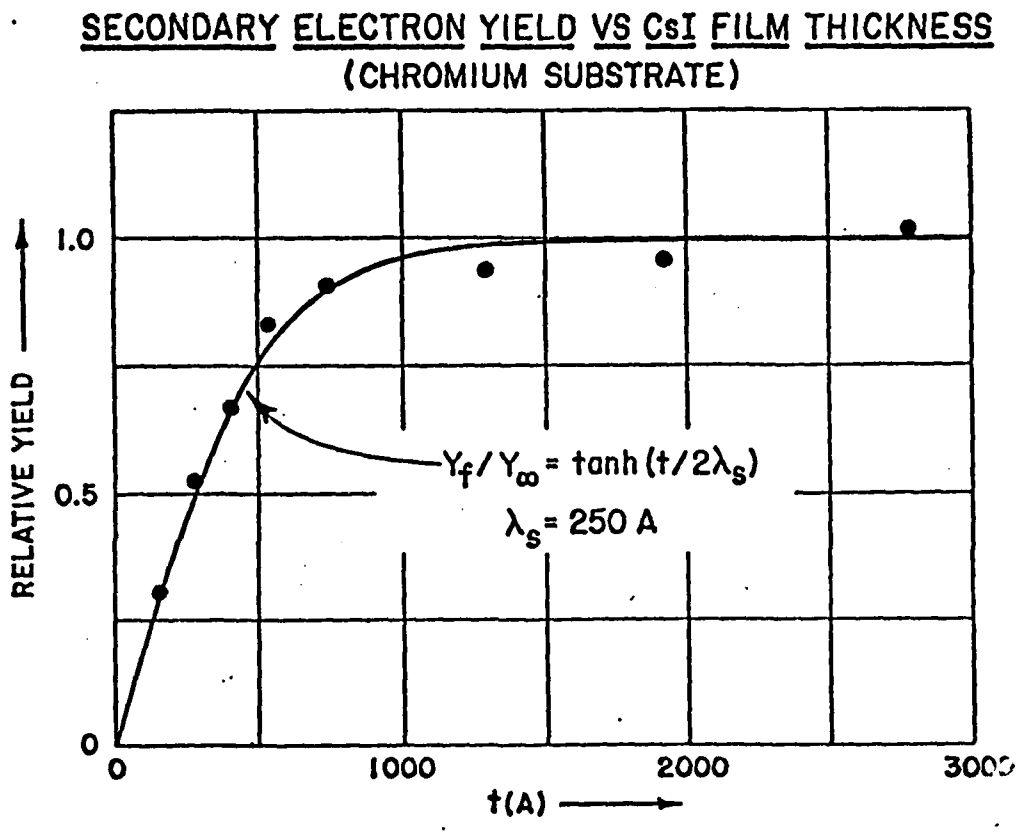

Figure 15. The front-surface secondary electron yield for CsI vs photocathode film thickness and fit according to a yield equation predicted by the x-ray photoemission model presented here. (The CsI was evaporated upon a chromium substrate of relatively very low photoemission efficiency.)

B. Back-Surface Photoemission-- Transmission Photocathodes

Gold and cesium iodide transmission photocathodes are currently being applied in x-ray streak cameras for time-resolved spectroscopy into the picosecond range.[11] We have presented the back-surface secondary electron emission yields-vs-photon energy data for the 0.1 to 10 keV region for these photocathodes in Fig. 16 and 17. The transmission photocathode films were of about 250 and 1000 A thickness, respectively, and were vacuum evaporated upon carbon foil substrates of about 50 micrograms per cm^2 mass thickness. The x-ray transmissions of the substrate carbon foils were measured and these values were used to obtain the secondary electron yield per normally incident photon as transmitted to the front-surface of the photocathode film. Carbon foil substrates were chosen because these have good mechanical strength, low attenuation for the low-energy x-rays and are conducting. Because of the very low photoemission efficiency of the carbon substrates, it is expected that these yield data are essentially independent of the substrate contribution and would be the same for the equivalent self-supporting film system.

In Figs. 18 and 19 are presented the back-surface yields vs photocathode film thickness for the gold and cesium iodide systems. Because of the very broad maxima

TRANSMISSION PHOTOCATHODE
SECONDARY ELECTRON YIELD, Y_b, VS PHOTON ENERGY
(ELECTRONS PER NORMALLY INCIDENT PHOTON ON 230 A GOLD FILM)

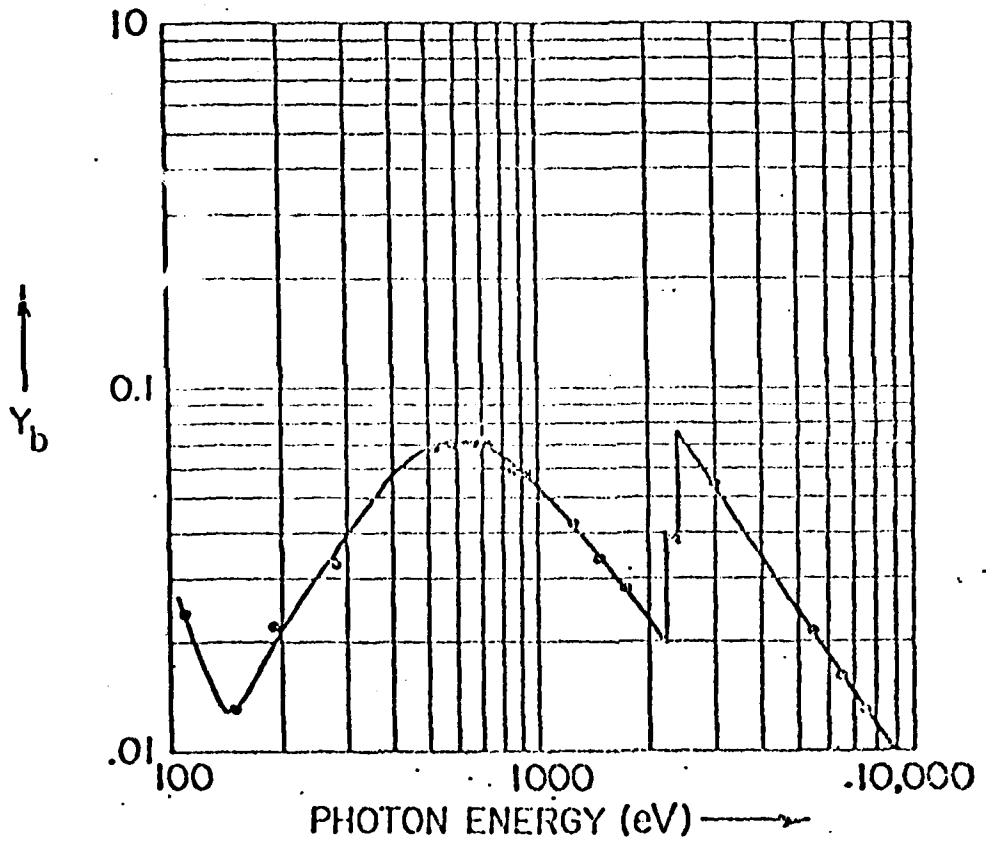

Figure 16. Back-surface secondary electron quantum yield for a 230 A Au transmission photocathode.

B. Back-Surface Photoemission-- Transmission Photocathodes

Gold and cesium iodide transmission photocathodes are currently being applied in x-ray streak cameras for time-resolved spectroscopy into the picosecond range.[11] We have presented the back-surface secondary electron emission yields-vs-photon energy data for the 0.1 to 10 keV region for these photocathodes in Fig. 16 and 17. The transmission photocathode films were of about 250 and 1000 A thickness, respectively, and were vacuum evaporated upon carbon foil substrates of about 50 micrograms per cm^2 mass thickness. The x-ray transmissions of the substrate carbon foils were measured and these values were used to obtain the secondary electron yield per normally incident photon as transmitted to the front-surface of the photocathode film. Carbon foil substrates were chosen because these have good mechanical strength, low attenuation for the low-energy x-rays and are conducting. Because of the very low photoemission efficiency of the carbon substrates, it is expected that these yield data are essentially independent of the substrate contribution and would be the same for the equivalent self-supporting film system.

In Figs. 18 and 19 are presented the back-surface yields vs photocathode film thickness for the gold and cesium iodide systems. Because of the very broad maxima

TRANSMISSION PHOTOCATHODE
SECONDARY ELECTRON YIELD, Y_b, VS PHOTON ENERGY
(ELECTRONS PER NORMALLY INCIDENT PHOTON ON 230 A GOLD FILM)

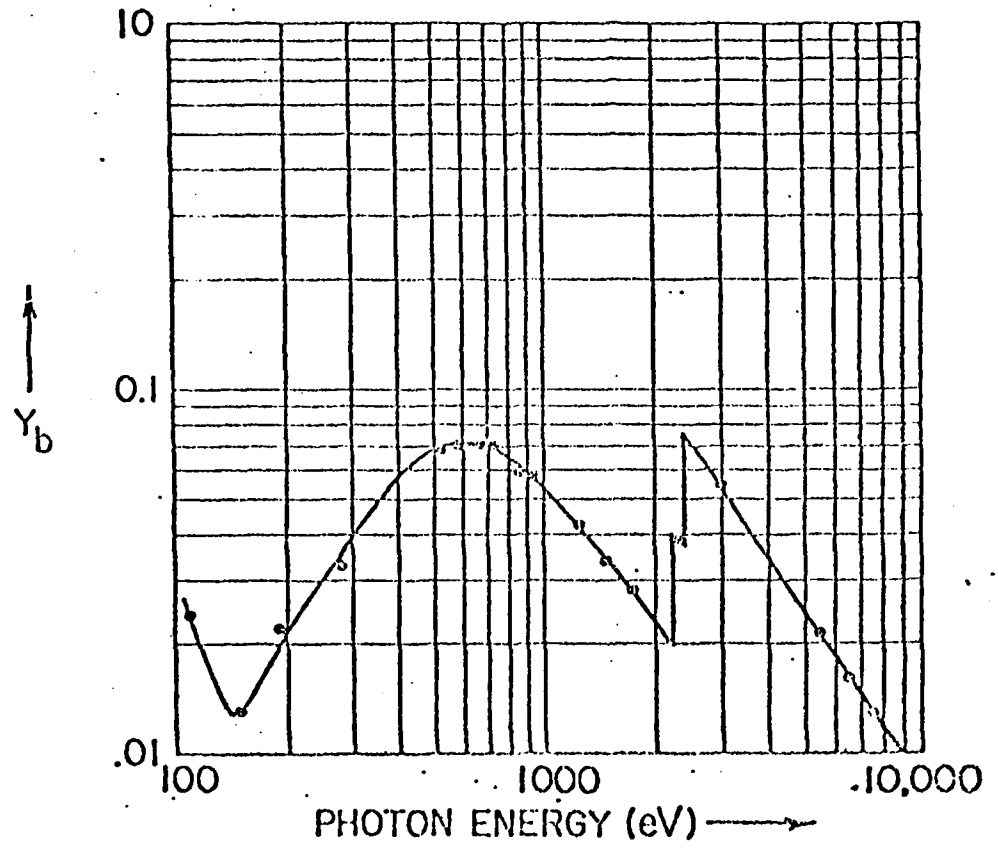

Figure 16. Back-surface secondary electron quantum yield for a 230 A Au transmission photocathode.

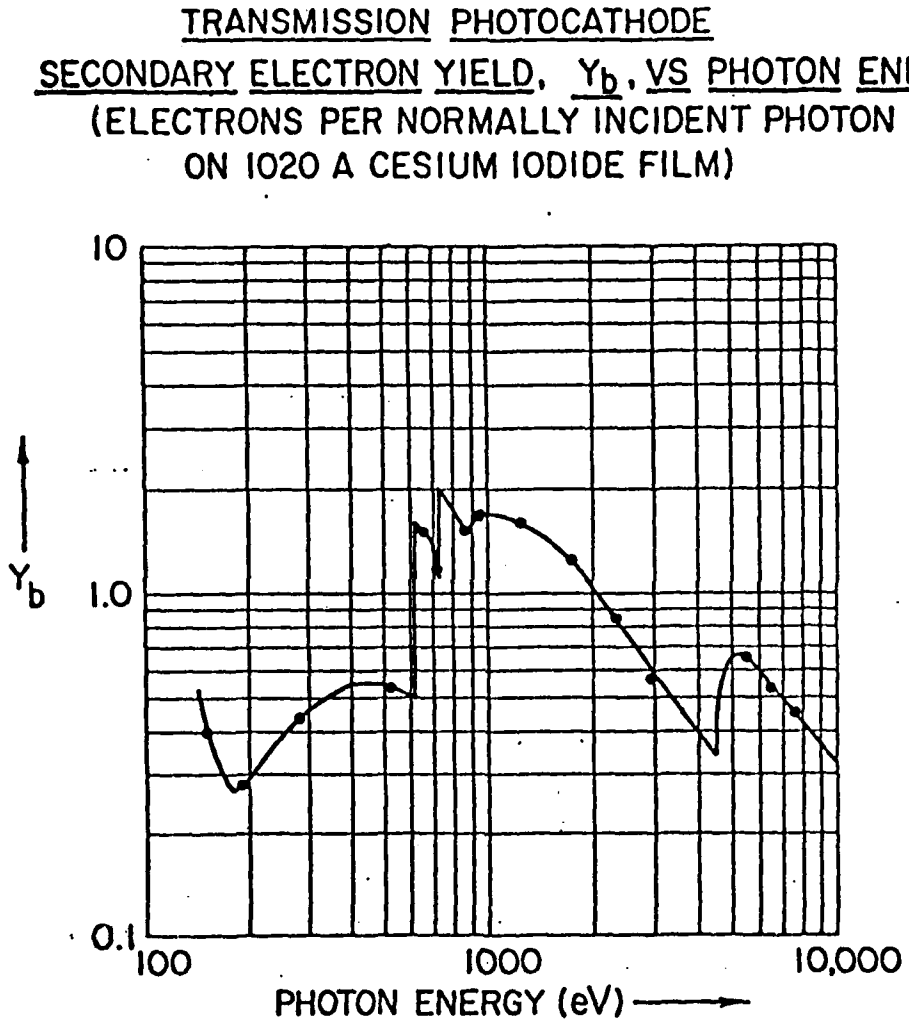

Figure 17. Back-surface secondary electron quantum yield for a 1020 A CsI transmission photocathode.

TRANSMISSION PHOTOCATHODE SECONDARY ELECTRON YIELD, Y_b, VS GOLD FILM THICKNESS, t

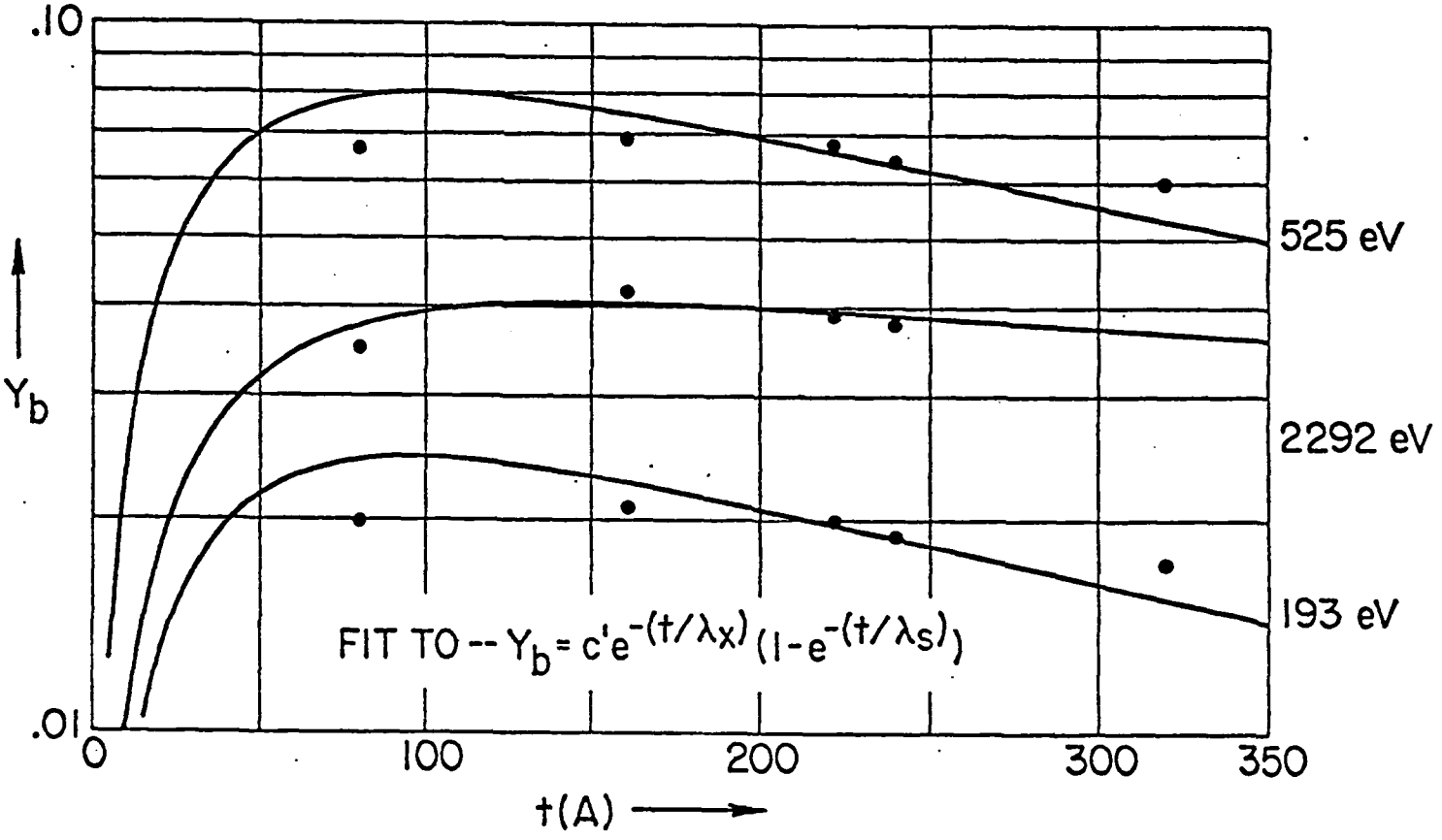

Figure 18. Back-surface secondary electron yield for Au-vs-transmission photocathode film thickness and fit according to a yield equation predicted by the x-ray photoemission model presented here.

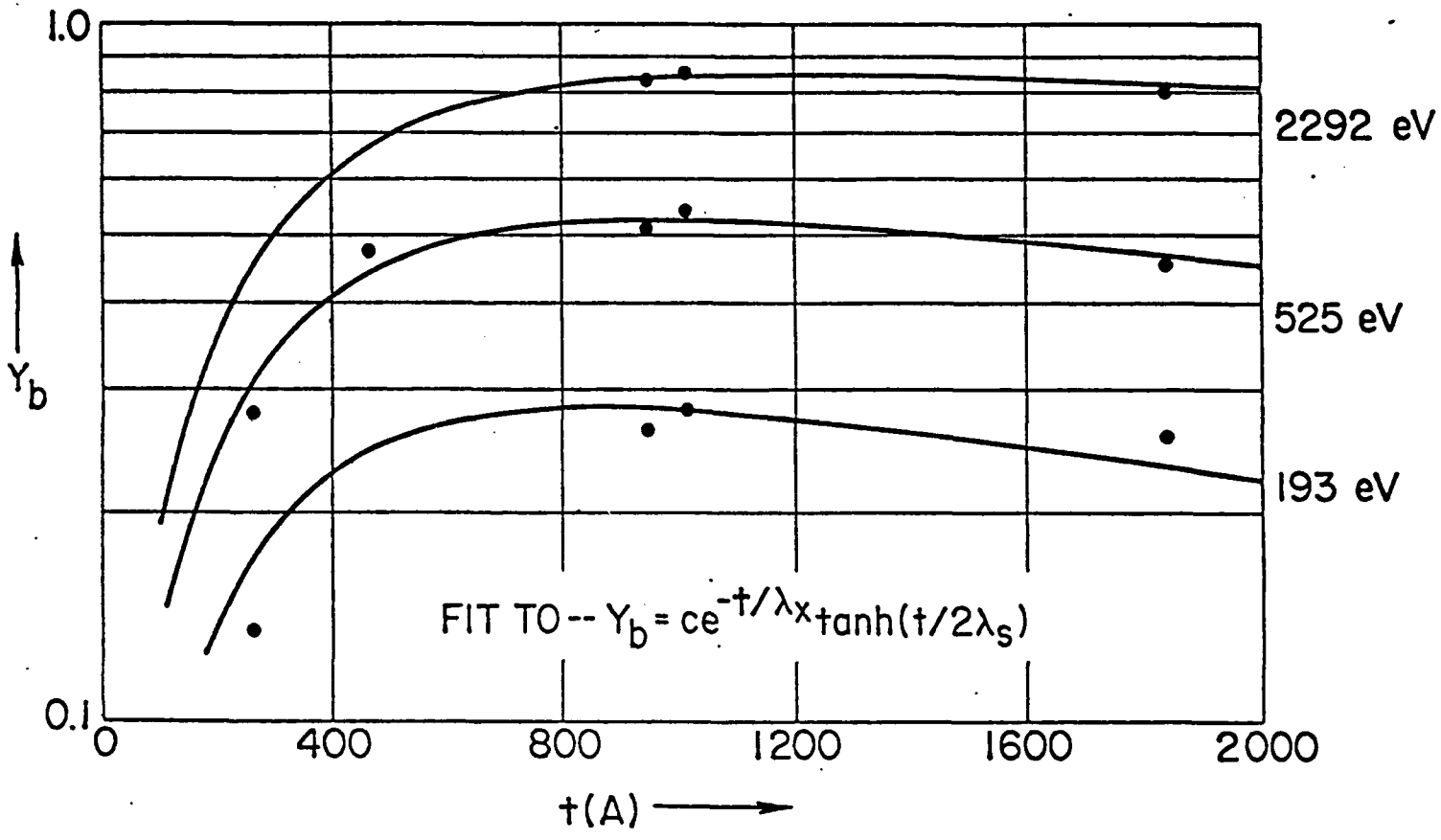

Figure 19. Back-surface secondary electron yield for CsI-vs-transmission photocathode thickness and fit according to a yield equation predicted by the x-ray photoemission model presented here.

characteristic of the yield-vs-thickness curves for the transmission photocathodes, we have chosen the thicknesses of 250 and 1000 A as appropriate for the Au and CsI transmission photocathodes which allow somewhat greater uniformity and strength without a serious decrease in yield from an optimum value for the low energy x-rays.

IV. A SIMPLE MODEL FOR FRONT AND BACK SURFACE X-RAY PHOTOEMISSION YIELDS AND FOR THE EFFECT OF PHOTOCATHODE THICKNESS: COMPARISON WITH EXPERIMENTAL RESULTS

In a previous work[10] we have presented a detailed phenomenological model for x-ray photoemission for thick photocathodes. Here we extend this description to include the effect of photocathode thickness for the thin metal or insulator photocathode for which both front and back surface photoemission are excited by incident x-radiation.

We had noted that the x-radiation energy that is deposited within the photocathode is converted through photoelectric absorption to that of photoelectrons and subsequently to emitted Auger electrons and fluorescent radiation. Nearly all of this deposited energy is transformed to that of primary electrons within the photocathode except for a small fraction that is associated with the primaries and fluorescence that escapes through the photocathode surface. The energy of these internal

primaries is initially and completely transformed to the excitation energy of secondary electrons (mostly by promoting valence band electrons to the conduction band and by the de-excitation of excited plasmons). Heuristically we can relate the number of secondaries, N, that are excited within a unit photocathode area of effective escape depth, λ_S, in a thick photocathode to the x-radiation energy deposited by the expression

$$N\bar{E}_{KS} \approx I_o \rho E \mu(E) \lambda_S \ , \qquad (1)$$

where $\bar{E}_{KS}$ is the mean energy of the excited secondaries; I_o is the number of photons per unit area normally incident and of energy, E; $\mu(E)$ is the mass photoionization cross section; and ρ is the mass density. Assuming that the number of secondaries emitted per inicident photon (the yield, Y_S, for a thick photocathode) is simply proportional to that number of internally excited secondaries within the escape volume, we may then predict that

$$Y_S \sim \frac{\rho E \mu(E) \lambda_S}{\bar{E}_{KS}} \ . \qquad (2)$$

We have not been able to detect any significant change in the energy distribution of the emitted secondary electrons with photon energy in the 0.1 to 10 keV region as is illustrated here in Figs. 13 and 14. This implies that the internal energy distributions are also independent

of the x-ray photon energy and that $\bar{E}_{KS}$ is a constant for a given photocathode material. We may therefore predict for the yield of secondary electrons from a thick photocathode the relation

$$Y_S = K_S \rho E\mu(E) \lambda_S \quad . \tag{3}$$

Applying the same reasoning for the emission of the primary electrons, we note that $\bar{E}_{KP}$ for the internal distribution of primaries should be essentially proportional to the incident photon energy, E, and we obtain from a relation analogous to (2)

$$Y_P = K_P \rho \mu(E) \lambda_P \quad . \tag{4}$$

Because λ_S, the escape length for secondaries, is independent of the photon energy, the secondary electron yield dependence upon the x-ray photon energy, E, should be approximately as $\underline{E\mu(E)}$. This is confirmed by a comparison of the $E\mu(E)$ curves that are presented along with the log-log plots of the experimental yield data in Figs. 8 through 11. (The total yield plotted in these figures is mostly that of secondary electron emission.)

An escape depth for the primaries which are emitted into the sharp, elastically scattered photoelectron and Auger electron lines (as depicted in Fig. 1) may be a mean free path, and, for the kilovolt region, may depend upon the

energy[9,12,13] as approximately $E_K^{.8}$. However the total primary yield that is measured here, Y_P, is mostly that of the fast electrons which have suffered many inelastic collisions before escaping (into the low energy tails of the line spectra as illustrated in Fig. 1) and for these, the effective escape depth, λ_P, is more accurately described as a practical range. Its energy dependence, therefore, might be obtained for the kilovolt region by a logarithmic extrapolation of the Bethe-Bloch continuous-slowing-down-approximation range given in the tables of Pages, et al. as approximately the relation, $\lambda_P(\text{CSPA}) = R_o E_K^{1.9}$.[14,15] We may thus predict then since the primary energies should increase as the photon energy, the primary yield, Y_P, depends upon photon energy as approximately $E^{1.9}\mu(E)$. It then follows from (3) and (4) that the ratio, Y_P/Y_S, should depend upon the x-ray photon energy in the kilovolt region as approximately $E^{.9}$. This dependence is suggested by the experimental data for Y_P/Y_T presented in Fig. 12 ($Y_P/Y_T = Y_P/(Y_S + Y_P) \approx Y_P/Y_S$ for $Y_P << Y_S$.)

In the detailed analysis of secondary electron photoemission that is presented in Ref.10 are predicted this photon energy dependence through the factor $E\mu(E)$ and also the secondary electron energy distributions for photoemission from metals, semiconductors and insulators for thick photocathodes. As in Kane's secondary electron transport model,[16] we have assumed in this analysis that an

electron-electron collision will drop the energy of a random-walking secondary electron to below the vacuum level and hence eliminate it from the group of electrons that may escape from the photocathode surface. Following Kane's notation, we define the linear scattering cross section (inverse mean free path) for electron-electron collisions as b. The electron-phonon collision cross section is defined as a for which the associated energy loss per collision is very small. For a given photocathode, a and b are assumed to be constants. In Ref. 10, we have used Kane's transport model to predict an isotropic distribution of secondaries just inside the photocathode surface and have then applied the usual escape cone integral over all the secondary energies to determine the secondary electron energy distribution and yield as emitted from the photocathode surface. In this model we neglected any enhancement of the secondary emission resulting from a reflection of those secondaries that are outside the escape cone (into the photocathode and possibly "wandering" back by a random walk to the surface and escaping). For metals, any reflecting secondaries would most likely suffer an electron-electron collision ($b >> a$) in order to return and would thereby be dropped to below the vacuum level. For insulators, for which electron-electron collisions are unlikely ($b << a$), it is suggested in Ref. 10 that the internal reflection of secondaries may

contribute to a small enhancement of photoemission. This enhancement factor, however, is independent of photon energy and thus is essentially constant for a given photocathode.

As outlined in Appendix I, we have applied a similar analysis for the case of thin photocathodes for which both front and back surface photoemission is involved as illustrated in Fig. 20. We have simply placed a limit of t for the thickness of the photocathode instead of infinity as in Kane's original analysis for a semi-infinite photocathode and as has been done by Pong, et al.[17] for a finite photocathode. We neglect any contributions to the yield from the front or back surface reflections because it can be shown that such are significant only if the photocathode thickness approaches a value equal to the escape length, λ_s. As will be shown below, a practical thickness for the x-ray photocathode will be several times greater than this escape length value. In addition to our considering enhancement of emission resulting from internal reflections to be small and constant, we have also considered the mean attenuation length for the photons within the photocathode, $(\mu\rho)^{-1}$, to be very large as compared with the mean free paths, b^{-1} and a^{-1}.

This simple extension of our x-ray photoemission model results in the following relations for the secondary electron emission yields for the front and back surfaces, Y_f and Y_b, as a function of the photocathode thickness, t:

Front Surface--

$$Y_f = K\rho E\mu(E)\left(\frac{c}{u(u+c)}\right)\left(\frac{1 - e^{-ut}}{1 + \delta e^{-ut}}\right) \qquad (5)$$

Back Surface--

$$Y_b = K\rho E\mu(E)\left(\frac{ce^{-\mu\rho t}}{u(u+c)}\right)\left(\frac{1 - e^{-ut}}{1 + \delta e^{-ut}}\right) . \qquad (6)$$

Here, as functions of the linear cross sections for electron-phonon and electron-electron scattering, a and b, we have introduced the following parameters:

$$c = (a + b)$$

$$u = \sqrt{c^2 - ac} = \sqrt{b^2 + ab}, \text{ and}$$

$$\delta = (c - u)/(c + u).$$

K is a material constant which depends upon the electronic constants of the photocathode material as the band-gap energy, E_G, and the electron affinity, E_A for insulators, and upon the Fermi energy, E_F, and the work function, W, for metals (as discussed in Ref.10).

As shown in Kane's one-dimensional random-walk analysis for secondary electron transport to the surface, u^{-1} is the escape length for a photocathode of infinite thickness and defined here as an average escape length, λ_s, measured normal to the surface. (The mean-free-paths for electron-phonon and electron-electron scattering, a^{-1}

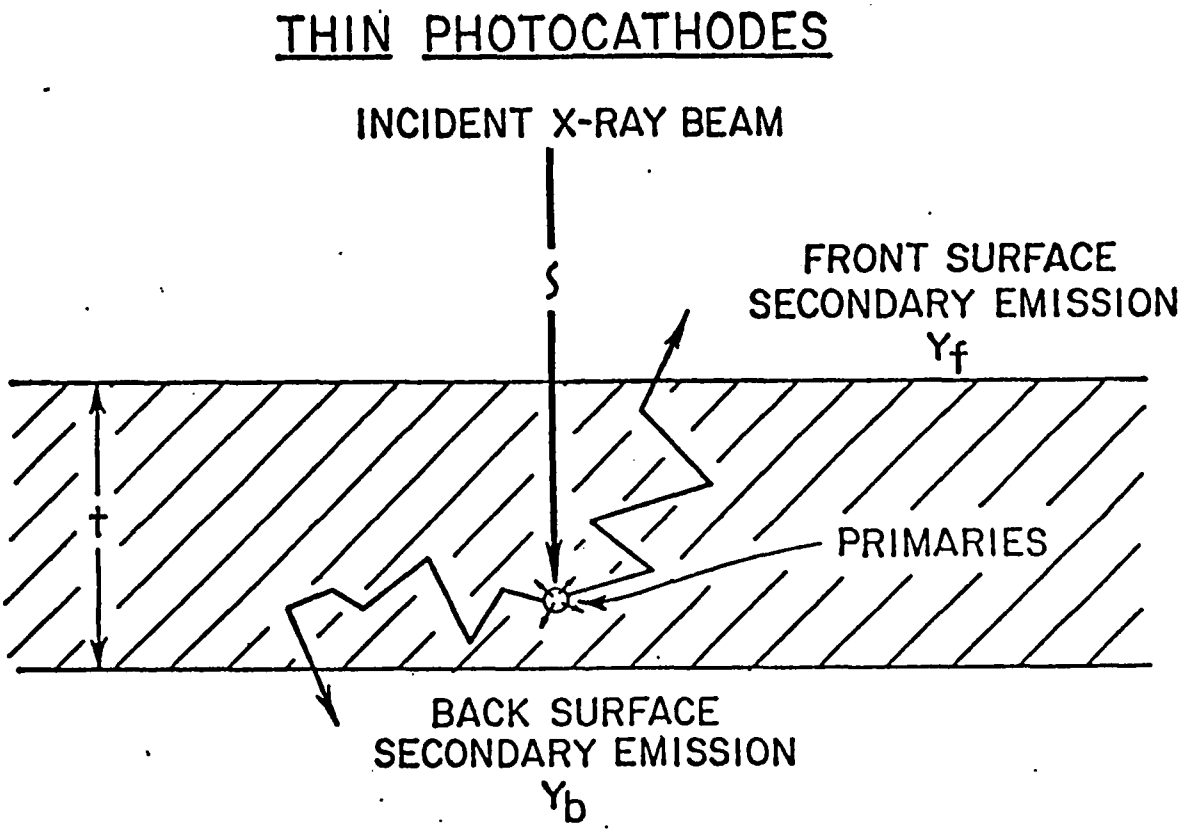

Figure 20. Front and back surface emission geometry for the transmission photocathode.

and b^{-1}, as adopted here from Kane's one-dimensional random-walk analysis, are the averages of the projections along the direction normal to the photocathode surface of the actual three-dimensional random-walk scattering path segments. These one-dimensional mean-free-paths have been shown by exact three-dimensional random-walk analyses to be approximately one-half the magnitude of the corresponding actual mean-free-paths.[10])

For insulators, $b \ll a$, and therefore $u \approx \sqrt{ab}$ and $\delta \approx 1$. Defining an escape length, λ_S, as equal to $(ab)^{-\frac{1}{2}}$ for insulators, we obtain from (5) and (6)

$$Y_f = K\rho E\mu(E)\lambda_S \tanh(t/2\lambda_S) \qquad (7)$$

and

$$Y_b = K\rho E\mu(E)e^{-(t/\lambda_X)}\lambda_S \tanh(t/2\lambda_S) \ . \qquad (8)$$

For metals, $b \gg a$, and therefore $c \approx b$, $u \approx b$ and $\delta \approx 0$. Defining an escape length, λ_S, for metals to be equal to b^{-1}, we may obtain from (5) and (6)

$$Y_f = K'\rho E\mu(E)\lambda_S(1 - e^{-(t/\lambda_S)}) \qquad (9)$$

and

$$Y_b = K'\rho E\mu(E)\lambda_S e^{-(t/\lambda_X)}(1 - e^{-t/\lambda_S}), \qquad (10)$$

Here λ_X is the x-ray attenuation length, $(\mu\rho)^{-1}$.

In Fig. 15 is shown a fit of Eq. (7) to the

experimental data of yield-vs-thickness for the insulator, cesium iodide, on a chromium-coated substrate. Because the trend of the experimental data is to pass through the origin and because the yield at 277 eV for chromium is very small as compared with that of CsI (about 3%), it is suggested that the substrate contributes a relatively small effect upon these yield data. The best fit parameter, λ_S, equal to 250 A, is in good agreement with the measurements of the escape length for secondary electrons emitted from CsI crystals and films by Iyesaar, et al.[18] of 215 A.

By maximizing the transmission photocathode yield, Y_b, as given in (8) and (10), we obtain the following expressions for the optimum thickness of insulator and metal photocathodes:

For insulators--

$$t_{opt} = \lambda_S \sinh^{-1}(\lambda_x/\lambda_S) \quad . \tag{11}$$

And for metals--

$$t_{opt} = \lambda_S \ell n(\lambda_x/\lambda_S) \quad , \tag{12}$$

For the insulator, cesium iodide (choosing λ_S equal to 250 A) with photon energies of 193, 525 and 2292 eV, the x-ray attenuation lengths are 3620, 5290 and 13,470 A, respectively, and the corresponding values for the optimum thicknesses are 840 A, 940 A and 1170 A, respectively.

For the gold photocathode (choosing λ_s equal to 40 A[19,20]) with the same photon energies of 193, 525 and 2292 eV, the x-ray attenuation lengths are 397, 440 and 1409 A, respectively, and the corresponding values for the optimum thicknesses are 92, 96 and 142 A, respectively. These values are well within the experimental precision limits suggested for the optimum thicknesses by the data presented in Figs. 18 and 19 to which we have fit the predicted Y_b-vs-t relations given in (7) and (10).

V. CONCLUSIONS.

The secondary electron quantum yield varies with the photon energy approximately as $E\mu(E)$ as has been demonstrated here for the metals, gold and aluminum, for the semiconductor, copper iodide, and for the insulator, cesium iodide. The primary electron yield varies less rapidly with photon energy and approximately as $E\mu^2(E)$. ($\mu(E)$ E^n with n typically between 2.5 and 3.)

The secondary electron yield for CsI is ten to one-hundred times higher than that for Au in the 0.1 to 10 keV region. This increased efficiency may be attributed in part to its larger escape depth (250 A as compare to 40 A) and to its low electron affinity. Its high quantum yield and relatively narrow secondary electron energy distribution suggests that CsI would be a very effective photocathode

for sensitive time-resolved x-ray spectroscopy into the picosecond region.

A simple model for x-ray photoemission has been extended to include the effect of photocathode thickness which does predict the photon energy dependence for the secondary and the primary electron quantum yields and the dependence of front and back surface secondary electron yield upon photocathode thickness. Relatively simple expressions have been derived and can be used as semiempirical equations for quantum yield and based upon the parameter, λ_S (the escape length for the corresponding semi-infinite photocathode) which may be determined experimentally from yield-vs-thickness data. The predictions of this phenomenological model are in good agreement with the experimental measurements.

ACKNOWLEDGEMENTS

The authors gratefully acknowledge the invaluable assistance in this work of Robert Hockaday, Priscilla Piano, Mary Pottenger and Murray Tester of this laboratory, Dr. Robert Day of the Los Alamos Scientific Laboratory, and of Dr. Robert Kauffman of the Lawrence Livermore Laboratory. This program is supported by a grant from the Air Force Office of Scientific Research, Grant AFOSR 79-0027, and by a supplemental Department of Energy/Lawrence Livermore Laboratory Subcontract, No. 9072209.

APPENDIX I

SECONDARY ELECTRON EMISSION FROM A FINITE PHOTOCATHODE: ONE-DIMENSIONAL, RANDOM-WALK ANALYSIS

Our derivation of relations (5) and (6) for the front and back surface photoemission from a finite x-ray photocathode is based upon a one-dimensional random-walk analysis method of Kane[16] and upon the following assumptions:

1. The number of emitted secondary electrons is proportional to the number that have transported to the emission surface by electron-phonon scattering only. Electron-electron scattering effectively drops the energy of the secondaries below that of the vacuum level.

2. The number of electrons is negligible that have electron-phonon scattered to the surfaces and then reflect back into the photocathode volume and manage to random-walk by electron-phonon scattering to these surfaces and to escape.

3. The probabilities per unit pathlength normal to the surfaces for electron-phonon and for electron-electron scattering, $\underline{a}$ and $\underline{b}$ respectively, are constants (independent of secondary electron energy).

4. The mean attenuation length for the x-ray photons, $(\mu\rho)^{-1}$, is very large as compared to the one-dimensional mean free paths, a^{-1} and b^{-1}, for electron-phonon and electron-electron scattering.

We would like to calculate first the probability $q(x)$, that an electron which is excited at a distance x from the front surface of a photocathode of thickness, t, will reach the front surface (at x = 0) by electron-phonon scattering only. This may be expressed as a sum

$$q(x) = \sum_{n=0}^{\infty} p_n(x) \tag{A1}$$

in which $p_n(x)$ is the probability that the excited electron will reach the surface by a random-walk of $\underline{n}$ collisions. This probability may be expressed in terms of the probability $p_{n-1}(y)$ (a path of n-1 collisions before reaching the surface) by the following recursive integral

$$p_n(x) = \frac{a}{2}\left[\int_o^x p_{n-1}(y)e^{-c(x-y)}dy + \int_x^t p_{n-1}(y)e^{-c(y-x)}dy\right] \tag{A2}$$

in which we are able to write explicitly the probability for the excited electron to have its first electron-phonon collision in the differential layer, dy, as

$$\frac{a}{2}\, e^{-c(x-y)}dy \quad \text{for } y < x$$

and

$$\frac{a}{2}\, e^{-c(y-x)}dy \quad \text{for } y > x \ ,$$

where c is the total linear cross section for secondary electron scattering, a + b.

In these expressions the factor of ½ simply accounts for the likelihood for the excited electron either to be initially heading toward a y position that is less than or greater than x. Thus the first integral in (2) is the contribution to $p_n(x)$ of all scatterings for which the first collision is in the volume between x and the front surface and the second integral is that for which the first collision is in the volume between x and the back surface. Using the definition for q(x) in (1) we may now rewrite (2) as the following relation:

$$\sum_{n=1}^{\infty} p_n(x) = q(x) - p_o(x) = \frac{a}{2}\left[\int_o^x q(y)e^{-c(x-y)}dy + \int_x^t q(y)e^{-c(y-x)}dy\right] \tag{A3}$$

where p_o is the probability that the electron may reach the front surface without scattering and is given by

$$p_o(x) = \tfrac{1}{2}e^{-cx} \quad . \tag{A4}$$

By differentiating (3) twice with respect to x, we obtain the differential relation

$$q''(x) - u^2q(x) = 0 \tag{A5}$$

which must have a solution of the form

$$q(x) = Ae^{ux} + Be^{-ux} \quad . \tag{A6}$$

Here u is equal to $\sqrt{c^2 - ac} = \sqrt{b^2 + ab}$ and A and B are thickness dependent.

We may now obtain A and B by substituting (6) into (3) (which must yield the same solution for A and B for all values of x between 0 and t). For x = 0, we obtain the probability that an electron which is excited at the surface will be heading toward the surface and, if not reflected, will escape, viz.,

$$q(0) = A + B = \frac{a}{2}\{\int_o^t (Ae^{uy} + Be^{-uy})e^{-cy}dy\} + \tfrac{1}{2} \quad . \tag{A7}$$

And, similarly, for x = t, we obtain the probability that an electron which is excited at the opposite surface will reach the surface at x = 0 and heading toward this surface, viz.,

$$q(t) = Ae^{ut} + Be^{-ut} = \frac{a}{2}\{\int_o^t (Ae^{uy} + Be^{-uy})e^{-c(t-y)}dy\} + \tfrac{1}{2}e^{-ct}. \tag{A8}$$

Completing the integrals in (7) and (8), we then use these two equations to solve for A and B, obtaining

$$A = \frac{-c\delta}{(u + c)[e^{2ut} - \delta^2]} \tag{A9}$$

and

$$B = \frac{c\, e^{2ut}}{(u + c)[e^{2ut} - \delta^2]} \, , \tag{A10}$$

where

$$\delta = \frac{c - u}{c + u} \quad .$$

The number of secondaries that are excited at x within a layer, dx, and per unit area of photocathode surface, can be written as the photon intensity, I, at x, multiplied by $E\mu(E)\rho dx/\bar{E}_s$ according to the simplified model description given above and discussed in more detail in Ref. 10. ($\mu(E)\rho$ is the fraction of the photons that are absorbed per unit and $\bar{E}_s$ is the mean energy of the secondaries.) Therefore, we may write for the x-ray photoemission from the front and back surfaces of a finite photocathode the following quantities to which Y_s and Y_b are proportional, viz., the number of secondaries heading toward and at these surfaces:

$$Y_f \sim E\mu(E)\rho \int_o^t q(x)e^{-\mu\rho x}dx \qquad \text{(A11)}$$

$$Y_b \sim E\mu(E)\rho \int_o^t q(t - x)e^{-\mu\rho x}dx \quad . \qquad \text{(A12)}$$

Finally, by substituting into these relations the expressions for A and B given in (9) and (10) and making the assumption that the x-ray attenuation length, $(\mu\rho)^{-1}$ is very large as compared to the escape length, u, we obtain the x-ray photoemission yields that were quoted in the text's Eqs. (5) and (6), viz.,

$$Y_f = KE\mu(E)\rho\frac{c}{u(u+c)}\frac{1-e^{-ut}}{1+\delta e^{-ut}} \qquad (A13)$$

and

$$Y_b = KE\mu(E)\rho\frac{c\,e^{-\mu\rho t}}{u(u+c)}\frac{1-e^{-ut}}{1+\delta e^{-ut}} \quad . \qquad (A14)$$

The constant, K, is the fraction of the electrons that are heading toward the emission surface and are just inside that surface which do escape. To determine this quantity, appropriate assumptions must be made for the internal secondary electron energy distribution which then allows a determination of the number of electrons with sufficient energy to escape, i.e., of energy greater than a work function or an electron affinity. (The energy distribution is a function of such parameters as the Fermi energy and the band-gap energy.) We may use the one-dimensional analysis described here to define a corresponding isotropic three-dimensional distribution of electron velocities at the surface, conserve the transverse momentum for the escaping electron and thereby determine the escape cone angle for an electron of a given energy. Integrating this "escape probability" over the allowed angles and energies yields the total escape fraction, K. This procedure has been described in Ref. 10.

REFERENCES

* Present address: Lockheed, LMSC Palo Alto Research Laboratory, Org. 52-11, Building 203, 3251 Hanover Street, Palo Alto, California 94304.

[1] J. L. Gaines and R. A. Hansen, *J. Appl. Phys. 47*, 3923 (1976).

[2] E. J. T. Burns and J. F. Thurston, *Appl. Spectrosc. 31*, 317 (1977).

[3] M. J. Bernstein and J. A. Smith, *IEEE Trans. Nucl. Sci. NS-26*, 1 (1979).

[4] E. B. Saloman, J. S. Pearlman and B. L. Henke, *Appl. Opt. 19*, 749 (1980).

[5] R. H. Day, P. Lee, E. B. Salomon and D. J. Nagel, LA-UR-79-1360, IEEE International Conference on Plasma Science, Montreal, Quebec, Canada, June 1979.

[6] B. L. Henke and K. Premaratne, *Proceedings of the International Conference on X-Ray and XUV Spectroscopy* (Sendai, Japan, August 1978); *Jap. J. Appl. Phys. 17*, Suppl. 17-2, p. 23 (1978).

[7] B. L. Henke and M. A. Tester, *Advances in X-Ray Analysis* (Plenum, New York, 1975), Vol. 18.

[8] W. B. Herrmannsfeldt, SLAC Report No. 166, September 1973, Stanford Linear Accelerator Center, Calif.

[9] B. L. Henke and J. A. Smith and D. T. Attwood, *J. Appl. Phys. 48*, 1852 (1977).

[10] B. L. Henke, J. Liesegang and S. D. Smith, *Phys. Rev. B19*, 3004 (1979).

[11] G. L. Stradling, H. Medecki, R. L. Kauffman, D. T. Attwood and B. L. Henke, *Appl. Phys. Lett.* (to be published).

[12] C. J. Powell, *Surf. Sci. 44*, 29 (1974).

[13] C. J. Tung, J. C. Ashley and R. H. Ritchie, *Surf. Sci. 81*, 427 (1979).

[14] M. S. Livingston and H. A. Bethe, *Rev. Mod. Phys. 9*, 263 (1937).

[15] L. Pages, E. Bertel, H. Jaffre and L. Sklavenitis, *Atomic Data 4*, 1 (1972).

[16] E. O. Kane, *Phys. Rev. 147*, 335 (1966).

[17] W. Pong, H. K. Nishihara and D. Chan, *Journal of the Optical Society of America, 62*, 487 (1972).

[18] T. É. Ïyésaar, A. M.-É. Saar and M. A. Élango, *Sov. Phys: Solid State 20*, 454 (1978).

[19] W. Pong, R. Sumida and G. Moore, *J. Appl. Phys. 41*, 1869 (1970).

[20] R. E. Thomas, *J. Appl. Phys. 41*, 5330 (1970).

DESCRIPTION OF A FIXED, ELLIPTICAL ANALYZER SPECTROGRAPH FOR PULSED SOURCE ANALYSIS

Shown in Fig. 1 are the essential features of the proposed spectrograph for the x-ray spectral analysis of an intense, pulsed x-ray source of small angular extent. An elliptically curved crystal or multilayer analyzer is utilized with the source at one of the foci and a small exit aperture (scatter aperture) at the second focal point. The elliptical analyzer curvature may be a cylindrical section, or it may be of double curvature and as a surface of revolution (an ellipsoidal section).

Considerable importance in the design of this spectrograph is placed here on achieving a minimum of background radiation and presenting a spectrum that can be simply and accurately interpreted to yield the source spectral characteristics. The small scatter aperture into the detector module effectively eliminates the stray radiation that may diffusely scatter or fluoresce from the analyzer. An optically flat, total-reflection mirror with an adjustable entrance slit along with an appropriate filter is used for an effective attenuation of high-order diffracted and the lower-energy radiation background. If the slit at the mirror is adjusted for a sufficiently small entrance aperture, a one-dimensional spatial distribution of the source intensity can be presented along the length of a given spectral line for an extended source (spatial resolution in the tenth milliradian range). As discussed below, the spectrum is formed by a relatively small analyzer dimension normal to this drawing section so that the instrument package is thin and can thus be "stacked" for multiple band spectral coverage.

1. Some Geometrical and Optical Properties

In order to establish a focal point for radiation from a small source and thereby an effective scatter aperture, the analyzer curvature is that for the ellipse

$$\rho = \frac{h}{1 - \epsilon\cos\beta} \quad , \tag{1}$$

where ϵ is its eccentricity and h is characteristic radial distance, ρ, for $\beta = \pm 90°$.

An important design feature is that the measured radiation can be normal to a circular arc detection surface (a film surface for photographic detection, a CCD array for electronic detection and for time-resolved spectroscopy, and for a proportional counter-goniometer circle in a calibration chamber). The angular position in

PULSED X-RAY SOURCE SPECTROSCOPY

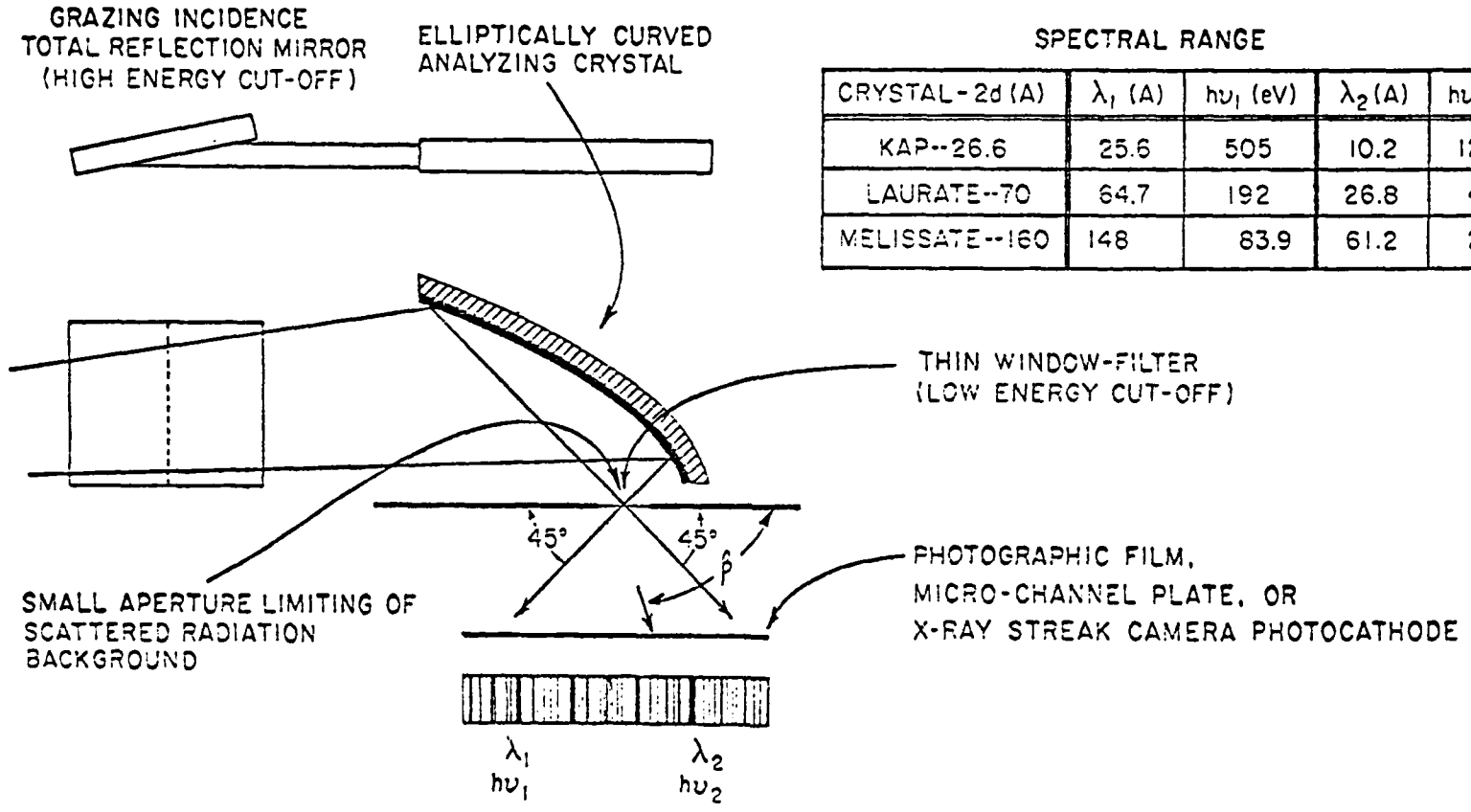

SPECTRAL RANGE

CRYSTAL - 2d (A)	λ_1 (A)	$h\upsilon_1$ (eV)	λ_2 (A)	$h\upsilon_2$ (eV)
KAP--26.6	25.6	505	10.2	1220
LAURATE--70	64.7	192	26.8	463
MELISSATE--160	148	83.9	61.2	203

Figure 1. A spectrograph for pulsed x-ray spectroscopy utilizing a fixed crystal or multi-layer analyzer. All wavelengths from a point source at one of the foci of an elliptically curved analyzer will focus at the other focal point and through a small scatter aperture into the detector module. For nearly parallel incident radiation, the analyzer is parabolic and the wavelength for first-order diffraction is given by $2d \sin(\beta/2)$. A grazing incidence mirror reflection of the incident beam provides a high-energy cut-off. A low-energy cut-off is effected by an appropriate filter at the scatter entrance aperture.

this detection circle, β, is related to the Bragg reflection angle off the analyzer, θ, by the equation

$$\theta = \tan^{-1}\left(\frac{1 - \varepsilon\cos\beta}{\varepsilon\sin\beta}\right) \qquad (2)$$

which reduces to simply

$$\theta = \beta/2 \qquad (3)$$

for applications with a large source distance (i.e., with an eccentricity, ε, equal to one for an approximately parabolic analyzer). Using the Bragg relation for first-order diffraction, $\lambda = 2d\sin\theta$ and Eq. (2), we present the photon energy vs β in Fig. 2 and the wavelength vs β in Fig. 3.

It can be shown that the number of photons per sec, S, that arrive at the detection circle relative to the number of photons per unit area per sec (I_o) at the analyzer is given by the relation

$$\frac{S}{I_o} = \frac{htC}{2}\ \frac{1 + \cos^2 2\theta}{\cos\theta}\ \frac{(1 + \varepsilon^2 - 2\varepsilon\cos\beta)^{3/2}}{\varepsilon(\varepsilon - \cos\beta)(1 - \varepsilon\cos\beta)^2}\ , \qquad (4)$$

where t is the width of the beam as allowed by the entrance slit and/or source size and is measured at the analyzer; h is the distance from the exit aperture to the analyzer surface as measured along the $\beta = 90°$ direction; ε is the eccentricity of the elliptical arc and given by

$$\varepsilon = \sqrt{1 + (h/R)^2} - (h/R), \qquad (5)$$

where R is the distance between the source and the exit aperture. It has been assumed here that the integrated reflection efficiency of the analyzer (area under its rocking curve) can be given by the approximate relation

$$R(\theta) \approx C\ \frac{1 + \cos^2 2\theta}{\sin 2\theta}\ . \qquad (6)$$

I_o is equal to $i_o \tau E/R^2$, where i_o is the photons/stearadian-sec source brightness and E is the reflection efficiency of the total-reflection mirror monochromator for a given wavelength, and τ is the corresponding filter transmission factor. Thus

$$\frac{S}{i_o} = \left(\frac{h}{R}\ \frac{t}{R}\ \frac{EC_1}{2}\right)T(\varepsilon,\beta)\ , \qquad (7)$$

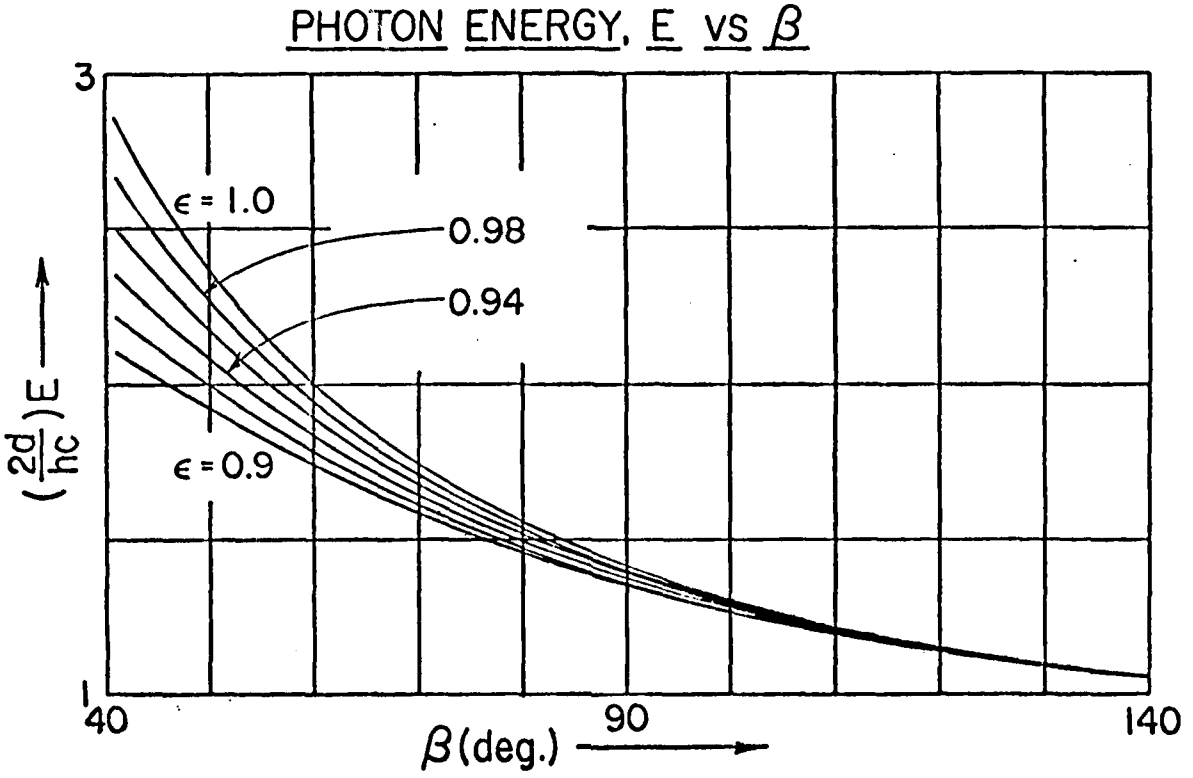

Figure 2

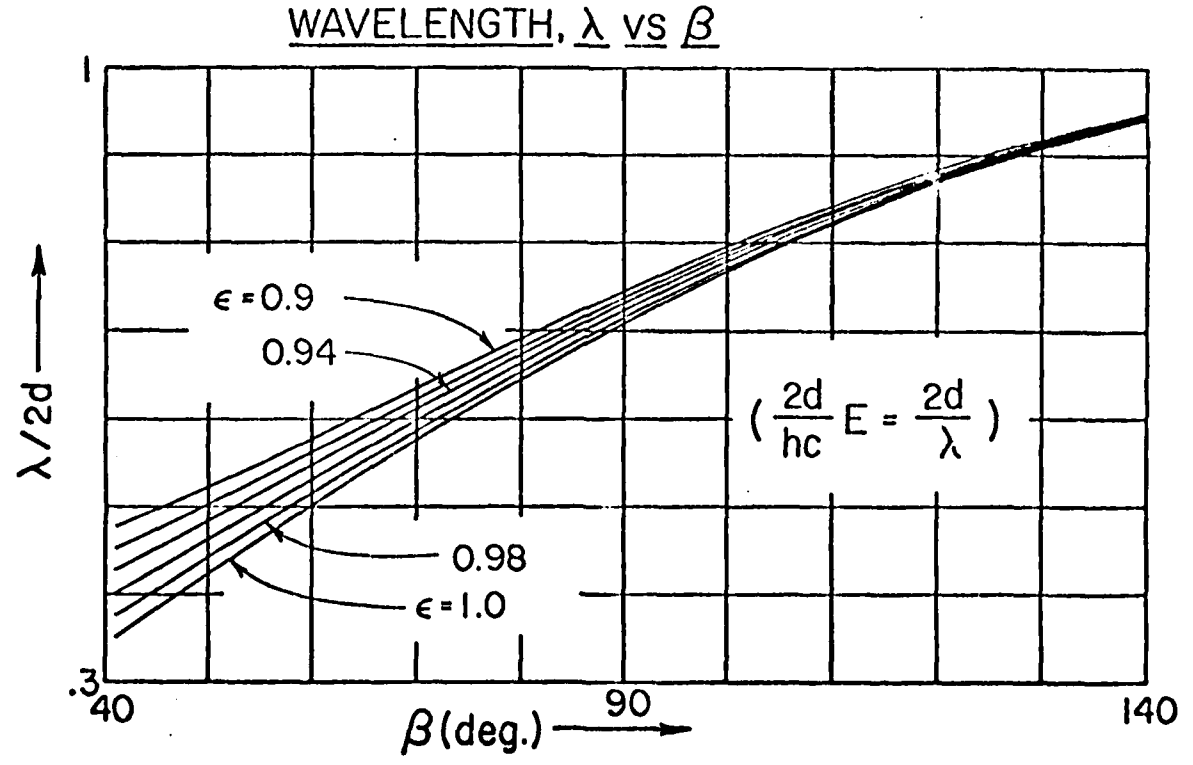

Figure 3

where the transmission function, $T(\epsilon,\beta)$, is given by

$$T(\epsilon,\beta)=K\left(\frac{S}{i_o}\right)=\left(\frac{1+\cos^2 2\theta}{\cos\theta}\right)\frac{(1+\epsilon^2-2\epsilon\cos\beta)^{3/2}}{\epsilon(\epsilon-\cos\beta)(1-\epsilon\cos\beta)^2}\ . \quad (8)$$

This transmission function, $T(\beta,\epsilon)$, has been plotted for values of ϵ equal to 0.9 and 1 in Fig. 4. Here the instrumental constant, K, is given by

$$K = \left(\frac{h}{R}\,\frac{t}{R}\,EC_\tau\right)^{-1} \quad (9)$$

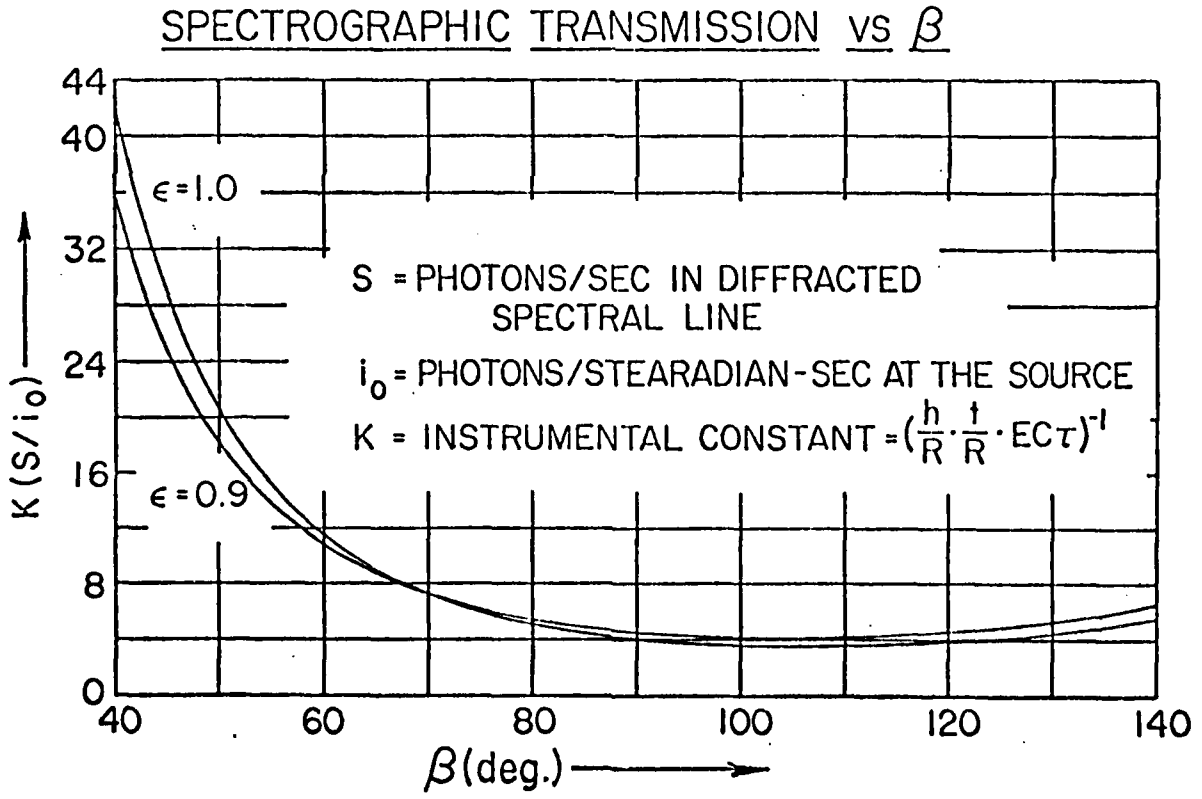

Figure 4

For a "point" source, a micromachined ellipsoidal section may be used on which the molecular multilayers can be directly deposited. For this ellipsoidal analyzer, a small circular scatter aperture into the detector module would be used.

For relatively simple, one-dimensional imaging of a source along the length of the spectral line, an elliptical cylinder section may be used as the analyzer. If not micromachined, it might be milled to about ten or twenty microinch surface smoothness and a .012" optical quality coverslip glass can be accurately pressed and epoxied onto the surface upon which the molecular multilayers can be deposited. Also, on such a curvature, a .010" thickness of crystals such as KAP can be precisely mounted. For the elliptical cylinder geometry, a slit shaped scatter exit aperture is used.

Because of the small width dimensions of this spectrograph unit, it is possible to "stack" two or more units for multiple-band spectroscopy. An example of such is described in Fig. 5. Here two ellipsoidal sections or a single elliptical cylinder section of double width can be used with the same multilayer surface. With an appropriate total-reflection filter band-pass primary monochromator, one analyzer section is "tuned" for first-order spectra and the other for second-order spectra. This allows spectroscopy, for example, with the lignoceric analyzer (of 130 A 2d-value) in the 100-500 eV region. In this example, the second-order attenuated background radiation that may appear in the low-energy band measured spectrum may be immediately recognized and quantitatively subtracted by a direct comparison with the parallel and coincident second-order spectra in the higher energy spectral band measurement.

An example of a "stacked" multiple band spectrograph is shown schematically in Fig. 6. Three different analyzers are used for maximum efficiency, first-order diffraction. For the band below the carbon edge in energy 100-250 eV, the lead salts of the straight carbon chain fatty acids are optimum. The lead behenate analyzer (2d=120 A) is suggested here. Between the carbon and the oxygen absorption discontinuities is the band of about 250-500 eV. Long-spaced organic crystals, natural or multilayer, have reduced efficiency in this region because of carbon absorption effects. The shortest carbon chain molecular multilayer that can be constructed, lead laurate (2d=70 A), would seem to be an optimum choice for this band. These multilayers can be deposited upon any substrate curvature. For the 500-1000 eV band, above the oxygen edge, potassium acid phthalate (KAP of 2d=26.6 A) is

TWO-BAND SPECTROGRAPH
USING 1st AND 2nd ORDER SPECTRA

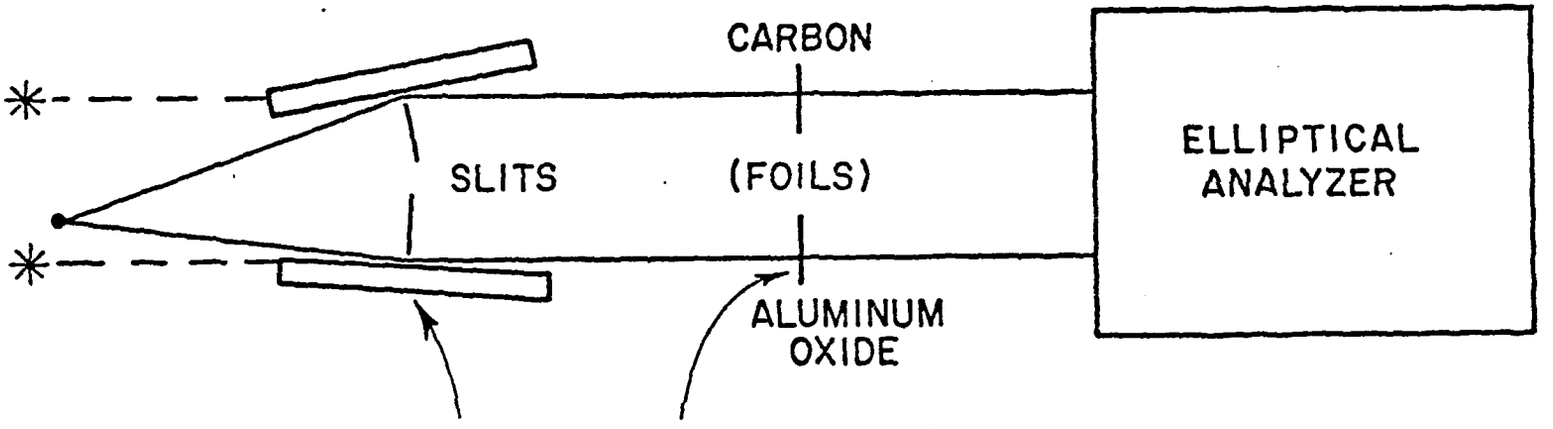

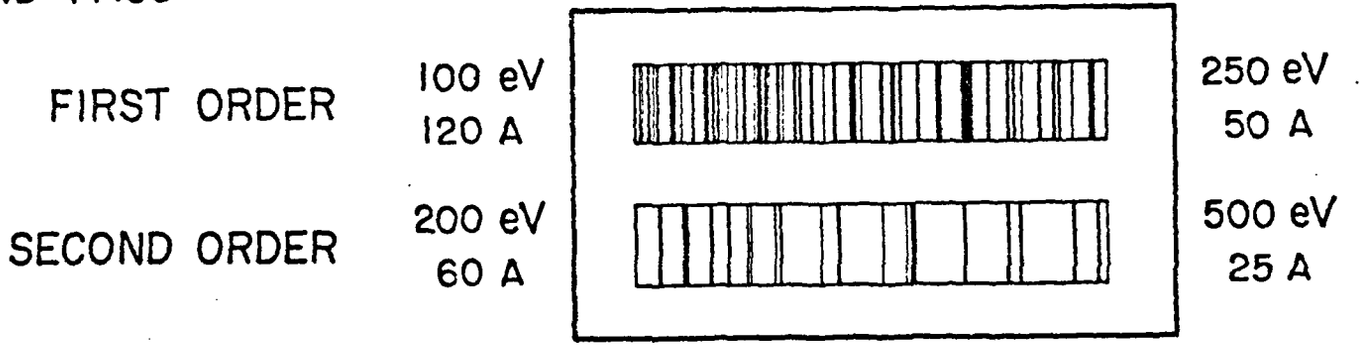

Figure 5

THREE-BAND SPECTROGRAPH USING "STACKED" ANALYZERS

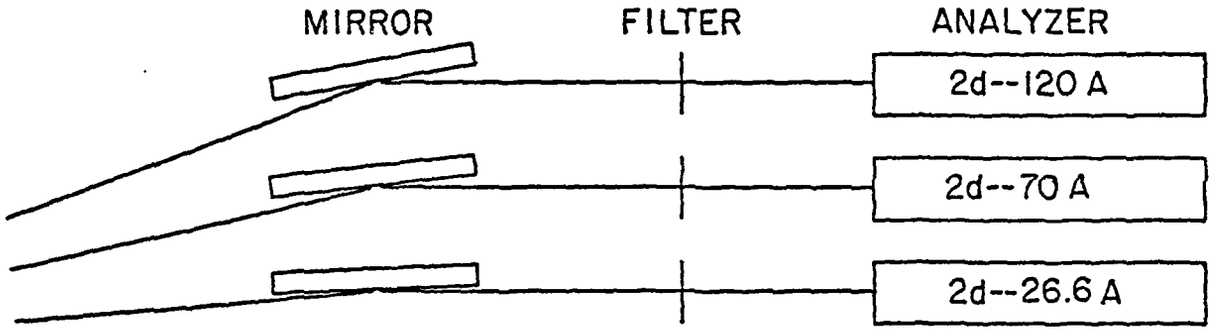

MIRROR*	FILTER	ANALYZER
SiO_2	CARBON	LEAD BEHENATE 2d--120 A
SiO_2	Al_2O_3	LEAD LAURATE 2d--70 A
SiO_2	ALUMINUM	KAP 2d--26.6 A

*FUSED QUARTZ OR PYREX

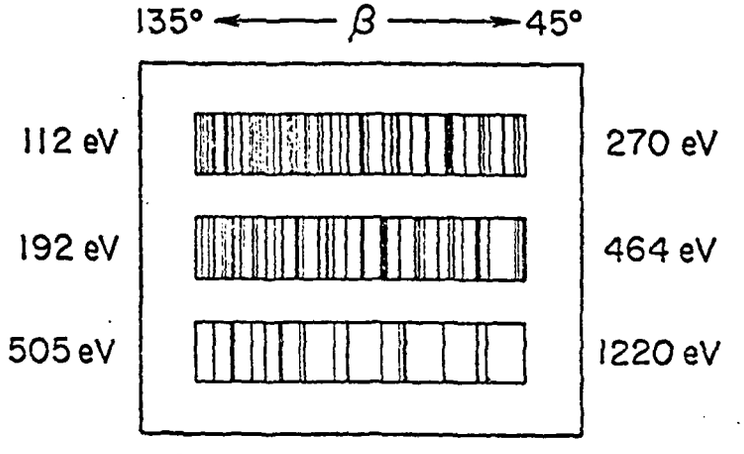

70 mm PHOTOGRAPHIC FILM ON HALF-CYLINDER FRAME

Figure 6

considered to be very satisfactory. Thicknesses of about .010" will allow the radii of curvatures indicated here provided that the cylinder axis is chosen parallel to the optimum crystal axis for bending. The rubidium acid phthalate crystal should also be optimum for this application.

Also suggested in Fig. 6 are the SiO_2 (fused quartz or Pyrex) high energy cut-off mirrors and the carbon, Al_2O_3 and aluminum filters respectively for the low-energy cut-off. The optimum mirror grazing incidence angle and the optimum filter thickness is determined by optimizing the band-pass characteristic presented by the combined effect of the transmission functions of the mirror, filter, analyzer, spectrograph (T, given in Eq. (8)) and the photographic film response function.

As is illustrated in Fig. 7, the one-dimensional imaging of source points along a spectral line formed on the detection circle is with a constant magnification, x'/x. This follows from the fact that the optical distance, $\rho + \rho'$, is a constant and equal to $(R^2 + h^2)^{1/2} + h$. We may write

$$\frac{x'}{x} = M = \frac{(R^2 + h^2)^{1/2} + \ell + h - s}{s} \tag{10}$$

M has essentially the same value throughout the spectral band when $h << R$ as given by

$$\frac{x'}{x} = \frac{R + \ell + h - d}{d} \tag{11}$$

Finally, it is important to note that with this spectrograph, it is possible to precisely define the contribution to the spectral line breadth that is instrumental and thus permit a measurement of the emission line width by deconvolution.* For example, for a point source, the instrumental broadening is caused principally by the rocking-curve breadth of the analyzer. For $R >> h$, we have noted that $\beta = 2\theta$, and it follows that the spectral line profile resulting purely from the rocking-curve of the analyzer, $I(\theta)$, becomes simply $I(\beta/2)$. In general, the width of the measured spectral line, ϕ, may by given by

$$\phi = \omega\left(\frac{d\beta}{d\theta}\right) , \tag{12}$$

*See the recent report of this program, "High-Efficiency Low Energy X-Ray Spectroscopy in the 100-500 eV Region," J. Appl. Phys. (attached).

where ω is the corresponding width of the analyzer rocking-curve and the function $(\frac{d\beta}{d\theta})$ can be derived to be

$$\frac{d\beta}{d\theta} = \frac{\varepsilon^2 + 1 - 2\varepsilon\cos\beta}{\varepsilon(\varepsilon - \cos\beta)} \quad . \tag{13}$$

This function has been plotted in Fig. 8.

2. Analyzer Block Construction

In order to equalize the thickness of the analyzer block as shown in Fig. 9 , its back surface is set at 30° to the ellipse axis. It is important that this block be as thin as practicable as a suitable geometry for the dipping process for depositing the molecular multilayers. As described earlier, the useful crystal region of the elliptical surface is between β values of 45 and 135°. At about 140°, it is proposed that this surface be continued as a straight tangential section in order to minimize the crystal bending at this sharper curvature end of the analyzer. This transition should be at position -s along the ellipse axis. The equation for this ellipse, with the focal point (exit aperture) as the origin and with an x_o-axis along the ellipse axis is given here as well as that with an x-axis rotated through angle θ from the ellipse axis. The optimum choice of θ will, of course, depend upon the milling procedure that is chosen.

As the source-to-exit-aperture distance, R, is changed, only the profile of the surface toward the source point significantly changes. This is indicated in Fig. 9 for R values equal to 30" and 90". Typical values of the radius of curvature, r, are listed in Table 1.

In Table 2 are listed for a set of working distances, R, the corresponding parameters for the analyzer profile, viz., the major and minor axes, a and b, for the ellipse, the x_o-coordinate of the transition point, -s, and the tangential surface parameters, m and p.

The chosen dimensions for a universal analyzer block suitable for all R-values are presented in Fig. 10. Precision-bored dowel holes are used for mounting the analyzer block in the spectrograph, in the calibration system, and also for stacking in the crystal dipping tank. These may also be useful in stacking these blocks for milling several at one time. Note: The second dowel hole, toward the source, should be elongated, plus and minus f/2, keeping the vertical dimension, f, constant. Specific parameters are also presented in Fig. 10 for the source distance equal to 12" and for h=1.000".

ONE-DIMENSIONAL IMAGING

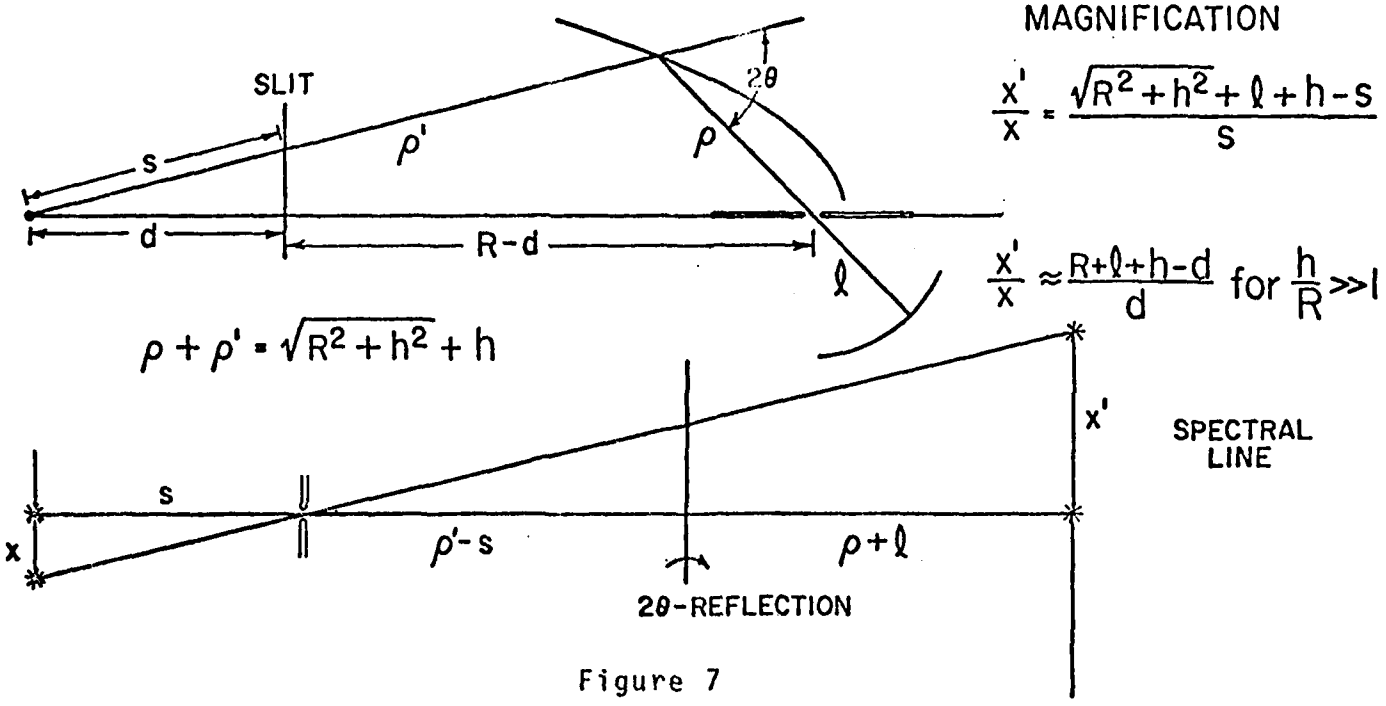

MAGNIFICATION

$$\frac{x'}{x} = \frac{\sqrt{R^2+h^2}+\ell+h-s}{s}$$

$$\frac{x'}{x} \approx \frac{R+\ell+h-d}{d} \text{ for } \frac{h}{R} \gg 1$$

Figure 7

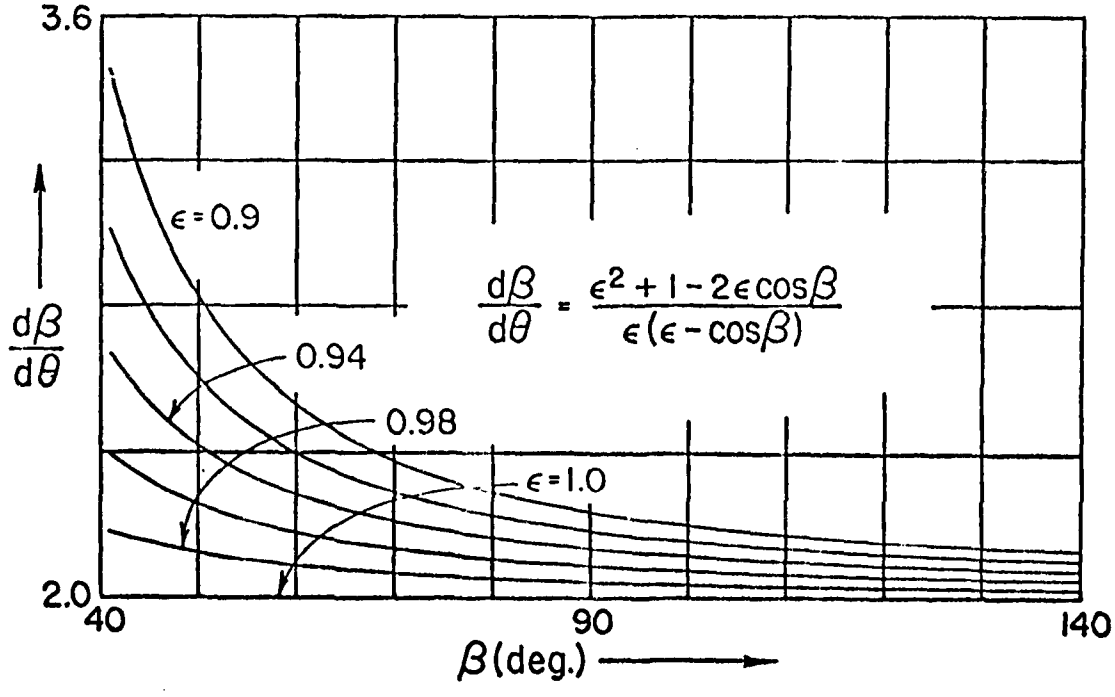

Figure 8

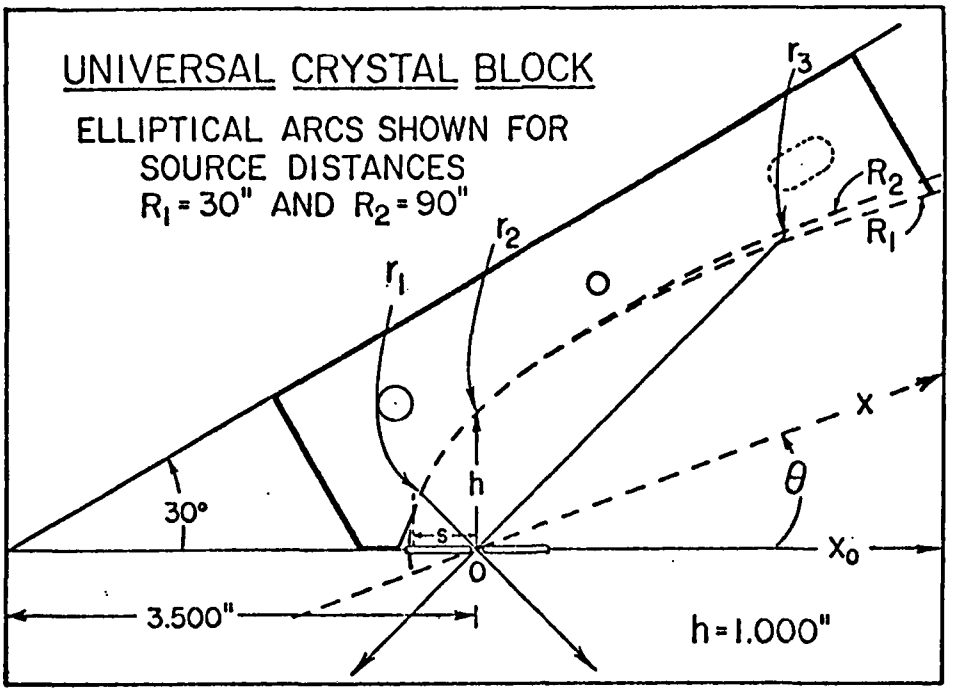

FOR $x_0 > -s$, $y_0 = b\sqrt{1-(\frac{x_0-R/2}{a})^2}$ FOR $x_0 < -s$ $y_0 = m(x_0+p)$

FOR ROTATED ELLIPSE--$y = x\tan(\beta-\theta)$

where $\beta = \cos^{-1}\left\{\frac{(\epsilon x + h\cos\theta)x - h\sin\theta\,[h^2+(\epsilon^2-1)x^2+2\epsilon x h\cos\theta]^{1/2}}{\epsilon^2x^2+h^2+2\epsilon x h\cos\theta}\right.$

RADII OF CURVATURE, r, FOR
ELLIPTICAL ANALYZER PROFILE

Table 1

R	ϵ	$r_1(135°)$	$r_2(90°)$	$r_3(45°)$
12"	.9201	1.242	2.509	9.445
30"	.9672	1.257	2.693	13.543
40"	.9753	1.260	2.726	14.468
50"	.9802	1.261	2.746	15.068
90"	.9890	1.264	2.782	16.228

$$r = \frac{h(1-2\epsilon\cos+\epsilon^2)^{3/2}}{(1-\cos\beta)^3}$$

Figure 9

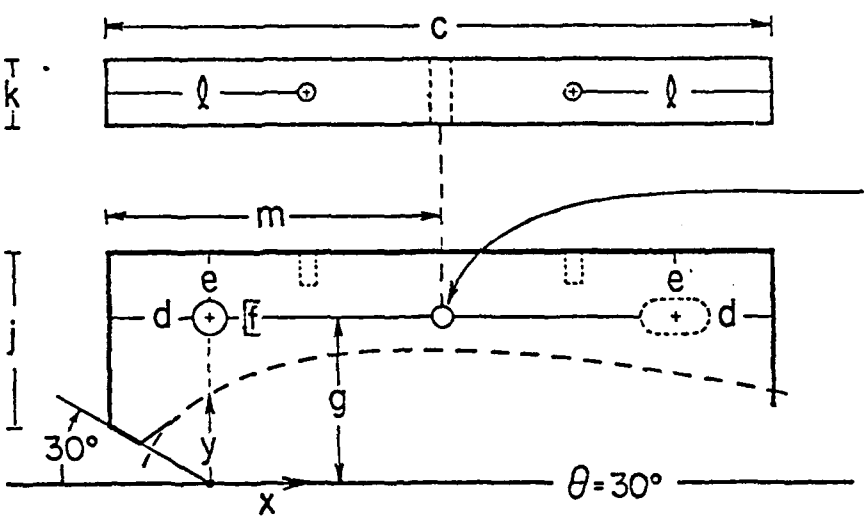

WIDTH, k = 0.500"
TAPPED 6-32 HOLES, 1/4" DEEP,
AT ℓ = 1.500"

CLEARANCE HOLE = 0.166" DIAMETER
AT m = 2.500"

c = 5.000" f = 0.250"
d = 0.750" g = 1.500"
e = 0.250" j = 1.317"

PARAMETERS VS SOURCE DISTANCE, R

Table 2

R	ϵ	a	b	s	m	p
12"	.9201	6.521	2.554	.449	2.625	.593
30"	.9672	15.508	3.938	.440	2.695	.577
40"	.9753	20.506	4.528	.438	2.710	.574
50"	.9802	25.505	5.050	.438	2.717	.573
90"	.9890	45.503	6.746	.436	2.732	.570

Figure 10

3. Calibration

A calibration facility has been developed for this laboratory (see Fig. 11) which applies a point source of characteristic line x-radiations in the 0.1-10 keV region. A precision goniometer is used to rotate a photon counting, proportional counter in angle, β, about the exit slit. The laboratory line source spectra will be fit by spectrographic transmission functions that are derived from the best available theoretical calculations and measurements on the total-reflection mirror characteristics, the multilayer characteristics, the filter transmission and finally on the detector response (photographic or photoelectric). This part of the program will be effectively supported by the current efforts of this project on the development of a state-of-the-art compilation of x-ray optical constants for the low energy x-ray region. (See Sec. I-D.)

CALIBRATION FACILITY

A demountable, 2-4 kilowatt x-ray source may be mounted at any desired working distance from the fixed-crystal using extension vacuum pipe sections. Specially chosen, characteristic lines (K, L and M) in the 0.1 to 10 keV region are used with appropriate filters on the x-ray tube and counter windows. Pulse height discrimination against background with sensitive, photon counting is obtained with flow-proportional counters that are "pressure tuned" for each wavelength. The monochromaticity of the direct beam is monitored by a multi-channel analyzer connected to the proportional counter. The orientation of the fixed crystal spectrograph with respect to the direct beam is adjustable from outside the vacuum chamber and this module can also be shifted in and out of the direct beam from outside. The proportional counter scans about a spectrograph axis using a precision goniometer and from 0° (direct beam) through 150° in 2θ.

CALIBRATION FACILITY FOR PULSED X-RAY SOURCE SPECTROMETERS

A. DEMOUNTABLE X-RAY SOURCE, SPECTROMETER AND PHOTON COUNTING SYSTEM

B. FLOW PROPORTIONAL COUNTER

C. PRECISION GONIOMETER

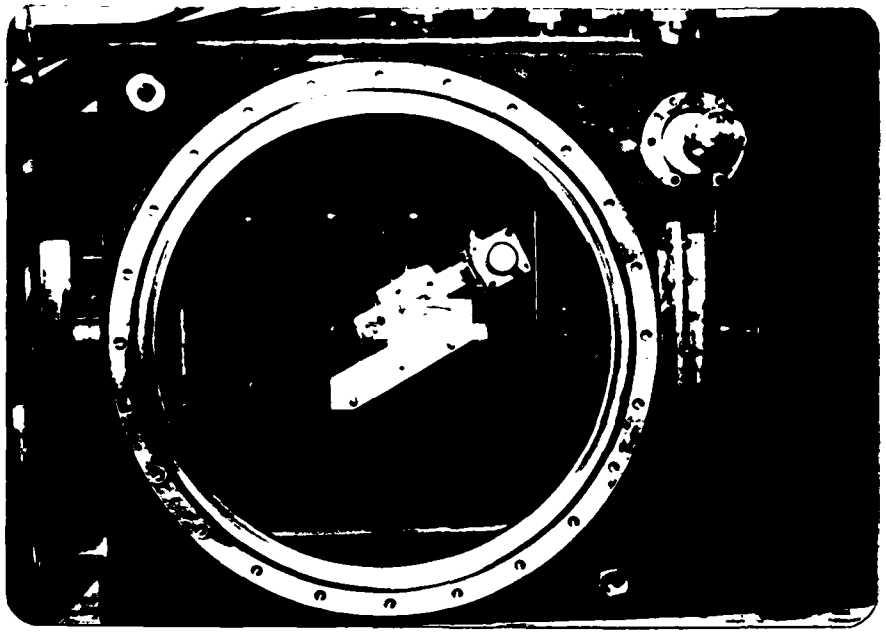

B

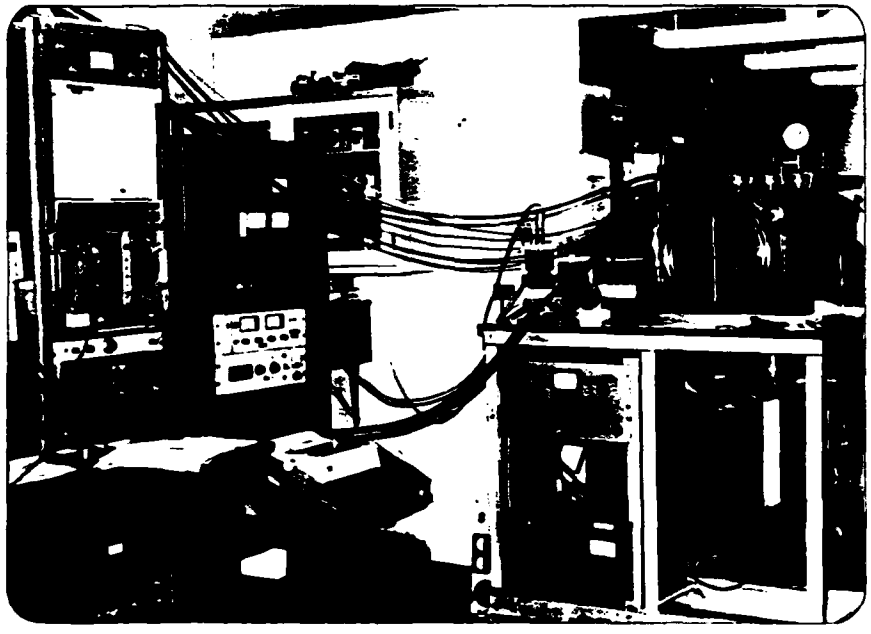

A

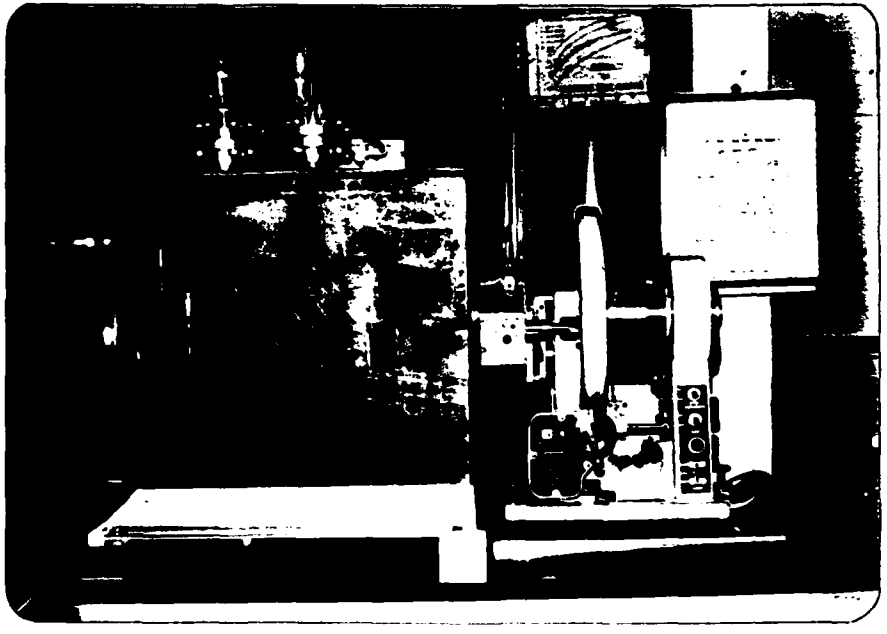

C

Outline for

LOW ENERGY X-RAY INTERACTION COEFFICIENTS: PHOTOIONIZATION, SCATTERING AND REFLECTION*

B. L. Henke, P. Lee, T. J. Tanaka,
R. L. Shimabukuro and B. K. Fujikawa

University of Hawaii
Honolulu, Hawaii 96822

I. INTRODUCTION

Important new needs for more complete and accurate interaction coefficient data for the low energy x-ray region and for all elements. Particularly needed for the development of spectroscopic analysis in the high temperature plasma diagnostics as involved in controlled thermonuclear fusion research and in the development and application of super-radiant x-ray sources.

In this work the best available reported (to 1980) experimental and theoretical photoionization cross section data have been compiled and reviewed particularly for the low energy x-ray region. The quantum dispersion theory has been used to generate the corresponding complex, atomic scattering factors. These, in turn, have been applied to the calculation of the optical constants, δ and β, for selected materials. (Experimental evidence suggests that the effect of molecular and crystalline state bonding upon the atomic photoionization and scattering cross sections is very small except for photon energies close to thresholds.) With these data, the specular and Bragg reflection coefficients are calculated for selected materials of particular importance in low energy x-ray spectroscopy.

*Work supported by AFOSR Grant 79-0027 and supplemental DOE/LLL Subcontract 9072209.

II. ORIGIN OF THE INTERACTION COEFFICIENT DATA: EXPLANATION OF TABLES

A. The Photoionization Cross Sections--A complete compilation for the photoionization cross sections in the 30-300 eV region as based upon about 130 referenced works including the new data from synchrotron and storage ring measurements. "Best fitting" procedures are discussed. Data is presented for all elements and for the 30 eV to 10 keV region at fifty characteristic line, laboratory wavelengths. The absorption edge energies are listed and the prominent, broad structural absorption features below 200 eV are identified.

B. The Atomic Scattering Factor, $f_1 + if_2$--The Kramers-Kronig dispersion relations are used to calculate from the photoionization cross section data (30 eV to 10 keV region) the corresponding values of f_1 and f_2 for all elements and for the 100 to 2000 eV region. These x-ray wavelengths (6 to 100 A) are large as compared to the dimensions of the atoms and therefore the spatial distribution of the electron charge about the nuclei is not an important consideration in the calculation of the low energy x-ray atomic scattering factors. However, the very strong anomalous dispersion effects in the low energy x-ray region have been included in these calculations.

C. The Optical Constants and Specular Reflection--The refractive index of materials for the x-ray region is expressed as $1 - \delta - i\beta$. Given the atomic densities for a material, the δ and β data may be calculated directly from the atomic scattering factors, f_1 and f_2. These data may then be applied to determine the refraction and reflection coefficients of materials using the Fresnel relations. Tables are presented here of δ and β and for the reflectivities of the total reflection mirror monochromator systems of berylium, vitreous carbon, fused quartz, nicel and tungsten. Also Tables of δ and β are presented for eleven crystal and multilayer analyzers (described below) that are of importance in low energy x-ray spectroscopy. Simple expressions are given as functions of δ and β that permit 1) making the necessary refraction correction for the Bragg equation as required in the precise determination of x-ray wavelengths, and 2) calculating the specularly reflected background component in crystal dispersed spectral analysis.

D. Crystal/Multilayer Structure Factors: Bragg Reflection--The atomic scattering factors are used to calculate the structure factors which characterize the scattering from unit cells of crystal and of multilayer systems. With the structure factor, $F_1 + iF_2$, and the associated δ and β values, the Darwin-Prins crystal theory has been applied to calculate the Bragg reflection coefficients--the integrated reflectivity, R_p; the peak reflectivity, P(%); the angular resolution (FWHM), ω; the absolute energy resolution, ΔE; and the resolving power, $E/\Delta E$. The integrated reflectivity, R_m, has also been calculated using the mosaic crystal theory. Bragg reflection coefficients are presented here for five acid phthalate crystals, six molecular multilayers (lead salts of the straight-chain fatty acids) and of three sputtered/evaporated multilayers of tungsten/carbon periodicity. These analyzers are of considerable importance at this time in low energy x-ray spectroscopy. These coefficients have been presented for the multilayer systems as a function of the number of layers, N. The predicted crystal/multilayer characteristics are in good agreement with those measured experimentally.

TABLE I. PHOTOIONIZATION CROSS SECTION, μ
ATOMIC SCATTERING FACTOR, $f_1 + if_2$

Atomic Weight = 83.80 Z = 36

μ(barns/atom) = μ(cm^2/gm) x 139.1 KRYPTON (Kr)

$E\mu(E) = 501.9\ f_2$ keVcm^2/gm

LINE	E(eV)	μ(cm^2/gm)	f_1	f_2	λ(A)	LINE	E(eV)	μ(cm^2/gm)	f_1	f_2	λ(A)
Na $L_{2,3}M$	30.5	1.21 05		7.37	407.1	Co Lα	776.2	5.19 03	28.79	8.03	16.0
Mg $L_{2,3}M$	49.3	1.03 04		1.01	251.5	Ni Lα	851.5	4.21 03	28.87	7.14	14.56
Al $L_{2,3}M$	72.4	3.77 03		0.54	171.4	Cu Lα	929.7	3.45 03	28.85	6.39	13.33
Si $L_{2,3}M$	91.5	4.55 03		0.83	135.5	Zn Lα	1011.7	2.84 03	28.72	5.72	12.25
Be K	108.5	1.21 04	3.23	2.62	114.0	Na Kα	1041.0	2.65 03	28.65	5.50	11.91
Sr Mζ	114.0	1.45 04	2.64	3.29	108.7	Ge Lα	1188.0	1.94 03	28.10	4.59	10.44
Y Mζ	132.8	2.48 04	1.17	6.55	93.4	Mg Kα	1253.6	1.71 03	27.75	4.27	9.89
S Lζ	148.7	3.82 04	1.60	11.30	83.4	Al Kα	1486.7	1.13 03	25.47	3.35	8.34
Zr Mζ	151.1	3.92 04	2.28	11.79	82.1	Si Kα	1740.0	4.30 03	20.33	14.91	7.13
Nb Mζ	171.7	3.99 04	4.96	13.64	72.2	Zr Lα	2042.4	3.38 03	30.15	13.76	6.07
B Kα	183.3	4.02 04	6.10	14.68	67.6	Nb Lα	2165.9	2.94 03		12.69	5.73
Mo Mζ	192.6	4.05 04	7.21	15.53	64.4	Mo Lα	2293.2	2.56 03		11.70	5.41
W N_5N_7	212.2	3.88 04	9.34	16.40	58.4	Cl Kα	2622.4	1.83 03		9.57	4.73
C Kα	277.0	3.33 04	15.46	18.36	44.7	Ag Lα	2984.3	1.31 03		7.82	4.16
Ag Mζ	311.7	2.83 04	18.44	17.59	39.8	Ca Kα	3691.7	7.50 02		5.52	3.36
N Kα	392.4	2.07 04	22.88	16.17	31.6	Ba Lα	4466.3	4.49 02		4.00	2.78
Ti Lℓ	395.3	2.04 04	23.07	16.09	31.4	Ti Kα	4510.8	4.37 02		3.93	2.75
Ti Lα	452.2	1.59 04	25.21	14.30	27.4	V Kα	4952.2	3.39 02		3.34	2.50
Va Lα	511.3	1.25 04	26.54	12.74	24.3	Cr Kα	5414.7	2.66 02		2.86	2.29
O Kα	524.9	1.19 04	26.78	12.43	23.6	Mn Kα	5898.8	2.10 02		2.47	2.10
Mn Lℓ	556.3	1.06 04	27.28	11.75	22.3	Co Kα	6930.3	1.35 02		1.86	1.79
Cr Lα	572.8	9.97 03	27.50	11.38	21.6	Ni Kα	7478.2	1.09 02		1.63	1.66
Mn Lα	637.4	7.99 03	28.18	10.14	19.5	Cu Kα	8047.8	8.91 01		1.43	1.54
F Kα	676.8	6.96 03	28.42	9.38	18.3	Zn Kα	8638.9	7.32 01		1.26	1.44
Fe Lα	705.0	6.42 03	28.53	9.01	17.6	Ge Kα	9886.4	5.04 01		0.99	1.25

ABSORPTION EDGE

L_I	1915 eV	6.43 A
L_{II}	1730 eV	7.168 A
L_{III}	1677 eV	7.392 A

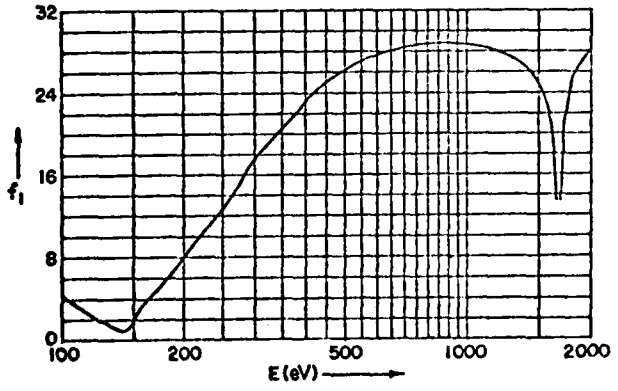

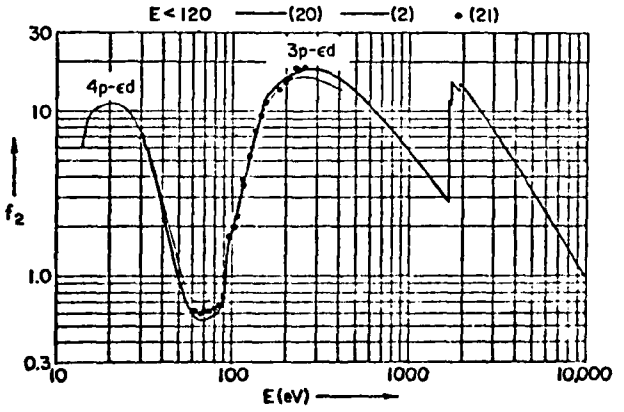

References: 2,10,15,20,21,50

APPENDIX I

A GENERAL DESCRIPTION OF THI^ RESEARCH PROGRAM

A. Significance of this Overall Program

When this project was initiated, there was relatively little research or application being undertaken with x-rays in the 10 to 100 A region or with the associated x-ray induced electron emissions in the 0 to 1000 eV region. Since then, there has been a steadily growing recognition of the considerable importance and significance of these radiations, primarily for the following reasons:

1. Structural and Chemical Analysis of Matter

Low Energy x-rays and electrons are ideally suited for the analysis of surfaces, microscopic and sub-microscopic systems because of the very large interaction cross sections that are characteristic of these radiations. The light elements, sodium to beryllium, emit characteristic x-rays only in this ultrasoft region of 10 to 100 A. In all elements, transitions of electrons from the valence band or molecular orbital into the nearby and relatively sharp inner electronic levels result in emissions which are always in the low energy x-ray region and which are sensitive to the chemical environment surrounding the atom. Finally, it has been established by this AFOSR research program (and by others) that the analysis for elementary and structural information of matter from the photoelectron and Auger electron emissions is optimized in the low energy x-ray excitation region.

2. High Temperature Plasma Diagnostics

Low energy x-rays are among the most abundant radiation components which are emitted by matter that has been "heated" to the one to ten million degree region. Such plasmas are typically involved in the current research and development of controlled thermonuclear energy sources as produced by laser or particle beams and inertially confined and by magnetic field compression and confinement.

The spectroscopic measurement of radiations from these plasmas can effectively complement the neutron spectroscopy in the determination of the time history of the plasma density and temperature and can uniquely determine the identity of concentrations of contaminating

species.

Because of the high intensities of x-radiation along with the neutron radiations that are typically around these plasmas, the x-radiation effects upon materials can be appreciable. There is considerable need at this time for more basic knowledge of the kinds of rates of structural changes of surfaces induced by intense soft x-radiation.

3. X-Ray Astronomy

During the past ten years, rocket and satellite research has demonstrated the great value of x-ray astronomy, particularly in the low energy region. In addition to the solar corona, strong galactic x-ray sources have been discovered and a nearly isotropic background of soft x-rays has been measured. Measurements to date seem to indicate an increase in x-ray flux as spectral measurements are directed into this low energy region for many important galactic sources, and a "turning over" of the low energy flux for extra-galactic sources due to cosmic absorption. The low energy x-ray spectroscopy of astrophysical plasma sources also yields critical information as to the effective temperatures and densities and the identification of the ionic species involved, as well as the radiation mechanisms. There is considerable need at this time for new techniques and methods of achieving high efficiency spectrographic measurement in the low energy x-ray region from space vehicles. There is also a need for basic knowledge of the effect of x-radiation on materials in space technology.

The scientific importance of low energy x-ray and electron physics is unquestionable--yet its theory and experiment remain among the most difficult and incomplete. It is the objective of this program to contribute as much as possible to the development of the physics and its applications in the low energy x-ray and electron region.

B. The Approach

Very early in this work it was considered to be of an important advantage to combine into a single research program the study of both the low energy x-ray and the associated electron interactions. Photoelectron spectroscopy was found to be very useful in the detailing of the photoionization process and in the revealing of x-ray spectral detail by photoconversion spectroscopy which

could not be resolved by present Bragg reflection spectroscopy. Similarly, in order to understand and qualitatively to apply photoelectron spectroscopy to surface state analysis, a thorough knowledge of the photoionization process and its cross sections was required.

Another important aspect of the approach of this program has been to place an equally strong emphasis on the development of new and efficient methods of low energy x-ray and electron spectroscopy as that upon measurement and application. Unlike many areas of radiation physics, in this low energy region precision measurement is very difficult and often impossible by the conventional methods or by available commercial instruments. A new type of high power, ultrasoft x-ray source was developed as demanded for excitation in both the x-ray and the electron spectrograph systems. New synthetic, long spacing, organic x-ray analyzing crystals were developed in order to achieve the necessary increase in efficiency over that of diffraction grating systems. Because this research area is still quite new and unsettled, the associated development of methods and instruments continues to be very important for a productive research program.

Since there have been relatively few workers who have been involved with the development of the basic experimental physics and of new methods and techniques, it has been found worthwhile to apply some of the effort of this program to helping other laboratories establish low energy x-ray and electron spectroscopy programs--for example, for high temperature plasma diagnostics, for rocket and satellite work and for materials analysis. This has been also done through participating in collaborative programs, accepting invitations to present working seminars at these laboratories, having groups working at our laboratory for one to two week periods, publishing occasional tutorial and technical type papers, and answering hundreds of requests for reports and scientific information on techniques, methods and cross sections. Nearly all of the work has been carried out with physics students, including undergraduates, who have spent usually three or four years on the project. Most of these students complete their graduate work in physics and proceed on to scientific careers in experimental physics.

C. PERSONNEL

The principal investigator, Burton L. Henke, will direct this research program by half-time participation during the academic year (at no cost to the research program) and by full-time participation during the summer. His curriculum vitae is presented in Appendix V.

Also on this project is a graduate assistant (fourth-year PhD candidate) who will be working half-time during the entire year.

It has been proposed that this program have the important participation of a post-doctoral research associate who is a specialist in radiation physics research. He would spend full-time on this project and would be fully supported along with a graduate student research assistant under a supplementary grant from the DOE via one of their lead laboratories.

This project has been very fortnuate to have been able to add to its personnel a full-time research associate, Mr. Murray Tester, and a research associate, Ms. Priscilla Piano, who participates half-time during the academic year and full-time during the interim and summer.

As noted in Appendix I-D, there are many colleagues in the University's Department of Physics and Astronomy, Chemistry and Geosciences whose research experience and interests highly quality them as collaborators in this research program.

Finally, it should be noted here that we usually have visiting scientists on this program. For example, during the past few years, for collaborative work in the area of low energy x-ray spectroscopy, these were Professor David S. Urch of Queen Mary College, University of London, supported by a NATO Fellowship; also, for an eight-month collaborative program in electron spectroscopy was Professor John Liesegang from La Trobe University, Bundoora, Victoria, Australia.

During the past three years, visiting professorships have been supported by the University of Hawaii and awarded to scientists who can interact well with our research programs. These have been Professor Rolf Manne of the University of Bergen, Norway, who is an outstanding quantum theorist in molecular orbital analysis; Professor Marvin Cohen of the University of California, Berkeley, a solid state theorist; and for this year, Professor James Samson,

AD-A096 376 HAWAII UNIV HONOLULU DEPT OF PHYSICS AND ASTRONOMY F/G 20/8
DEVELOPMENT AND APPLICATION OF LOW ENERGY X-RAY AND ELECTRON PH--ETC(U)
JAN 81 B L HENKE AFOSR-79-0027
UNCLASSIFIED AFOSR-TR-81-0147 NL

2 OF 2
AD A 096376

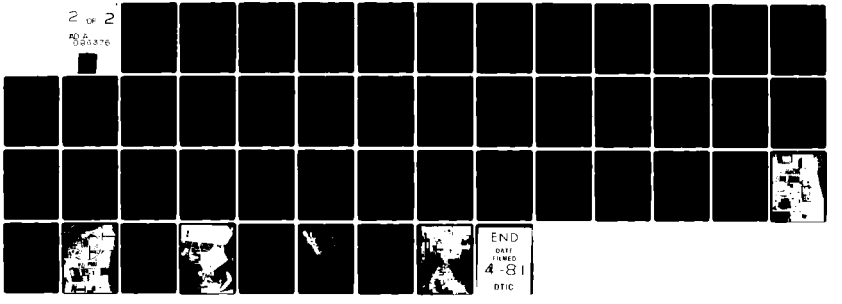

University of Nebraska, who is a well recognized authority on the experimental measurement of photoionization cross sections for the euv region and who has been an invaluable resource person for this program. This coming year, the visiting professorship has been given to Professor Thomas Feuchtwang of Pennsylvania State University who is also a very active and successful authority in solid state physics.

The recent post-doctorates who have participated in this program on one-year appointments as separately supported by supplemental grants through the DOE have been Dr. Jerel A. Smith who proceeded on to A.R.A.C.O.R. in Sunnyvale, California, Dr. James P. Knauer who subsequently accepted a position at Lockheed Palo Alto Research Labs, and Dr. Ping Lee who is currently on leave from the University of California's Los Alamos Scientific Laboratory until December 1980. All three are now doing applied research in the x-ray diagnostics of high temperature plasmas.

D. INSTITUTIONAL SUPPORT

1. Related Research Programs

This principal investigator was introduced to the University of Hawaii while working on rocket x-ray astronomy experiment launchings off the island of Kauai in 1963-65. At the Manoa campus on Oahu, he found certain programs in progress which complemented his own research interests in the low energy x-ray and electron region. Related research currently includes the following:

a. Low Energy Photoemission Electron Spectroscopy Applied to Solid State Analysis
(Professor W. Pong)

This work is concerned with electron interactions and photoelectron spectra in the photon excitation energy region just below that of specific interest to this project (<20 eV).

b. Solar Coronal Plasma Physics
(Professors J. Jeffereis and F. Orrall)

An important emphasis of the program of the Institute for Astronomy at the University of Hawaii is on solar phenomena, including both theoretical and experimental programs. The University operates a large solar observatory on Mount Haleakala on the island of Maui.

c. Rocket Astronomy in the Vacuum Ultraviolet Region
(Professor H. McAllister)

High-resolution spectrographs for the vacuum ultraviolet have been designed and constructed here. They are currently being flown on Aerobee rockets at White Sands Missile Range. To this time, this work has been directed to solar studies.

d. X-Ray Analysis of Materials
(Professors G. Andermann, R. Cramer, C. Fadley, R. Jones, K. Seff and M. Manghnani)

This work includes geochemical and physical chemical materials analysis using conventional x-ray energies and methods of fluorescence for elementary and valence band analysis, crystallographic analysis, low energy electron diffraction (LEED), and electron spectroscopy (ESCA).

2. Research Facilities

It should be noted that the University of Hawaii has completed at this time a 25-million-dollar expansion phase of research facilities in the physical sciences and engineering.

In the new physics research building is a specially-designed laboratory for this project on low energy x-ray and electron analysis. In Appendix IV are shown photographs of the low energy x-ray and electron spectrographic systems. The total laboratory space is about 2,000 square feet; its design is shown in Fig. 5 of Appendix IV. The special facilities of this laboratory have been developed by this AFOSR project over a ten-year period and probably represent one of the best of such facilities. Included are a complete ultrasoft x-ray spectrographic system, an electron spectrographic system, specialized apparatus for crystal research, analytical equipment for sample preparation, a calculator-computer system for data analysis (Hewlett-Packard 9810A plus 1861A typewriter output, a 9862A plotter, a 9865A cassette memory unit and a 9863A tape reader), and a terminal to the new PDP-11/03-KA computer.

Also available to this project in the new physics building are general research facilities valued at about $700,000, including complete experimental machine shops.

APPENDIX II

A. RESEARCH PUBLICATIONS BY THE PRINCIPAL INVESTIGATOR AND CO-WORKERS

B. INVITED RESEARCH PAPERS PRESENTED BY THE PRINCIPAL INVESTIGATOR ON THIS RESEARCH PROGRAM - 1970 TO 1980.

APPENDIX II

A. RESEARCH PUBLICATIONS BY THE PRINCIPAL INVESTIGATOR AND CO-WORKERS ON THIS RESEARCH PROGRAM

1. "Low Engle X-Ray Diffraction with Long Wavelengths," *Phys. Rev. 89*, 1300 (March 15, 1953).

2. "Diffraction of Long Wavelength X-Rays," Special Technical Report No. 24, Office of Naval Research; Special Technical Report No. 3, Atomic Energy Commission, June 1953.

3. "Submicroscopic Structure Determination by Long Wavelength X-Ray Diffraction," *J. Appl. Phys. 26*, 903-917 (1955) (w/ Jesse W. M. DuMond).

4. "Slide Rule for Radiographic Analysis," *Rev. Sci. Instr. 27*, 1043-1045 (1956) (w/ Bruno Lundberg).

5. "Conditions for Optimum Visual and Photometric 'Contrast' in Microradiograms," *X-Ray Microscopy and Microradiography* (Academic Press, New York, 1957), pp. 240-248 (w/ B. Lundberg and A. Engström).

6. a."Monochromatic Sources of Ultrasoft X-Radiations for Quantitative Microradiographic Analysis," *X-Ray Microscopy and Microradiography* (Academic Press, New York, 1957), pp. 71-88

   and

   b."High Resolution Contact Microradiography with Ultrasoft Polychromatic X-Rays," *X-Ray Microscopy and Microradiography* (Academic Press, New York, 1957), pp. 218-233 (w/ A. Engström, R. C. Greulich and B. Lundberg).

7. "Semiempirical Determination of Mass Absorption Coefficients for the 5 to 50 Angstrom X-Ray Region," *J. Appl. Phys. 28*, 98-105 (1957) (w/ R. White and B. Lundberg).

8. "Ultrasoft X-Ray Physics and Applications," Summary Technical Report No. 1, AFOSR TN-57-436, ASTIA Document No. AD 136 426.

9. "High Resolution Microradiography," Technical Report No. 2, AFOSR TN-58-803.

10. "Ultrasoft X-Ray Interaction Coefficients," Technical Report No. 3, AFOSR TN-59-895, August 1959.

11. "X-Ray Microscopy," Technical Report No. 4, AFOSR AF 49 (638)-394, File No. 1-1-20 and *The Encyclopedia of Microscopy*, George L. Clark, Ed. (Reinhold Publishing, New York, 1961), pp. 675-693.

12. "Measurement in the 10 to 100 Angstrom X-Ray Region," *Advances in X-Ray Analysis* (Plenum, New York, 1961), Vol. 4.

13. "Microanalysis with Ultrasoft X-Radiations," Technical Report No. 6, AFOSR AF 49(638)-394, 1961.

14. "Ultrasoft X-Ray Analysis of Micron Systems," *Norelco Reporter*, IV, 82 (1957).

15. "Ultrasoft X-Ray Interaction Coefficients," *Proceedings, 2nd International Symposium on X-Ray Microscopy and Microanalysis* (Elsevier Publishing, Netherlands, 1960) (w/ Jack C. Miller).

16. a."Projection X-Ray Microscopy at Pomona College," *Norelco Reporter*, VII, 137 (1960).

    b."Isolation of Selected Elements with an Electron Microscope," *Norelco Reporter*, VII (1961).

17. "Microstructure, Mass and Chemical Analysis with 8 to 44 Angstrom X-Radiation," *Proceedings, 7th Annual Conference on Industrial Applications of X-Ray Analysis*, University of Denver, 1958.

18. "Microanalysis with Ultrasoft X-Radiations," *Advances in X-Ray Analysis* (Plenum, New York, 1962), Vol. 5.

19. "Small Energy Losses of Electrons in Solids; Design of a Low Energy Electron Spectrometer," (informal notes, 1960) (w/ Charles Greenhall).

20. "Production, Detection and Application of Ultrasoft X-Rays," *X-Ray Optics and X-Ray Microanalysis* (Academic, New York, 1963).

21. "Sodium and Magnesium Fluorescence Analysis--Part I: Method," *Advances in X-Ray Analysis* (Plenum, New York, 1963), Vol. 6.

22. "Surface Analysis by Soft X-Ray Excitation of Auger and Photoelectrons," (technical notes, 1963) (w/ J. Merritt).

23. "X-Ray Fluorescence Analysis for Sodium, Fluorine, Oxygen, Nitrogen, Carbon and Boron," *Advances in X-Ray Analysis* (Plenum, New York, 1964), Vol. 7.

24. "Oxygen Determinations in Silicates and Total Major Elemental Analysis of Rocks by Soft X-Ray Spectrometry," *Analyt. Chem. 37*, 727-729 (1965) (w/ A. K. Baird).

25. "Some Notes on Ultrasoft X-Ray Fluorescence Analysis--10 to 100 Angstrom Region," *Advances in X-Ray Analysis* (Plenum, New York, 1965), Vol. 8.

26. "Spectroscopy in the 15 to 150 Angstrom Ultrasoft X-Ray Region," 4th International Symposium on X-Ray Microscopy and X-Ray Microanalysis, Orsay, France, *Optique des Rayons X et Microanalyse*, R. Castaing, P. Deschamps and J. Philibert, Eds. (Editions Scientifiques Hermann, Paris, 1966), pp. 440-453.

27. "Valence Electron Band Analysis by Ultrasoft X-Ray Fluorescence Spectroscopy," *J. Appl. Phys. 37*, 922 (1966) (w/ Eric N. Smith).

28. "Application of Multilayer Analyzers to 15 to 150 Angstrom Fluorescence Spectroscopy for Chemical and Valence Band Analysis," *Advances in X-Ray Analysis* (Plenum, New York, 1966), Vol. 9.

29. "Design Notes on an Intermediate Resolution Experiment for the Measurement of the Ultrasoft X-Radiations of the Solar Corona," Technical Report No. 7, AFOSR 66-2446 (September 1966).

30. "X-Ray Absorption in the 2 to 200 A Region," Technical Report, AFOSR 67-1254 (June 1967) (w/ R. L. Elgin, R. E. Lent and R. B. Ledingham).

31. "Techniques of Low Energy X-Ray and Electron Physics--50 to 1000 eV Region," *Proceedings of the 2nd Symposium of Low Energy X- and Gamma Ray Sources and Applications*, Austin, Texas, March 1967.

32. "Techniques of Low Energy X-Ray and Electron Physics--50 to 1000 eV Region," *Norelco Reporter*, XIV, No. 3-4, (1967) (w/ R. L. Elgin, R. E. Lent and R. B. Ledingham).

33. "X-Ray Absorption in the 2 to 200 A Region," *Norelco Reporter*, XIV, No. 3-4 (1967).

34. "Some Recent Work in Low Energy X-Ray and Electron Analysis," *Advances in X-Ray Analysis* (Plenum, New York, 1969), Vol. 12 (w/ R. E. Lent).

35. "An Introduction to Low Energy X-Ray and Electron Analysis," *Advances in X-Ray Analysis* (Plenum, New York, 1970), Vol. 13.

36. "X-Ray Absorption Tables for the 2 to 200 A Region," *Advances in X-Ray Analysis* (Plenum, New York, 1970), Vol. 13.

37. *Advances in X-Ray Analysis*, Vol. 13, a special volume on low energy x-ray and electron analysis, edited by Burton L. Henke, John B. Newkirk and Gavin R. Mallett (Plenum, New York, 1970).

38. "Measurement of Primary Electron Interaction Coefficients (500 to 1500 eV Region," *Colloque International du C.N.R.S., Processus Electroniques Simples et Multiples du Domaine X et X-UV* (Paris, September 1970), *Le Journal de Physique*, Colloque C4, Supp. 10, Vol. 32, October 1971, pp. 115-123.

39. "Surface Characterization by Low Energy Photoelectron Spectroscopy," *Proceedings of the 6th International Congress on X-Ray Optics and Microanalysis* (Osaka, Japan, September 1971), pp. 367-384.

40. "The Measurement of Inner Shell Ionization Cross Sections for the 100-1000 eV Region as Involved with X-Ray and Electron Interactions within Solids," *Proceedings of International Conference on Inner Shell Ionization Phenomena* (Atlanta, Georgia, April 1972), published as *Inner Shell Ionization Phenomena and Future Applications*, edited by R. W. Fink *et al.* (Technical Information Division of the U.S. Atomic Energy Commission, Oak Ridge, Tennessee, 1973).

41. "Ultrasoft X-Ray Reflection, Refraction and the Production of Photoelectrons (100-1000 eV Region)," *Proceedings of Spring Meeting of the American Physical Society* (Washington, D. C., April 1972), published in *Bulletin of the American Physical Society*.

42. "The Measurement of Low Energy Electron and X-Ray Interaction Coefficients for Solids," *Proceedings of the 7th National Conference of the Electron Probe Analysis Society of America* (San Francisco, July 1972).

43. "Ultrasoft X-Ray Reflection, Refraction and Production of Photoelectrons (100-1000 eV Region)," *Physical Review A6*, 94-104 (1972).

44. "Electron Interactions within Solids--Electron Spectroscopy" and "Light Element Analysis" *Proceedings of the U.S.-Japan Seminar on Fundamentals of Scanning Electron Microscopy* (Osaka, Japan, November-December 1972).

45. "Low Energy X-Ray and Electron Absorption within Solids (100-1500 eV Region)," Interim Report, AFOSR 72-2174 (August 1973) (w/ Eric S. Ebisu).

46. "Low Energy X-Ray and Electron Absorption within Solids (100-1500 eV Region)," *Advances in X-Ray Analysis* (Plenum, New York, 1974) (w/ Eric S. Ebisu).

47. "Ultrasoft X-Ray Bragg and Specular Reflection: The Effects of Anomalous Dispersion," Interim Report, AFOSR 72-2174 (August 1974) (w/ Rupert C. C. Perera and Ronald H. Ono).

48. "Demountable Ultrasoft X-Ray Source," (informal notes, August 1974).

49. "Techniques of Low Energy X-Ray Spectroscopy (0.1 to 2 keV Region)," *Advances in X-Ray Analysis* (Plenum, New York, 1975) (w/ Murray A. Tester).

50. "Techniques of Low Energy X-Ray Spectroscopy (0.1 to 2 keV Region)," Interim Report, AFOSR 75-2762 (November 1974) (w/ Murray A. Tester).

51. "Valence Band Spectroscopy in the Ultrasoft X-Ray Region (50 to 100 A), *Advances in X-Ray Analysis* (Kendall/Hunt, Dubuque, 1976), Vol. 19 (w/ Kazuo Taniguchi).

52. "Parameters for the Calculation of X-Ray Absorption Coefficients for H (1) through Ge (32) in the 100-1500 eV Region," *Advances in X-Ray Analysis* (Kendall/Hunt, Dubuque, 1976), Vol. 19 (w/ Mark L. Schattenburg).

53. "Quantitative Low Energy X-Ray Spectroscopy (50-100 A Region)," *J. Appl, Phys.* 47 (1976) (w/ Kazuo Taniguchi).

54. "Sulfur $L_{II,III}$ Emission Spectra and Molecular Orbital Studies of Sulfur Compounds," *J. Chem. Phys. 64* (1976) (w/ Kazuo Taniguchi).

55. "X-Ray Calibration Sources for the 100-1000 eV Region," *Proceedings of the 1976 ERDA Symposium on X- and Gamma-Ray Sources and Applications* (University of Michigan, Ann Arbor, May 1976).

56. "Secondary Electron Energy Distributions for Gold as Excited by C-Kα (277 eV) and Al-Kα (1487 eV) X-Rays," *Appl. Phys. Lett. 29* (1976) (w/ J. A. Smith and D. T. Attwood).

57. "0.1 to 10 keV X-Ray-Induced Electron Emissions from Solids--Models and Secondary Electron Measurements," *J. Appl. Phys. 48*, 1852 (1977) (w/ J. A. Smith and D. T. Attwood).

58. "High Efficiency Low-Energy X-Ray Spectroscopy in the 100-500 eV Region," *J. Appl. Phys. 49*, 480 (1978) (w/ R. C. C. Perera, E. M. Gullikson and M. L. Schattenburg).

59. "Cl-$L_{II,III}$ Fluorescent X-Ray Spectra Measurement and Analysis for the Molecular Orbital Structure of ClO_4^-, ClO_3^- and ClO_2^-," *J. Chem. Phys. 68*, 3692 (1978) (w/ R. C. C. Perera and D. S. Urch).

60. "Some Recent Studies in Low Energy X-Ray Physics," *Proceedings of the 8th International Conference on X-Ray Optics and Microanalysis* (Boston, August 1977).

61. "Models and Measurement for the Response of Dielectric X-Ray Photocathodes," Scientific Reports, AFOSR 75-2762-F and DOE E(04-3)235-PA15, March 1978.

62. "Low Energy X-Ray Emission Spectroscopy in the 100-500 eV Region: Molecular Orbital Interpretation," (PhD Thesis by R. C. C. Perera) Special Scientific Report, AFOSR 75-2762-F, May 1978.

63. "The Secondary Electron Emission Photocathode Characteristics for Time Resolved X-Ray Spectroscopy," *Proceedings of the International Conference on X-Ray and XUV Spectroscopy* (Sendai, Japan, August 1978); *Jap. J. Appl. Phys. 17*, Suppl. 17-2, p. 23 (1978) (w/ K. Premaratne).

64. "C-K and Cl-L Emission Spectra and Molecular Orbital Analysis of CCl_4" *Proceedings of the International Conference on X-Ray and XUV Spectroscopy* (Sendai, Japan, August 1978); *Jap. J. Appl. Phys. 17*, Suppl. 17-2, p. 23 (1978) (w/ R. C. C. Perera).

65. "A Soft X-Ray Spectrometer for the Study of Plutonium and Plutonium-based Materials," *X-Ray Spectrometry 7* (1978) (w/ P. L. Wallace, W. L. Haugen and E. M. Gullikson).

66. "Soft X-Ray Induced Secondary Electron Emission from Semiconductors and Insulators: Models and Measurements," *Phys. Rev. B19*, 3004 (1979) (w/ J. Liesegang and S. D. Smith).

67. "Low Energy X-Ray Emission Spectra and Molecular Orbital Analysis of CH_4, CCl_4 and $CHCl_3$," *J. Chem. Phys. 70*, 5398 (1979) (w/ R. C. C. Perera).

68. "The Characterization of Photocathodes for Application to Time-Resolved X-Ray Spectroscopy," Technical Progress Report, AFOSR 79-0027 and DOE DE-AS03-76SF00235, April 1979.

69. "Multilayer X-Ray Spectrometry in the 20-80 A Region: A Molecular Orbital Analysis of CO and CO_2 in the Gas and Solid States," *X-Ray Spectrometry 9*, 81 (1980) (w/ R. C. C. Perera).

70. "X-Ray Spectrometry in the 100-1000 eV Region," *Nucl. Instrum. Methods 177*, 161 (1980).

71. "Evaluation of High Efficiency CsI and CuI Photocathodes for Soft X-Ray Diagnostics," *Appl. Opt. 19*, 748 (w/ E. B. Saloman and J. A. Pearlman).

72. "The Characterization of X-Ray Photocathodes in the 0.1-10 keV Photon Energy Region," *J. Appl. Phys.* (March 1981) (w/ J. P. Knauer and K. Premaratne).

73. "Low Energy X-Ray Interaction Coefficients: Photoionization, Scattering and Reflection," to be published (w/ P. Lee, T. J. Tanaka, R. L. Shimabukuro and B. K. Fujikawa).

APPENDIX II

B. INVITED AND CONTRIBUTED RESEARCH PAPERS PRESENTED BY THE PRINCIPAL INVESTIGATOR

1970 TO 1980

1970

- Seminar for Phillips Petroleum Corp., Tulsa, Oklahoma
- Seminar for Shell Development Company, Emeryville, California
- Seminar at Department of Physics, University of Arizona
- Colloquium on *Processus eletroniques simples et multiples du domaine X et X-UV* sponsored by the Centre National de la Recherche Scientifique and held in Paris, France, September 1970 (principal investigator participated as a guest of the French government)

1971

- Sixth International Conference on X-Ray Optics and Microanalysis, Osaka, Japan, September 5-10, 1971
- Post Conference Seminar on Scanning Electron Microanalyzers sponsored by the Japan Society of Applied Physics, Tokyo, Japan, September 14, 1971
- Seminar at Tohoku University, Sendai, Japan, September 1971

1972

- Discussion: Possibilities of low energy analysis, particularly as applied to membranes; with Dr. Poen S. Ong, M. D. Anderson Cancer Research Center X-Ray and Electron Probe Analysis Laboratory, Houston, Texas, April 1972
- International Conference on Inner Shell Ionization Phenomena, Atlanta, Georgia, April 1972
- Seminar at ORTEC, Inc., Oak Ridge, Tennessee, April 1972
- Spring Meeting of American Physical Society, Washington, D. C., April 1972
- Presentation: Slides on recent spectroscopic techniques and measurements of cross sections, Naval Research Laboratories, Washington, D. C., April 1972
- Seminar at Pomona College (and associated colleges at Claremont, California) April 1972
- Seminar at IBM Research Laboratory, San Jose, California, July 1972
- Seminar at University of California Livermore Radiation Laboratory, Livermore, California, July 1972
- U.S.-Japan Seminar on Fundamentals of Scanning Electron Microscopy, Osaka, Japan, November-December 1972
- Seminar at Rigaku Denki Co., Ltd., Osaka, Japan, December 1972

1973

- Seminar at Los Alamos Scientific Laboratory (University of California), Los Alamos, New Mexico, January 1973
- Seminar at Kirtland Air Force Base and Sandia Corp., Albuquerque, New Mexico, January 1973
- Seminar at Materials Analysis Laboratory, Wright-Patterson Air Force Base, Ohio, August 1973
- Twenty-second Annual Conference on Applications of X-Ray Analysis, Denver, Colorado, August 1973
- U.S.-Japan Seminar on Electron Probe Microanalysis (University of Hawaii), Honolulu, Hawaii, September 1973

1974

- Seminar at Lawrence Livermore Laboratory, Livermore, California, August 1974
- Twenty-third Annual Conference on Advances in X-Ray Analysis, Denver, Colorado, August 1974
- Seminar at Los Alamos Scientific Laboratory (University of California), Los Alamos, New Mexico, August 1974
- Seminar at Kirtland Air Force Base and Sandia Corp., Albuquerque, New Mexico, August 1974

1975

- A two-day symposium on *Low Energy X-Ray and Electron Spectroscopy* held at the University of Hawaii, June 12-13, 1975. This research group joined others from our Chemistry Department as host for this meeting which was also part of the 13th Northwest Regional Meeting of the American Chemical Society. Papers presented on this project's research program were:

  1. *Some Current Research in Low Energy X-Ray and Electron Physics* (B. L. Henke)
  2. *Effect of Chemical State upon Sulfur $L_{II,III}$ Fluorescence Spectra* (w/ Kazuo Taniguchi)
  3. *Effect of Chemical State upon the Characteristic Energy Loss Spectra of Molecular Gases* (w/ Taylor Norcross)

  (A total of 42 papers were presented for this symposium from U.S. and international laboratories.)

- Twenty-forth Annual Conference on Applications of X-Ray Analysis, Denver, Colorado, August 1975
- Seminar at Los Alamos Scientific Laboratory (University of California) Los Alamos, New Mexico, August 1975
- Seminar at Lawrence Livermore Laboratory, Livermore, California, August 1975
- Seminar at Kirtland Air Force Base, Albuquerque, New Mexico, and discussions with E. J. T. Burns, August 1975

1976

- American Physical Society Topical Conference on Diagnostics of High Temperature Plasmas, Knoxville, Tennessee, January 1976
- ERDA Conference on X- and Gamma-Ray Sources and Applications, University of Michigan, Ann Arbor, Michigan, May 1976
- Seminar at Lawrence Livermore Laboratory, Livermore, California, May 1976

1977

- Seminar at Lawrence Livermore Laboratory, Livermore, California, August 1977
- Seminar at Los Alamos Scientific Laboratory, Los Alamos, New Mexico, August 1977
- Eight International Conference on X-Ray Optics and Microanalysis, Boston, Massachusetts, August 1977

1978

- *A Systematic Study of the Characteristics of X-Ray Photocathodes*, Poster presentation, American Physical Society Second Topical Conference on High Temperature Plasma Diagnostics, Santa Fe, New Mexico, February 28 - March 3, 1978
- *Application of Low Energy X-Ray Spectroscopic Techniques to High Temperature Plasma Diagnostics*, Physics seminar lecture, Los Alamos Scientific Laboratory, June 1978
- *The Optimization of X-Ray Photocathodes for Time Resolved X-Ray Spectroscopy in Laser-Produced Fusion Research*, Physics colloquium lecture, University of California Lawrence Livermore Laboratory, June 1978
- Participated in a workshop on the Absolute Calibration of X-Ray Photocathodes as Applied in X-Ray Detectors (XRD's) sponsored by the National Bureau of Standards at the Lawrence Livermore Laboratory, June 1978. The results of the calibrations of two detectors that were calibrated by each of the six participating laboratories, including this one, were evaluated.
- *The Secondary Electron Emission Photocathode Characteristics for Time Resolved X-Ray Spectroscopy*, International Conference on X-Ray and XUV Spectroscopy, Sendai, Japan, August 28 - September 1, 1978
- *C-K and Cl-L Emission Spectra and Molecular Orbital Analysis of CCl_4* International Conference on X-Ray and XUV Spectroscopy, Sendai, Japan, August 28 - September 1, 1978
- *A Review of X-Ray Photocathode Characteristics that Affect Picosecond Streak Camera Operation*, 1978 American Physical Society Annual Meeting of the Division of Plasma Physics, Colorado Springs, October 30 - November 3, 1978
- *Physics and Application of Multilayer 'Crystals' for Spectral Analysis in the 50-100 Å Region*, Invited paper, American Crystallographic Assn. Meeting (Joint with Japanese Crystallographic Society), Honolulu, Hawaii, March 26-30, 1979.

1979

- Seminar at Lawrence Livermore Laboratory, June 20, 1979
- Seminar at Los Alamos Scientific Laboratory, June 26, 1979
- Seminar at Kirtland Air Force Base and Sandia Laboratories, Albuquerque, New Mexico, June 28, 1979
- Seminar at Maxwell Laboratories, Inc., San Diego, June 29, 1979
- *X-Ray Spectroscopy in the 100-1000 eV Region*, Invited review paper, Japan-U.S.A. Seminar on Synchrotron Radiation Facilities, East-West Center, University of Hawaii, November 5-9, 1979
- *The Characterization of X-Ray Photocathodes*, 21st Annual Meeting of the Division of Plasma Physics, American Physical Society, Boston, November 12-16, 1979
- Seminar at Department of Physics, Pomona College, Claremont, California, November 1979
- Seminar at Massachusetts Institute of Technology, Center for Space Research, Cambridge, Massachusetts, November 1979

1980

- Seminar at Lawrence Livermore Laboratory, August 1980
- Seminar at Los Alamos Scientific Laboratory, August 1980
- Seminar at Kirtland Air Force Base and Sandia Laboratories, Albuquerque, New Mexico, August 1980
- *Some Recent Developments in Low Energy X-Ray Spectroscopy*, 1980 Annual Meeting of the Division of Plasma Physics, American Physical Society, San Diego, November 10-14, 1980

APPENDIX III

FIRST-PAGE ABSTRACTS OF SELECTED EXAMPLES OF
SOME RESEARCH PUBLICATIONS

ADVANCES IN X-RAY ANALYSIS Volume 13 (1970)

681-page text

Edited by Burton L. Henke
Department of Physics and Astronomy
University of Hawaii
and John B. Newkirk
and Gavin R. Mallett
Denver Research Institute
The University of Denver
Denver, Colorado

FOREWORD

This conference has attempted to achieve a balance in the presentation of papers on the application of current methods to established problem areas and on the introduction of new methods and applications. It has recognized the relevance of papers on basic physics and chemistry and on the total interaction of x-rays with matter. In order to achieve sufficient depth, a topic is chosen each year for special emphasis. This conference had as its central theme, "The Interactions and Applications of Low Energy X-Rays."

Those who were invited as speakers and as contributors to this volume are among the outstanding workers in the application of low energy x-ray and the associated photo-Auger electron interactions. These include A. K. Baird and W. L. Baun on Light Element Analysis and Long Wavelength Instrumentation; J. E. Holliday, D. W. Fischer, R. J. Liefeld and D. J. Nagel on Bonding and Valence State; H. Friedman and W. P. Reidy on X-Ray Astronomy; and R. Nordberg on Photo-Auger Electron Spectroscopy.

Upon reading over the papers as presented here, one cannot help but be impressed by the steady, dynamic growth and expansion of the field of applied x-ray analysis, beginning about thirty years ago with quantitative elementary analysis and extending to the present time with dramatic and exciting applications to x-ray astronomy.

It has been most appropriate and indeed a privilege to have Dr. Herbert Friedman as a speaker and contributor to this volume. He was among the few who pioneered the application of x-ray spectroscopy as an analytical technique and now he is noted as one of the first to open the new field of x-ray astronomy.

Burton L. Henke
Invited Co-Chairman

JOURNAL DE PHYSIQUE *Colloque C4, supplément au n° 10, Tome 32, Octobre 1971, page C4-115 - 123*

MEASUREMENT OF PRIMARY ELECTRON INTERACTION COEFFICIENTS (500 TO 1 500 eV REGION)

BURTON L. HENKE

Department of Physics and Astronomy, University of Hawaii, Honolulu, Hawaii

Résumé. — Etant donné que les électrons d'énergie incidente comprise entre 500 et 1 500 eV n'ont d'interaction appréciable qu'avec peu de couches atomiques dans les solides, des mesures précises et l'application de leurs coefficients d'interaction sont difficiles. La statistique des interactions et la sensibilité à la disposition géométrique de la cible nécessitent une attention particulière. Nous présentons ici une méthode pour l'étude de telles interactions, basée sur la déposition contrôlée d'une couche monoatomique de cations métalliques bivalents comme cible, sur un support formé d'une double couche de stéarate du type de Langmuir-Blodgett. Pour vérifier la méthode, nous avons mesuré les sections efficaces des cations de barium à 466 eV, 706 eV et 1 349 eV, et celles du zinc et du plomb à 706 eV. Les valeurs mesurées sont en accord avec des mesures récentes de faisceau atomique sur le barium et avec un modèle théorique simple. Nous considérons que des mesures de ce type sont d'une grande importance dans le développement de l'analyse chimique quantitative de surface par spectroscopie d'électrons et de rayons X de basse énergie.

Abstract. — Because electrons of incident energy in the 500-1 500 eV range interact appreciably within only a few atomic layers in solids, precisely measuring and applying their interaction coefficients becomes difficult. The statistics of the interactions and the sensitivity to the geometric arrangement of the target atoms require special attention. A method for the study of such interactions is presented here that is based upon the controlled deposition of monatomic layers of bivalent metal cations as targets within the framework of stearate double layers of the Langmuir-Blodgett type. To demonstrate the method, cross sections of the barium cation have been measured at 466 eV, 706 eV and 1 349 eV, and those of zinc and lead at 706 eV. The measured values are shown to be consistent with recent atomic beam measurements on barium and with simple theoretical models. Measurements of this type are considered to be of great importance in the development of quantitative surface chemical analysis by low energy X-ray and electron spectroscopy.

1. Introduction. — This work is concerned with the measurement of primary electron interactions in solids for incident electron energies in the 500-to-1 500 eV region. Such electrons have an associated wavelength of about 0.5 Å. Their mean free paths within condensed matter are generally less than 100 Å.

Although a considerable amount of theoretical work on the passage of electrons through matter has been presented and from a variety of approaches, very few experimental measurements have been reported for kilovolt-electron interactions in solids [1]. Interesting questions remain to be answered as to the relative roles of elastic and inelastic scattering, and of collective and individual electron energy loss mechanisms.

The ionization of matter by keV electrons should be similar in both mechanism and magnitude to that by MeV protons, for example [2]. Important new insights might be gained by comparing measurements with electrons in this region to the relatively large amount of data reported in recent years on heavy particle cross sections in the MeV region.

Finally, important analytical techniques based upon chemical and structural analysis by electron and X-ray spectroscopy demand a precise knowledge of X-ray and electron cross sections. Although many important applications involve radiations in the 100-to-1 000 eV region, it has been only relatively recently that low energy X-ray cross sections have become available to any extent [3, 4]. There remains an appreciable need for further work on low energy X-ray interaction coefficients and an even greater need for work on the low energy electron cross sections.

2. Electron spectroscopy of thin films. — The electron spectrograph which is used for the present work is shown in figure 1 and has been described previously [5]. It employs hemispherical plates as the electrostatic analyzer. These have inner and outer diameters of 18.5 and 21 inches. For this work the slits were set at 0.3 % energy resolution and to receive only photoelectrons which leave nearly normally from the surface of the sample (maximum angles off normal are plus-minus 3°). Al-K_α photons (1 487 eV) were used to excite the samples as generated by an

Phys. Rev. A
pp. 94-104

PHYSICAL REVIEW A VOLUME 6, NUMBER 1 JULY 1972

Ultrasoft-X-Ray Reflection, Refraction, and Production of Photoelectrons (100–1000-eV Region)*

Burton L. Henke
University of Hawaii, Honolulu, Hawaii 96822
(Received 14 February 1972)

The reflection, refraction, and associated production of photoelectrons by ultrasoft x rays (10–100 Å) can be important bases for the determination of material constants such as the linear x-ray absorption coefficients and the electron mean free paths. These may then be used to establish directly the photoionization cross sections and the electron-collision cross sections which account for the dominant energy-absorbing processes within solids for this energy region. Because the effective sample depths for these interactions are typically less than 100 Å, they constitute an important practical basis for surface characterization. By applying the exact theory for the reflection-refraction of a plane electromagnetic wave at an absorbing dielectric interface to the shorter-wavelength region (<10 Å), it can be shown that the conventional approximate theory of x-ray reflection is adequate. However, the more exact theory must be applied in the region of longer x-ray wavelengths (>50 Å). Although the derivations of the exact theory are tedious, the results can be expressed in relatively simple form as functions of two material constants α and γ, which are identifiable as the unit decrements to a complex dielectric constant, of the grazing-incidence angle, and of a parameter which is a function of this grazing angle and which becomes the angle of refraction for small angles of incidence. X-ray absorption coefficients and electron mean-free-path values have been determined from x-ray reflection and refraction and photoelectron excitation data. These values have been shown to agree reasonably well with such material constants as determined by transmission measurements through thin samples.

I. INTRODUCTION

It is well known that x rays do reflect from surfaces with high efficiency in the grazing-incidence region. The characteristic reflectance curve, which falls off to zero value with increasing angle, is the basis for an important method for determining the optical constants of the reflecting medium and its surface structure.[1,2] Also, a precise knowledge of this "total-reflection" characteristic curve is important in the design of mirror monochromators,[3] of optimized diffraction gratings, and of astronomical telescope systems for the x-ray region.

As will be described below, the refracted x-ray beam, when used to produce photoelectrons, can also be an important basis for the determination of certain constants of the medium and of its surface structure.[4]

In order to relate experimental reflection, refraction, and associated photoelectron excitation data to the optical constants, one may apply a relatively simple electromagnetic model based upon approximations permitted by the small values of the grazing-incidence angles and of complex refractive-index unit decrements which obtain for the

Reprinted from

PROCEEDINGS OF THE SIXTH INTERNATIONAL CONFERENCE ON X-RAY OPTICS AND MICROANALYSIS

pp. 367-384

Edited by G. SHINODA, K. KOHRA and T. ICHINOKAWA

UNIVERSITY OF TOKYO PRESS, 1972

Surface Characterization by Low Energy Photo-Auger Electron Spectroscopy

B. L. HENKE and M. W. ANDERSON

Department of Physics and Astronomy, University of Hawaii, Honolulu, Hawaii, U.S.A.

Low energy photoelectron spectroscopy (100 to 1000 eV region) has shown considerable promise as an effective method for the microanalysis of sample surface layers no thicker than 100 Å. Quantitative information can be obtained about the elementary chemistry, chemical bonding, and structure within the surface. Essentially, all elements throughout the periodic table can yield photoelectron lines within this low energy region which are suitable for such analysis.

A relatively simple electron spectrograph system has been developed. Its sensitivity is sufficiently high to permit the measurement of photoelectron lines from single atomic layer thicknesses at better than 0.5% energy resolution.

In order to develop methods for correlating photoelectron spectral information with surface characteristics, electron interaction cross sections are being measured, and simple models for predicting line intensities are being evaluated.

I. INTRODUCTION

Photo-Auger electron spectra in the 100--1000 eV region are relatively easy to obtain and are rich in information that is characteristic of the chemistry, density, and structure of the first 100 Å or less of the sample surface. The quantitative analysis of such spectra can constitute an effective technique for solving problems in the difficult areas of surface characterization. Examples of two such areas, noted for their extreme importance, are catalysis and biological membranes.

In order to develop practical methods for quantitative photo-Auger electron analysis, certain steps are necessary: A choice must be made for an optimum set of parameters that are amenable to measurement and can precisely define the electron signal generation within the sample. Correspondingly, photo-electron-sample interaction models that directly relate measured intensities to sample chemistry and structure must be developed and tested. Finally, from theory and measurement, the necessary tables for the appropriate fundamental interaction cross sections must be established.

The objective of this paper is to describe some current work in this laboratory that is addressed to the development of methods for photo-Auger electron analysis of surfaces. A proposal for an interaction model, an experimental test of its validity, and descriptions of new methods for the measurement of basic interaction coefficients are presented.

II. A MODEL FOR PHOTOELECTRON INTENSITY ANALYSIS

Figure 1 shows the essential geometry of the model adopted here for the generation of the unscattered, no-loss photoelectron signal. Monoenergetic, parallel X-radiation of wavelength λ is incident upon a plane surface at an angle, ϕ, refracting into an amorphous sample with angle ϕ'. The linear absorption coefficient for this radiation within the sample is equal to μ. In a sample layer at depth x and thickness dx, photoelectrons are generated in an effective sample area which is the projection of the limiting slit area, A_0. The atomic cross section for the crea-

Interim Report
August 1974
168 pages

ULTRASOFT X-RAY BRAGG AND SPECULAR REFLECTION: THE EFFECTS OF ANOMALOUS DISPERSION

B. L. Henke, R. C. C. Perera and R. H. Ono

ABSTRACT

For the low energy x-rays (100-1000 eV region), atomic scattering becomes of practical importance as it is involved in Bragg reflection from crystal analyzers and in specular reflection from mirror systems. But the cross section for coherent scattering in this energy region is very small as compared with that for photoionization, the latter being more amenable to direct measurement and also to theoretical calculation. Assuming dipole descriptions only need to be considered here where the wavelengths are long as compared with orbital dimensions, the current theoretical partial photoionization cross section calculations have been applied to yield oscillator densities which permit a numerical solution of semi-classical dispersion integrals to obtain the atomic scattering factors. These factors account for the strong anomalous dispersion that is characteristic of low energy x-ray scattering. For the long x-ray wavelengths, it is assumed that all atomic electrons scatter from a volume that is small as compared with the wavelength, in phase in all directions. The atomic scattering factors, in turn, are applied with electromagnetic theory to calculate optical constants for the solid and structure factors that characterize the crystalline state. With these, the classic models for x-ray reflection as the Darwin-Prins perfect crystal theory and the mosaic, imperfect crystal theory, have been specialized for the low energy x-ray region and applied to calculate the reflection properties of specific, practical analyzers for the ultrasoft x-ray wavelengths as the acid phthalate crystals and the Langmuir-Blodgett multilayers with d-spacings in the 25 to 150 A range. And with the optical constants, the Fresnel equations have been expressed for the long x-ray wavelengths and for the large angle region to calculate the specular reflectivities for the fused quartz and the aluminum mirror systems. These theoretical Bragg and specular reflection characteristics have been compared to those as measured for the same systems and generally good agreement has been found between theory and experiment. Finally, this approach for the calculation of anomalous dispersion effects has yielded a relatively simplified description of the general properties of dispersive analyzers for the low energy x-ray region.

LOW ENERGY X-RAY AND ELECTRON ABSORPTION WITHIN SOLIDS

(100-1500 eV Region)

Burton L. Henke and Eric S. Ebisu

University of Hawaii

Honolulu, Hawaii 96822

ABSTRACT

Quantitative analysis by x-ray fluorescence and photoelectron and Auger electron analysis can be effectively extended through a precise knowledge of the total and subshell photoionization cross sections. Light element and intermediate element analysis, as based upon K and L series fluorescence respectively, involve x-ray interactions in the low energy region. Optimized analysis for essentially all the elements by x-ray induced photoelectron and Auger electron spectroscopy involves both x-ray and electron interactions in the low energy region. Unfortunately, theory and measurement for interaction cross sections in this 100-1500 eV region are difficult, particularly for the heavier elements. Nevertheless, recent advances in experimental and computerized-theoretical techniques for the determination of low energy interaction coefficients do permit establishing appreciably more complete tabulations of cross sections than are currently available in this energy region.

In this paper, the types of interaction cross section data that are needed for quantitative x-ray and electron analysis are defined. Such data that are available from experiment and from theory are reviewed and compared. Some newer techniques for the measurement of cross sections are discussed. And finally, new "state of the art" tables are presented for the mass absorption coefficients of all of the elements and of some special laboratory materials. These are tabulated specifically for twenty-six of the most commonly applied characteristic wavelengths in the 8-110 A region and are based upon the best currently available theoretical and experimental data.

Advances in X-Ray Analysis (Plenum, New York, 1974), Vol. 17, pp. 150-213.

COMPARISON — THEORY AND EXPERIMENT

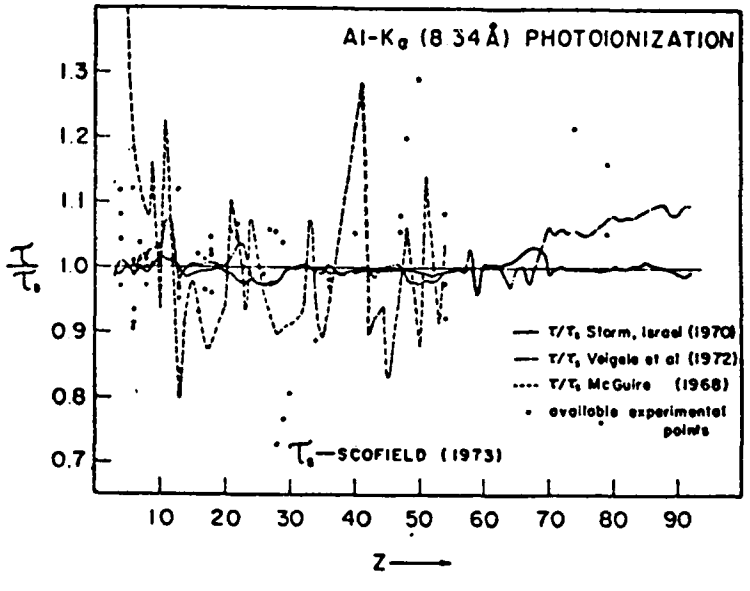

Figure 1

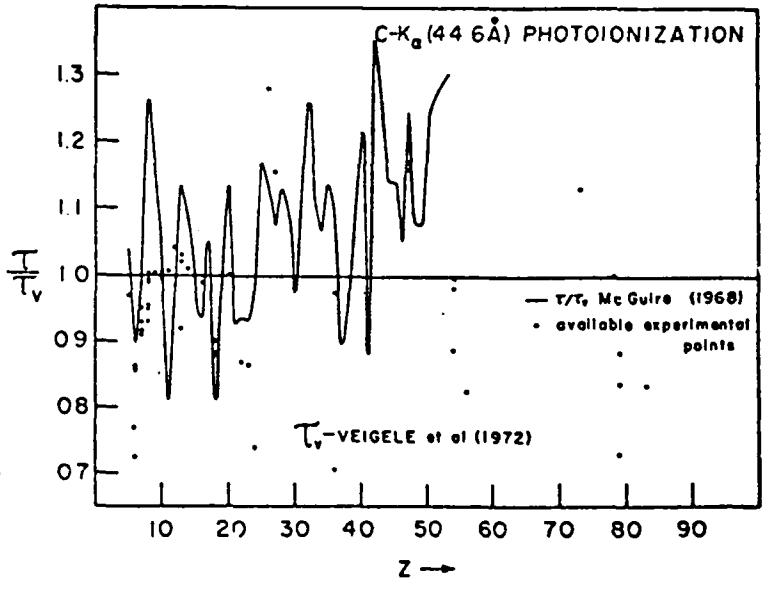

Figure 2

Advances in X-Ray Analysis (Plenum, New York, 1975) Vol. 18, pp. 76-106

TECHNIQUES OF LOW ENERGY X-RAY SPECTROSCOPY

(0.1 TO 2 keV REGION)

Burton L. Henke and Murray A. Tester

University of Hawaii•

Honolulu, Hawaii 96822

ABSTRACT

Presented here is a report on the development of practical techniques for laboratory spectroscopy in the 5 to 150 A wavelength region as may be applied, for example, to light element and surface state analysis, high temperature plasma diagnostics and to the design and calibration of x-ray astronomy measurements.

I. INTRODUCTION

X-ray spectroscopy in the low energy region at or below one kilovolt has become of considerable practical importance for light element analysis, valence band or orbital energy analysis, surface characterization and high temperature plasma diagnostics. The light elements, Mg through Be, emit characteristic x-radiation only in this region. The sensitive transitions from the outer orbitals into the first inner shells yield valence band spectra which are always in the ultrasoft wavelength region. Fluorescence analysis based upon the ultrasoft K, L or M characteristic wavelengths typically involve sampling depths of surfaces in the sub-micron range. And, finally, the spectra emitted by high temperature plasmas in the one-to-ten million degree range emit most strongly in this low energy region and do characterize the plasma temperature and electron-ion densities--such plasmas are involved in controlling nuclear reaction research and are of particular importance in laser-induced x-ray sources, and are also often observed from astronomical sources via rocket and satellite studies.

Advances in X-Ray Analysis (Kendall/Hunt, Dubuque, 1976) Vol. 19, pp. 627-641

VALENCE BAND SPECTROSCOPY IN THE ULTRASOFT X-RAY REGION (50 TO 100 A)

Burton L. Henke and Kazuo Taniguchi

University of Hawaii

Honolulu, Hawaii 96822

ABSTRACT

Transitions from the valence electron levels into the first relatively sharp inner sub-shell levels result in characteristic x-ray emissions in the 100-200 eV region. These spectra sensitively reflect the chemical state of the atoms which are representative of the sub-micron thickness of the sample surface under low energy x-ray excitation and of the first few molecular layers of the sample under electron excitation.

An optimized measurement method for this 50-100 A spectral region is based upon single crystal spectrometry using a lead stearate analyzer which has high dispersion and efficiency and an energy width of about one eV in this wavelength range. Spectra are recorded using "tuned" proportional counter detection. In the work reported here, low energy x-ray excitation is used in order to minimize the possibility of radiation damage of the sample.

Each spectrum is calibrated for both energy and instrument transmission using known, sharp M lines of elements such as molybdenum, zirconium and yttrium which will bracket the spectral range under measurement. A simple method has been developed for "stripping" from the measured spectra the Lorentzian crystal width and the Gaussian collimation width in order to allow an estimation to be made of the actual emission line widths as well as the relative intensities.

In this report, as an illustrative application example, S-$L_{II,III}$ spectra are presented for a series of sulfur compounds in both solid and gas states. Manne's approximate molecular orbital interpretation of the x-ray emission spectra has been adopted and extended to apply to the $L_{II,III}$ spectra for second row elements.

Advances in X-Ray Analysis (Kendall/Hunt, Dubuque, 1976) Vol. 19, pp. 749-767

APPENDIX

PARAMETERS FOR THE CALCULATION OF X-RAY ABSORPTION COEFFICIENTS FOR H (1) THROUGH Ge (32) IN THE 100-1500 eV REGION*

Burton L. Henke and Mark L. Schattenburg
Department of Physics and Astronomy
University of Hawaii
Honolulu, Hawaii 96822

In a recent paper[1] we compiled absorption coefficient tables for all elements through atomic number 94 (and for some often used laboratory compounds) for twenty-six K, L, and M characteristic wavelengths as commonly involved in low energy x-ray spectroscopy in the 8.34 to 114 A region. These tables were based upon a "state-of-the-art averaging" of available experimental data and the theoretical data of Veigele, et. al.[2] and of Scofield[3]. Our best experimental data (on the inert gases) were fit closely by the theoretical photoionization cross section curves (except for Xenon at the longer wavelengths) thereby verifying that for this low energy region coherent and incoherent scattering contributions to x-ray absorption are essentially negligible and that only small adjustments in the theoretical data were appropriate at this time.

In order to facilitate the programming of absorption corrections in quantitative, low energy x-ray analysis, we have listed here the parameters which define a least squares fit to all of the absorption data for the first thirty-two elements (through Germanium) using polynomials of the form

$$\log (10^{-3}\mu) = a + b \log E + c (\log E)^2 + d (\log E)^3$$

(μ in cm^2/gm, E in eV and log terms to base ten.)

These polynomials were used to plot the associated absorption curves within the listed absorption edge energies. In order to compare these curves to available experimental data the measured values have also been plotted (solid dots indicate our measurements and crosses indicate most other reported measurements). The sources of the experimental data are listed in Reference 1.

Using these parameters, we have programmed a small laboratory computer to generate tables and plots for compound absorbers. Included here are the calculated absorption curves for the molecules C_2H_6, C_2F_6, H_2S, and CCl_4 along with our directly measured absorption cross sections for these compounds in order to illustrate the additivity of atomic cross sections for this low energy region.

[1] B. L. Henke and Eric S. Ebisu, Advances in X-Ray Analysis, Vol. 17, (Plenum Press, New York, 1974).

[2] W. J. Veigele, Atomic Data Tables 5, 51 (1973).

[3] J. H. Scofield, Technical Report No. 51326 (1973), University of California Radiation Laboratory.

*This work is supported by the Air Force Office of Scientific Research Grant No. 75-2762.

J. Appl. Phys,
page 1027-1037

Quantitative low-energy x-ray spectroscopy (50–100-Å region)*

Burton L. Henke and Kazuo Taniguchi

University of Hawaii, Department of Physics and Astronomy, Honolulu, Hawaii 96822
(Received 27 August 1975)

The quantitative analyis of emission spectra in the 10–100-Å region has become of considerable importance for nigh-temperature plasma diagnostics (10^6–10^7°K region) and for molecular orbital and solid-state-band analysis. Because measurement intensities are typically low in these applications, achieving an optimum spectrographic measurement is essential. In order to present specific procedures and methods for optimizing and calibrating a low-energy spectrographic measurement, a molecular orbital analysis in the 70–90-Å region (S-$L_{II,III}$ emission spectra) has been carried out quantitatively in energy and intensity using a recently described single-crystal (lead stearate) spectrographic approach with about 1 eV resolution. Radiative yields, Y, for the radiation process being investigated are determined by the relation, $Y = Z/(X_0RSTQ)$, where Z is the area (intensity x angle) under the spectrographic line, X_0 the excitation function, $R(\lambda)$ the coefficient of reflection of the analyzer, $S(\lambda)$ the effective source thickness, $T(\lambda)$ the window transmission, and $Q(\lambda)$ the quantum counting efficiency of the detector. The determination of each of these parameters has been considered in detail.

PACS numbers: 32.10.F, 32.10.Q, 52.70., 07.85.

I. INTRODUCTION

Low-energy x-ray spectroscopy in the 10—100-Å wavelength region (100—1000-eV energy region) has become of considerable interest as applied in two types of research:

(1) High-temperature plasma analysis. Ionized gases (plasmas) in the 10^6—10^7°K temperature range radiate strongly in the 100—1000-eV x-ray region (1 eV corresponds to about 10^4°K). Because such high-temperature plasmas are characteristic of important astrophysical sources, their analysis is a fundamental aspect of the relatively new science of x-ray astronomy. And now it has become possible to generate such plasmas in the laboratory which radiate sufficiently strongly in the x-ray region for spectroscopic analysis. These are developed magnetohydrodynamically and magnetically confined, or by pulsed laser or electron beams and inertially confined. An important application of such high-temperature plasma analysis is for controlled thermonuclear fusion research. The x-ray measurements can yield information as to the temperature, density, time history, and spatial characteristics of the plasma.[1]

(2) Molecular orbital and solid-state-band analysis. When an atom is singly ionized with a vacancy created in one of its higher inner core levels, this vacancy is then promoted to one of the outermost electronic levels and a radiative transition typically in the 100—1000-eV region may result. The electronic structure of the initial ionization state of the atom is relatively insensitive to its molecular or condensed matter environment, but that of the final ionized state is strongly affected by this atomic environment. The major features of the associated x-ray emission spectra can yield direct information as to the populations, energy levels, and widths (or band structure) of the outer electronic levels. Because the strong radiative transitions obey the dipole selection rules, information as to the symmetry character of the outer electronic states may also be gained. Finally, the degree of localization of certain outer levels relative to a particular ionized atom can often be revealed by the existence of molecular orbitals rather than band structure and by comparative analyses of such spectra originating from inner core vacancies on adjacent atoms. Such low-energy x-ray emission spectra can be directly applied, using standard sample systems, for the identification of unknown valence states. These spectra can be applied to establish and to test molecular orbital and/or band theory models for which computer analysis is rapidly becoming more practical and precise.[2,3]

Typically, low-energy x-ray emission spectra of interest are of low intensities. At these transition energies, radiative transition rates are small as compared with those for the competing Auger and Coster-Kronig processes. For this reason it is generally required that the low-energy spectroscopy be by methods of optimum efficiency. Usually, the characteristically low emission intensities will not permit the use of double crystal spectrometry or of high-resolution grating spectrographs. The basic spectrographic approach that is used in this laboratory is shown in Fig. 1. It is

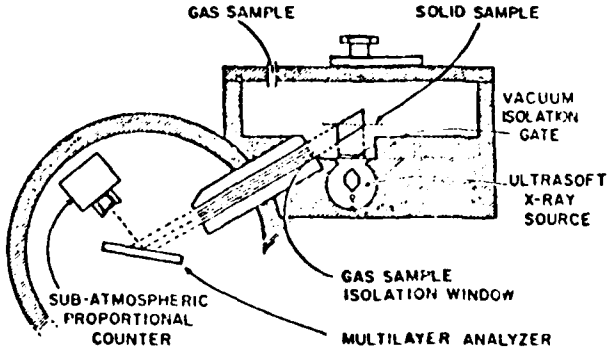

FIG. 1. A single-crystal spectrographic approach for low-energy x-ray spectroscopy applying closely coupled 2-kW demountable x-ray source, large d-spacing crystal analyzer, and tuned subatomospheric pressure proportional counter.

X-RAY CALIBRATION SOURCES FOR THE 100-1000 eV REGION*

Burton L. Henke

University of Hawaii
Department of Physics and Astronomy
Honolulu, Hawaii 96822

In order to calibrate windows, detectors and dispersive analyzers for low energy x-ray spectroscopy, certain characteristic line sources have been found to be particularly useful. These are obtained directly from an appropriate anode of a two-kilowatt demountable x-ray source, or from a fluorescent secondary radiator that is coupled closely to the x-ray source as shown in Fig. 1. Often the characteristic lines may be effectively isolated by filter and/or by pulse height discrimination with a proportional counter.[1] This is possible in the low energy x-ray region because the spectral line series are simpler and the line intensity relative to the associated continuum background is considerably higher than that for the ordinary x-ray region. This is illustrated in the spectra presented in Figs. 2 through 13 of fluorescent line sources in the 100 to 1000 eV region (10 to 100 A region). Also presented are typical absolute intensities as measured off a crystal analyzer and directly from the fluorescent radiator. The absolute characteristic radiation output intensities from three often-used anode sources for the excitation of the fluorescent lines are listed in Fig. 1. All intensities were measured with a calibrated proportional counter and with the window set to accept the full pulse height distribution. The measured intensities were divided by the appropriate x-ray tube window transmission. (Typical window transmissions are 50 to 80%.) The demountable x-ray source that is used in this laboratory is described in Fig. 14.

DIRECT SOURCE INTENSITY - I

PHOTONS / SEC - STEARADIAN - KILOWATT

(FOR CHARACTERISTIC RADIATION)

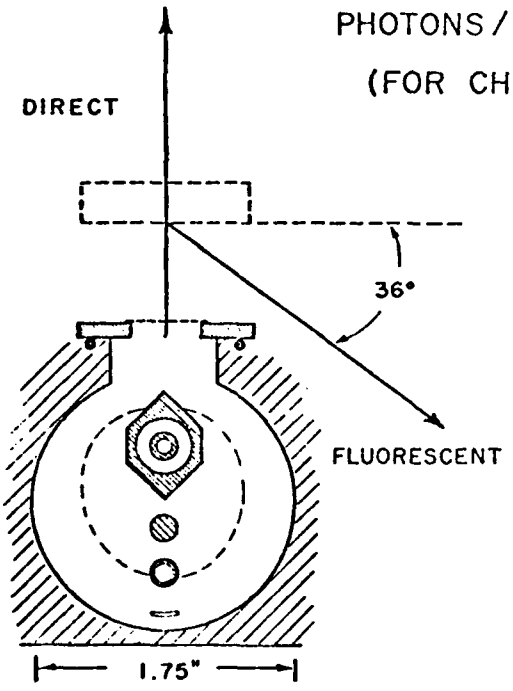

ANODE	RADIATION	I
ALUMINUM	Al-K_α (8.34 Å/1490 eV)	6 x 10^{13}
COPPER	Cu-L_α (13.3 Å/930 eV)	6 x 10^{13}
GRAPHITED COPPER	C-K_α (44.7 Å/277 eV)	2 x 10^{14}

Fig. 1. Showing the direct and fluorescent x-ray source geometries. Also listed are typical, absolute characteristic radiation output intensities from aluminum, copper and graphited anodes as used in the excitation of the fluorescent spectra shown in Figs. 2 through 13.

*To be published in the Proceedings of the 1976 ERDA Symposium on X- and Gamma-Ray Sources and Applications.

J. Chem. Phys.
page 3021-3035

Sulfur $L_{II,III}$ emission spectra and molecular orbital studies of sulfur compounds

Kazuo Taniguchi* and Burton L. Henke

Department of Physics and Astronomy, University of Hawaii, Honolulu, Hawaii 96822
(Received 27 August 1975)

The fluorescent sulfur $L_{II,III}$ emission spectra have been quantitatively measured and analyzed for the relative strengths (radiative yields) of the allowed transitions, and for the corresponding emission linewidths. These were investigated for the sulfur compounds in the solid, vapor, and gas states—Na_2SO_4, K_2SO_4, $CdSO_4$, Na_2SO_3, K_2SO_3, C_4H_4S, H_2S, SO_2, and SF_6. The S $L_{II,III}$ spectra for the solid compounds (all strongly ionic) revealed essentially the same localized molecular orbital character about a central sulfur atom as for the molecular compounds—showing no significant influence of the cations and no evidence of crystal band structure. The measured molecular orbital energies and radiative yields were found to be generally consistent with the eigenvalue and eigenvector calculations based upon current CNDO and *ab initio* molecular orbital approximation methods. The measured sulfur $L_{II,III}$ spectra for the compounds reported in this paper have been interpreted according to the valence orbital configuration as obtained from the CNDO/2 method. This is done while recognizing that other reported molecular orbital calculations on these molecules often indicate different orderings. The molecular orbital energies as derived from the $L_{II,III}$ spectra have also been compared with those obtained from photoelectron spectroscopy, demonstrating, generally, very good agreement between these two methods. Because the $L_{II,III}$ spectra for second row elements probe the $3s$ and the $3d$ character of the valence band and the K_β spectra probe the $3p$ character of the valence band, it has been found very useful to combine the results of these x-ray emission techniques in order to gain a complete analysis of valence band electronic populations and symmetries. It has been shown that the $L_{II,III}$ emission analysis can be a uniquely powerful tool for the determination of the role of the $3d$ atomic orbital in the chemical bonding of the second-row elements.

I. INTRODUCTION

X-ray spectroscopy has long been a basic method for studying the elemental compositions of materials and the electronic structure of atoms. Siegbahn,[1] in the early 1900's, developed the technique for measuring x-ray emission and absorption spectra of many elements. It has been known since 1920 that the x-ray spectrum of an element varies according to its state of chemical combination. Lindh[2] noted the chemical effect upon the K-absorption spectra for sulfur compounds. Later, Lindh and Lundquist[3] were able to observe the chemical combination effect in x-ray emission spectra.

Skinner and O'Bryan[4,5] showed the importance of x-ray spectroscopy in their investigations of valence electron band structure. Sommerfeld and Bethe,[6] and later Seitz,[7] applied solid state valence band theory to the interpretation of x-ray spectra. As described in many reviews,[8-12] the valence band theoretical interpretation of the x-ray spectra of solids developed most effectively from the area of soft x-ray spectroscopy. In recent years Best,[13] Nefedov and Fomichev,[14] Manne,[15] and Urch[16] have shown that the valence band x-ray spectra, resulting from transitions between the inner vacancies and the outer orbitals of an atom in the molecule, can be interpreted with the help of molecular orbital theory. Urch[17] was the first to interpret the sulfur $L_{II,III}$ x-ray emission spectra by theoretical approach. He proposed that the role of the $3d$ atomic orbital of sulfur is more important than previously speculated. Manne[15] interpreted the x-ray emission spectra of gaseous molecules by molecular orbital theory. He proposed that the relative intensities of x-ray transitions from the molecular orbitals were related to the eigenvectors of an LCAO (linear combination of atomic orbitals) molecular orbital. This same relation has been used for some solid compounds[17-25] and satisfactory results have been obtained. Many investigators[12-25] have shown that molecular orbital theory could be used effectively for the interpretation of the effect of chemical bonding upon the valence electron x-ray emission spectrum.

Today the valence molecular orbital structure is fairly well understood, particularly from the theoretical point of view. Most of the experimental results have been obtained from the K_β emission spectra (see, for example, Refs. 18-27). For the second row elements, K_β emission spectra result from transitions from the valence orbital levels to the $1s$ level, thereby revealing only the $3p$ character in the valence band spectra. $L_{II,III}$ emission spectra result from transitions from valence orbital levels to the $2p$ level for the second row elements, and, therefore, by measuring these spectra, we can investigate the $3s$ and $3d$ character in the valence band. By analyzing the $L_{II,III}$ emission spectra along with the K_β emission spectra and/or the photoelectron spectra, a more comprehensive view of the molecular orbital structure in the valence band can be gained.

The sulfur $L_{II,III}$ emission spectra for solids have been previously obtained by Henke[28] and by Merritt and Agazzi[29] through the secondary excitation method, and by Meisel *et al.*[30] and Nefedov and Fomichev[14] through electron excitation. Very recently Sadovskii *et al.*[31] measured the sulfur $L_{II,III}$ fluorescence spectra for gaseous compounds and interpreted these with the help of molecular orbital theory. Most reported measurements and interpretations of $L_{II,III}$ emission spectra to date have been incomplete and inexplicit, however. In recent years, the photoelectron spectra from molec-

Reprinted from Applied Physics Letters Vol. 29, No. 9, 1 November 1976
pp. 539-541

Secondary electron energy distributions for gold as excited by C K_α (277 eV) and Al K_α (1487 eV) x rays

Burton L. Henke and Jerel A. Smith

University of Hawaii, Honolulu, Hawaii 96822

David T. Attwood

Lawrence Livermore Laboratory, Livermore, California 94550
(Received 29 June 1976; in final form 27 August 1976)

The secondary electron energy distributions for a gold photocathode as excited by C K_α (277 eV) and Al K_α (1487 eV) x rays have been measured. The shapes of the energy distributions are essentially the same for these two x-ray photon excitation energies. For thick evaporated gold samples on glass substrates (at 150°C and 3×10^{-8} Torr), the secondary electron energy distributions peak at about 1 eV and have a FWHM of about 4 eV. As measured immediately after ion cleaning, the distributions peak at about 2 eV and have a FWHM of about 6.6 eV. Approximately 5 h after ion cleaning, the measured distributions appear as those obtained before ion cleaning. The work function of the evaporated gold photocathode temporarily increases by 1 eV upon ion cleaning.

PACS numbers: 79.60.Cn, 73.30.+y

The photoelectric conversion of x-ray intensity into secondary electrons[1] has become of considerable interest and importance in the development of detectors and of streak[2-5] and framing[6] cameras for application to the diagnostics of high-temperature plasma sources of intense x radiation. The photocathode response as a function of the incident x-ray photon energy is required for quantitative measurement. The energy spread (the secondary electron energy distribution) must be known in order to evaluate the time resolution of the picosecond streak cameras now under development.

There have been no precise measurements of x-ray-induced secondary electron distributions reported to this time. The mechanisms for the internal excitation, transport, and escape of the secondary electrons are not well known. Considerably more experimental data must be obtained before an adequate theory for the x-ray generation of secondary electrons can be presented. We have initiated a program of measurement of the secondary electron distributions for practical photocathode materials as excited by calibrated monoenergetic x-ray line sources[7,8] in the 100–10000-eV region. A report is now in preparation[9] that describes the models and methods which we have chosen for these measurements along with our first measurements on the gold photocathode. In this letter, we present an outline of our measurement procedure and some of these first results.

Because the secondary electrons are of low energy (typically in the 0–30-eV region) a precise measurement of the secondary electron distribution is obtained by preaccelerating the electrons into the entrance aperture of a high-resolution electron spectrograph. As shown in Fig. 1, this is accomplished by establishing a uniform field, parallel to the optical axis, by using a plane accelerating grid close to the photocathode. The region between the grid and the entrance aperture of the spectrograph is field free. (Typically, such preacceleration is also involved in streak camera optics,

J. Appl. Phys.
page 1852-1866

0.1–10-keV x-ray-induced electron emissions from solids—Models and secondary electron measurements

Burton L. Henke and Jerel A. Smith

University of Hawaii, Honolulu, Hawaii 96822

David T. Attwood

Lawrence Livermore Laboratory, Livermore, California 94550
(Received 15 September 1976; accepted for publication 14 December 1976)

Analytical models are presented describing the x-ray-excited emission of "no-loss" photoelectrons and Auger electrons and the energy distribution of emitted secondary electrons. The secondary electron energy distribution is given in terms of the electron kinetic energy E_K, work function W, photon energy E_o, and mass photoionization coefficient $\mu(E_o)$, as proportional to $E_o\mu(E_o)E_K(E_K+W)^{-4}$. Techniques of electron spectral measurements utilizing uniform field preacceleration and limited acceptance angle spectrometers are discussed. Secondary electron energy distributions are measured at about 10^{-8} Torr from thick evaporated films of gold and aluminum at photon energies 277, 1487, and 8050 eV. The shapes of these distributions do not depend significantly upon photon energy. The full width at half-maximum (FWHM) of these distributions are 3.9, 6.7, and 4.4 eV for Au and ion-cleaned Au and Al photocathodes, respectively. The data agree well with the model predictions.

PACS numbers: 79.60.Cn, 73.30.+y, 72.10.Bg

I. INTRODUCTION

This work is in sequel to and in support of a recent presentation by the authors of some measurements on the secondary electron energy distributions from gold as excited by C-K_α (277 eV) and Al-K_α (1487 eV) x-ray photons.[1] It is an attempt to present the basic physics for the measurement and for the interpretation of the x-ray-induced electron emissions from uniform isotropic solids.

In Fig. 1 are shown the typical characteristics of an electron spectrum induced by an x-ray beam incident upon a solid. Illustrated here are the sharp photoelectron and Auger electron "no-loss" lines with their characteristic energy loss tail structure, along with the low-energy secondary electron distribution. In contrast to uv-excited electron spectra, here the photoelectrons and the principal sharp Auger electron emissions are well outside the low-energy secondary electron energy region. The secondary electron spectrum peaks at about 1 to 2 eV and has a full width at half-maximum (FWHM) that is usually below 10 eV. In this 0–30 eV interval are typically from 50 to 90% of the total number of electrons emitted for photon excitation in the 100–10 000-eV region.

The x-ray-excited electron spectra constitute a unique "window" into the solid and its electron excitation, transport, and escape processes. When a thorough understanding of the physics of these processes is gained, electron spectroscopy can provide an important quantitative basis for the physical and chemical analysis of solids. The electron spectroscopy for chemical analysis (referred to as ESCA or XPS) has become a well-recognized research area within the last ten years.[2]

The photoelectric conversion of x-ray intensity into electron emission can provide an important practical basis for x-ray intensity measurement. X-ray photoelectric detectors are vacuum devices and, unlike gas ionization detectors, can be windowless. A unique advantage of the photoelectric detector is that it can be applied effectively over a wide band of photon energies.[3,4]

A very recent application of secondary electron detectors has been in the development of streak and framing cameras for the diagnostics of x-ray bursts from laser-produced plasmas. The time spread in the photoconverted secondary electron emission per photon is probably of the order of 10^{-14} sec, and the energy spread is of the order of 10 eV. An x-ray source can be imaged and photoconverted to an electron source which may then be reimaged down a streak or framing camera tube with an accelerating electron lens system. The time history of an x-ray event can be obtained by a fast transverse deflection of this image, e.g., to form a "streak" pattern with a time resolution in the picosecond range.[1,5–9]

In order to support research and application in x-ray photoemission, considerably more theoretical and experimental work should be done on the development of a quantitative relationship between the electron emission spectrum, the incident photon energy, and the characteristics of the photocathode. There is no complete theory of x-ray photoemission that is available

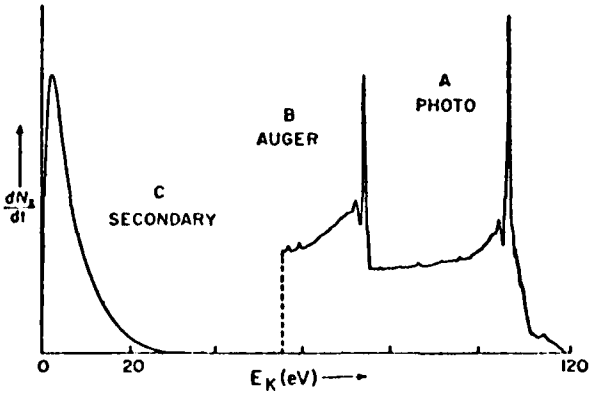

FIG. 1. A typical x-ray-excited photoemission spectrum.

Proceedings of the Eighth International Conference on X-Ray Optics and Microanalysis, Boston, August 1977.

SOME RECENT WORK IN LOW ENERGY X-RAY PHYSICS. B. L. Henke
Department of Physics and Astronomy, University of Hawaii, Honolulu, Hawaii 96822.

1. X-Ray Sources--High intensity, monochromatic excitation sources are essential for quantitative studies of the emission processes for photoelectrons, Auger and secondary electrons and for fluorescent x-rays. Such sources are also needed for the calibration of the detectors and analyzers employed for these studies and for subsequent applications. In the low-energy x-ray region (10-100 A/100-1000 eV) the direct radiation from an x-ray tube anode, with the appropriate filter and anode voltage, may be sufficiently monochromatic because the line radiation often dominates the associated continuum radiation. The line-continuum profiles have been measured and will be presented here for several useful K, L, and M characteristic line sources in order to illustrate the effect of filters and anode voltage. The absolute brightness of these sources (in photon/sec-stearadian) will also be presented.

2. Electron Spectroscopy--The electron spectroscopy of x-ray produced photoemissions has recently become an important tool in surface analysis. Photoelectron and Auger electron spectroscopy most effectively probe core electron states and the secondary electron spectroscopy probes the valence electron band states of the surface material. The basic processes that determine the photoemission spectra are the excitation, transport and the escape processes. In order that electron spectroscopy can be fully realized as a quantitative tool, considerably more must be known of the physics of these processes. This is particularly the case for secondary electron emission which is the most complex and for which there is no complete theory at this time.

Theoretical model results will be presented here along with examples of recently measured secondary electron energy distributions of metals and dielectrics. The secondary emission spectra rise sharply from zero electron kinetic energy to a peak value of about one eV and with a FWHM usually in the two to five eV region. These are being measured with a resolution of .04 eV using a hemispherical electrostatic analyzer. A uniform pre-acceleration field is employed which permits the application of a simple and accurate correction for a change in electron optical brightness associated with preacceleration (acceptance energy of the spectrograph is set at 15 volts).

It is hoped that measurements as these will also be helpful in gaining a more complete understanding of the secondary electron contrast dependence upon the surface state in scanning electron microscopy, and in the choice of x-ray photocathode materials particularly as used for pulsed x-ray measurements for temporal resolutions in the picosecond region.

3. X-Ray Spectroscopy--The low energy x-ray spectroscopy has been demonstrated to be a very useful tool for light element analysis, valence band and molecular orbital analysis, and for high temperature plasma diagnostics. The light elements emit only in the long wavelength x-ray region. Spectra from all elements involving transitions from the valence or molecular orbital levels to the nearby, relatively sharp core levels are in the one-to-several hundred eV region and do sensitively portray important outer electronic state structure. Plasma in the ten-million degree range (astrophysical and CTR, for example) emit most strongly in the low energy x-ray region. To accomplish this type of x-ray spectroscopy, the simpler and higher efficiency crystal spectroscopy is sometimes more appropriate than the grating spectroscopy even though the latter is inherently capable of higher resolution.

Presented here will be some examples of atomic and molecular, fluorescent spectroscopy of gaseous and solid samples using the multilayer analyzer (Langmuir-Blodgett type). The measured reflection coefficients and resolution for the lead myristate crystal will be presented in detail. And a simple method for unfolding the spectrographic lines and for decomposing overlapping spectra in order to gain spectral resolutions in the 0.5 eV range will be described.

J.Appl.Phys.
pp. 480-494

High-efficiency low-energy x-ray spectroscopy in the 100–500-eV region

Burton L. Henke, Rupert C. C. Perera, Eric M. Gullikson, and Mark L. Schattenburg

University of Hawaii, Honolulu, Hawaii 96822
(Received 21 July 1977; accepted for publication 1 September 1977)

The lead myristate multilayer analyzer has provided a basis for a relatively simple and efficient spectroscopy for the low-energy x-ray emissions in the 20–80-Å region (where conventional crystal spectroscopy and grazing incidence grating spectroscopy are generally inefficient). The percent reflectivity, the integrated coefficient of reflection, and the Bragg diffraction width of the lead myristate analyzer have been measured and found to be consistent with the predictions of a simple theoretical model for multilayer diffraction. This multilayer spectroscopy at large Bragg angles has a high efficiency (high instrument transmission) as compared to grazing incidence grating spectroscopy in this 20–80-Å region. However, the resolution is limited to that set by the diffraction width of the lead myristate analyzer of about 1 eV. Because the collimator-crystal broadening function can be precisely defined, a simple and effective deconvolution procedure can be applied with this multilayer spectroscopy to bring the resolution into the sub-electron-volt region. To demonstrate the efficiency of lead myristate spectroscopy in the 20–80-Å region, spectra were measured and analyzed from x-ray excited fluorescent sources which are characteristically of low intensity. (X-ray excitation yields a minimum of background spectra and of radiation damage.) These include the $L_{2,3}$ atomic spectrum of argon and the C-K molecular spectrum of CO_2, both in the gas phase, and the Cl-$L_{2,3}$ and O-K spectra from solid lithium perchlorate. Many samples undergo appreciable radiation-induced chemical change during the exposure time that is required for measurement—even with an optimally fast spectrograph and with fluorescent excitation. A method has been developed to evaluate and to correct for radiation damage by distributing the exposure over an effectively large sample volume either by gas flow or by rotating through multiple samples during measurement. Several spectral scans were made on the $LiClO_4$ using six samples. The total exposure time for each data point in each scan was recorded which permitted an extrapolation into a "zero" exposure spectrum. Finally, Fe-$L_{2,3}$/O-K spectrum (from Fe_2O_3) in the 17–25-Å region is presented to illustrate the effectiveness of the lead myristate analyzer in third-order diffraction. For this multilayer, the third-order diffraction efficiency is one-third that of the first order and is nearly twice that of the second order for this wavelength region.

PACS numbers: 07.85.+n, 32.30.Rj, 52.70.Kz, 33.20.Rm

I. INTRODUCTION

There are two areas in which low-energy x-ray spectroscopy is of particular importance at this time—the diagnostics of high-temperature plasmas[1] and the determination of the chemical and solid-state electronic structure of atomic systems.[2]

In the controlled thermonuclear fusion research, a critical temperature region of current interest is in the (1–10) × 10^6 °C range. The plasmas involved emit radiations most characteristically in the low-energy x-ray region (100–1000 eV/10–100 Å). The detailed spectroscopy of these plasma radiations can yield information as to the plasma density, temperature, and the identity and amount of contaminating elements. The low-energy x radiation from pulsed plasma sources (as produced by lasers or exploding wires) can be very efficiently converted to relatively sharp distributions in energy of secondary electrons[3] that are amenable, with streak camera techniques, to time-history measurements approaching psec resolutions.

Often, the energy and the symmetry of the outer electronic states of atomic systems can be sensitively revealed through the spectra associated with the transitions from these states into a nearby relatively sharp core level. Such spectra can yield valuable data complementary to that which are available from photoelectron Auger electron spectroscopy on the structure of valence bands, solid-state bands, and molecular orbitals.[4] These sensitive first transitions into the core levels typically result in low-energy x-ray spect. at a few hundred eV or less.

Using, for example, the acid phthallate crystals (2d value of about 26.6 Å), the conventional x-ray crystal spectroscopy has been very effectively extended down to about 500 eV.[5] Extreme ultraviolet diffraction grating spectroscopy has been extended with high efficiency (with relatively large angles of grazing incidence) up to about 100 eV.[6] We have found that a very efficient spectroscopy in the gap region of 100–500 eV is by using the multilayer analyzers as the lead stearate and lead myristate of 2d values equal to 100 and 80 Å, respectively. We have recently presented the detailed characteristics and application of the lead stearate analyzer.[7,8] In this paper, we extend the presentation of the methods and techniques of low-energy x-ray spectroscopy as specially applied with the lead myristate analyzer.

In Secs. II–V, we present an analysis and measurements of the x-ray optical characteristics of this multilayer analyzer, an optimized spectroscopic and data analysis procedure for gaining maximum overall efficiency and resolution, and, finally, we present some examples of applications to atomic and molecular low-energy x-ray spectroscopy.

II. REFLECTION PARAMETERS FOR THE LEAD MYRISTATE MULTILAYER

Lead salts of the fatty acids deposited as Langmuir-Blodgett multilayers have been demonstrated to be highly efficient

 0021-8979/78/4902-0480$01.10

Cl-$L_{II,III}$ fluorescent x-ray spectra measurement and analysis for the molecular orbital structure of ClO_4^-, ClO_3^-, and ClO_2^-

Burton L. Henke, Rupert C. C. Perera, and David S. Urch[a)]

University of Hawaii, Honolulu, Hawaii 96822
(Received 28 September 1977)

J. Chem. Phys.
pp. 3692-3704

The chlorine $L_{II,III}$ low energy x-ray spectra from sodium perchlorate, chlorate and chlorite have been obtained using carbon K_α (277 eV) photon excitation and a lead myristate analyzing "crystal" ($2d = 80$ A). X-ray induced decomposition was observed for each of these compounds. By taking repeated spectral scans, systematically distributed over six samples, it was possible to extrapolate to "zero-dose" Cl-$L_{II,III}$ spectra. A specially developed least-squares fitting program was applied to precisely determine the energy and strength of each spectral component which utilized the known collimation and crystal broadening functions and yielded energy resolutions of less than 1 eV. Broad low-energy satellite structures were observed for all the oxy-anions and for chloride (NaCl) and have been compared to similar satellites as measured in the Ar-$L_{II,III}$ spectrum. These structures were thus identified as resulting from multielectron processes. The other peaks in the Cl-$L_{II,III}$ spectra of the oxy-anions could be understood as corresponding to transitions from molecular orbitals with Cl 3*s* or 3*d* character. These results have demonstrated that 3*d* orbitals do play a definite role in the formation of chemical bonds in the oxy-anions of chlorine and that the importance of this role increases with the oxidation state of the chlorine. Satisfactory correlations have been obtained with the complementary K_β x-ray emission and photoelectron spectra and with molecular orbital theory for the same anions.

I. INTRODUCTION

Transitions between the molecular orbital states and the nearby and relatively sharp core level states result in low energy x-ray spectra that typically lie in the 100–300 eV (40–100 Å) region. Such spectra can sensitively portray the orbital structure of the molecule (or, in many cases, of an ionic group). For the second-row elements, the nearest core levels are the $2p_{1/2}$–$2p_{3/2}$ spin-orbit split states. The atomic binding energies of these $L_{II,III}$ levels, for example, for 15 P, 16 S, 17 Cl, and 18 Ar are 136–135, 165–164, 202–200, and 247–245 electron volts, respectively. In a particular chemical environment, these core levels of a given atom may shift as much as 10 eV. Such core level chemical shifts can be measured by x-ray photoelectron spectroscopy (XPS). The molecular orbital energies are of the order of 10 eV and can also be measured directly by ultraviolet photoelectron spectroscopy (UPS). The x-ray emission spectra directly yield the difference in the energy of the molecular orbitals and the core level states. However, unlike the photoelectron spectra, the x-ray emission spectra reveal appreciable information about the symmetries of the molecular orbital states. The $L_{II,III}$ spectral intensities are determined mostly by the *s* and *d* character of the orbitals and the K_β spectral intensities are determined mostly by the *p* character of the orbitals. If the $L_{II,III}$ or K_β spectrum originates from an atom of a molecule or of a strongly ionic group that contains only one such atom, it is then relatively easy to approximately calculate the energy and the relative intensity of the x-ray spectral components. Such theoretical predictions can simply be based upon one-electron integrals with the molecular orbital states described as linear combinations of the *s*, *p*, and *d* atomic orbital functions (LCAO approximation). The calculated eigenvectors are used to obtain the dipole transition probabilities. From such MO calculations the relative amounts of *s*, *p*, and *d* contribution can readily be estimated.

In an earlier work, Henke and Smith[1] were able to demonstrate the feasibility of obtaining the $L_{II,III}$ spectra of phosphorous, sulfur, and chlorine in different chemical states by applying spectrographic techniques of such efficiency as to minimize the effects of radiation decomposition. Recently, the S–$L_{II,III}$ spectra have been more precisely measured and analyzed by Henke and Taniguchi[2,3] for the SO_3^{-2} and SO_4^{-2} ions for polycrystalline samples and for the molecules containing single sulfur atoms and in the gas or vapor states—H_2S, SO_2, SF_6, C_4H_4S. The molecular orbital information derived from these spectra were compared to that obtained from the complementary photoelectron and K_β spectroscopy and to the predictions of molecular orbital theory. In this present work, the Cl–$L_{II,III}$ spectra for the ClO_2^-, ClO_3^-, and ClO_4^- ions for polycrystalline samples are measured, analyzed and compared to the photoelectron, K_β and MO calculated[4] data for the same ionic systems. Also, important comparisons with the measured atomic $L_{II,III}$ spectra for Ar and NaCl are presented.

A striking difference in the experimental determinations of the $L_{II,III}$ spectra of the sulfur and the chlorine compounds has been that the latter undergo considerably greater chemical change as induced by the excitation radiation that is required for the spectral measurement. That radiation decomposition might be important in the soft x-ray spectra of chloro-anions had been discussed by Best[5] in the electron excitation of Cl K_β spectra and had also been suggested by Urch[6] in attempting to interpret the early spectra of Henke and Smith.[1] Subsequently, both Prins[7] in x-ray photoelectron experiments and Sadovskii *et al.*[8] in measuring Cl–$L_{II,III}$ emission

a)Permanent address: Department of Chemistry, Queen Mary College, Mile End Road, London, E1 4NS, England.

 0021-9606/78/6808-3692$01.00

PHYSICAL REVIEW B VOLUME 19, NUMBER 6 15 MARCH 1979
pp. 3004-3021

Soft-x-ray-induced secondary-electron emission from semiconductors and insulators: Models and measurements

Burton L. Henke, John Liesegang,* and Steven D. Smith
University of Hawaii, Department of Physics and Astronomy, Honolulu, Hawaii 96822
(Received 27 July 1978)

Secondary-electron energy distribution curves (EDC's) and the total secondary-electron yields relative to such for gold have been measured for seven semiconductors for which electron-electron scattering losses within the emitter were considered dominant and for nine insulators (alkali halides) for which electron-phonon scattering losses were expected to be dominant in the transport process. The secondary-electron spectra were excited by Al-$K\alpha$ (1487 eV) photons and were measured from evaporated dielectric films (of about 0.3 μ thickness) on conducting substrates with an electrostatic hemispherical analyzer of about 0.03-eV resolution. Some of the dielectric photoemitters have appreciably narrower energy distributions and higher yields than has gold; CuI and CsI have EDC widths at half-maximum of about one-third of that for gold, and yield values of 11 and 30 times greater. The FWHM and secondary-electron yield for gold were measured to be about 4 eV and 0.50 electrons per normally incident photon, respectively. The shapes of the EDC's were found to be essentially unchanged for photon excitation in the 0.1–10-keV region. Strong structural features appear only in the alkali halide EDC's, and it is proposed that these are mainly the result of single-electron promotion of secondaries from the valence band by plasmon deexcitation. A relatively simple model for x-ray photoemission has been developed which assumes that direct excitation of secondaries by photoelectron and Auger-electron "primaries" is the dominant excitation mechanism, and accounts for both electron-electron and electron-phonon scattering in the transport process. Free-electron conduction-band descriptions are assumed. The theoretical and experimental curves are in satisfactory agreement.

I. INTRODUCTION

There has been a considerable amount of effort on the theory and application of secondary-electron emissions using electron excitation in the kilovolt region (as applied, for example, in scanning microscopy) and using extreme ultraviolet excitation (as applied in band-structure analysis). There has been relatively little theoretical or experimental work reported on the generation of the secondary electrons using x-ray excitation (which is of considerable current interest as applied to the measurement of the intensity and the temporal history into the picosecond region of pulsed x-ray sources with the diode detector, the streak, and the framing cameras in high-temperature plasma diagnostics).

With electron and extreme ultraviolet generation of the secondary-electron distribution, the effective escape depths of the electrons can be very dependent upon the attenuation mechanism of the exciting radiation. With x-ray excitation of the photoelectron and subsequent emission of the associated Auger-electron "primaries" which in turn generate the internal secondary-electron distribution, the electron escape depths are usually independent of the x-ray attenuation process. This is because the x-ray penetration is very large as compared to the effective electron escape length. Thus with x-ray excitation, often a more direct and precise interpretation of the secondary-electron energy distribution can be made in terms of models for the excitation, transport, and escape processes.

In an earlier work,[1] the electron energy dependence of the secondary-electron energy distribution from metals as excited by x-rays in the 0.1–10-keV region was measured and found to be consistent and predictable by applying currently available theoretical descriptions for the excitation, mean free paths, and escape for secondaries in metals. In this present work, we have measured the energy dependence and relative yields of the secondary electrons as excited by soft x rays (principally at 1487-eV photon energy) for a representative series of semiconductors and insulators. For these systems, the secondary-electron generation processes are more complex, particularly for the insulators for which multiple scattering has an appreciable role in the transport process. In order to test available theoretical expressions for the secondary-electron excitation and for the mean free paths for pair production and for electron-phonon interactions for the energy region below 10 eV, we have used the relatively simple rate equation developed by Kane[2] for a description of the multiple scattering transport process. We believe this approach will be helpful at this time in guiding the application of more exact transport theories, analytical and numerical, in later studies.

In Sec. II, we present the "semiclassical," simple case for x-ray excited secondary-electron generation for the "no-loss" transport (no multi-

Proceedings of the International Conference on X-Ray and XUV Spectroscopy, Sendai, 1978;
Japanese Journal of Applied Physics, Volume 17 (1978) Supplement 17-2, pp. 477–482

The Secondary Electron Emission Photocathode Characteristics for Time Resolved X-Ray Spectroscopy

Burton L. HENKE and Kandatege PREMARATNE

Department of Physics and Astronomy
University of Hawaii, Honolulu, Hawaii 96822, U.S.A.

Recently the secondary electron energy distributions and the relative secondary electron yields for the 0.1 to 10 keV photon excitation region have been measured for gold, aluminum and for sixteen representative semiconductors and insulators (alkali halides), and a simple phenomenological model for X-ray photoemission has been developed. This work is discussed here as it might be applied to the application of streak cameras for time resolved X-ray spectroscopy.

§1. Introduction

Time resolved X-ray spectroscopy has recently become of considerable value in studies of high temperature plasmas in the one second range (magnetically confined fusion) to the picosecond range (laser produced fusion). Mode-locked laser systems are available that can generate high intensity pulses of X-radiation from matter in the picosecond region. Ultra-fast spectroscopy is needed for the characterization of such X-ray sources and of the effects of their radiation bursts upon materials. Pico second X-ray spectroscopy may be a valuable tool for the measurement of the lifetimes of metastable atomic and molecular states and of certain photochemical processes.[1–3]

A proven method for accomplishing time resolved X-ray spectroscopy is that with the X-ray streak tube.[4–6] An X-ray beam is dispersed according to its photon energy along a slit-defined photocathode using a non-focusing crystal or a diffraction grating (or by a series of absorption filter and/or total-reflection monochromator channels). The secondary electrons from this slit source are used to form a line image at an image intensifier (needed particularly for ultra-fast spectroscopy). This line image is "streaked" to establish a time base using a pair of deflecting plates. The optical output of the image intensifier is recorded photographically. A schematic of such an X-ray streak tube is shown in Fig. 1. As indicated here, two types of imaging can be used, either an electron lens system[7,8] or a simple, proximity-focusing microchannel plate system.[9,10]

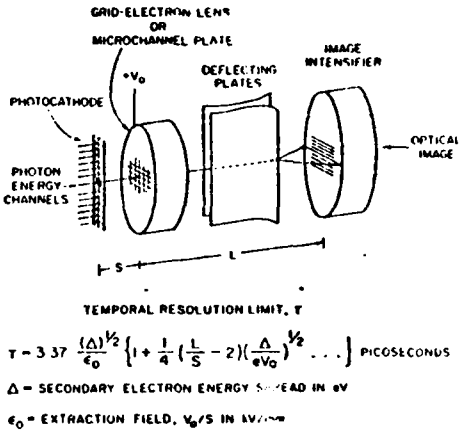

Fig. 1. Schematic of an X-ray streak tube as applied for time resolved X-ray spectroscopy. The temporal resolution limit, τ, is the difference in arrival time at the image intensifier for axially emitted electrons from the photocathode of initial velocities equal to zero and to v_0. The corresponding energy spread, Δ, of the secondary electron emission is $1/2 \cdot mv_0^2$.

The intensity-and-photon-energy response and the temporal resolution of the streak camera are ultimately determined by the characteristics of the photocathode. In the sections that follow, we have attempted to review (1) the basic relationship between the photoemission and the electron-optical characteristics of the X-ray streak tube, and (2) the experimental and theoretical determination of the relevant photoemission properties of metal and dielectric X-ray photocathodes as have been recently investigated in this laboratory.[11–13]

Proceedings of the International Conference on X-Ray and XUV Spectroscopy, Sendai, 1978;
Japanese Journal of Applied Physics, Volume 17 (1978) Supplement 17-2, pp. 112-115

C-K and Cl-L Emission Spectra and Molecular Orbital Analysis of CCl_4

Rupert C. C. PERERA*,** and Burton L. HENKE

Department of Physics and Astronomy,
University of Hawaii, Honolulu, Hawaii 96822

The C-K and Cl-$L_{II,III}$ low energy X-ray spectra from solid CCl_4 have been obtained using monoenergetic X-ray excitation and a lead myristate multilayer analyzing crystal. The Cl-L spectra was also measured in the vapor phase and compared with that measured in the solid phase. The deconvolved C-K and Cl-$L_{II,III}$ spectra are compared with the available Cl-Kβ and UPS spectra and with the results of CNDO/2, MINDO/3 and extended Hückel MO calculations.

§1. Introduction

The X-ray emission spectra from gaseous chlorinated methane derivatives have been previously reported by many authors. LaVilla and Deslattes[1] studied the chlorine-Kβ emission spectra and Ehlert and Mattson[2] reported the carbon-K and chlorine-L spectra from four chlorinated derivatives of methane. The photoelectron spectra of chloromethanes were measured by Potts *et al.*[3] using 21 eV and 40 eV excitations and by Turner *et al.*[4] using 21 eV excitation. The experimental photoelectron spectra are in good agreement. Hopfgarten and Manne[5] provided a molecular orbital interpretation of available photoelectron and X-ray emission spectra of chloromethanes on the basis of the extended Hückel molecular orbital calculations.

In this laboratory,[6,7] the C-K and Cl-L emission spectra of CCl_4 and $CHCl_3$ and the C-K emission spectra of CH_4 were measured in the solid phase. The C-K emission spectra of methane and the Cl-L emission spectra of chloromethanes were also measured in the gas phase. Molecular orbital analysis of these chloromethanes were based upon the CNDO/2 and MINDO/3 SCF-MO calculations and upon results of available extended Hückel MO calculations.[5] As an example, the spectra and molecular orbital analysis of CCl_4 will be presented here.

§2. Experimental

Basic details of the experimental approach have been given elsewhere.[7,8] For high efficiency, an oxidized copper excitation source was used to create the C-1s hole and a carbon excitation source was used to create the Cl-2p hole. The X-ray tube was operated at 8 kV and 150 mA. A lead myristate multilayer[8] was used as the analyzer. A "pressure tuned"[9] constant flow proportional counter filled with propane at subatmospheric pressure was used as the detector.

In measuring the chlorine-$L_{II,III}$ spectra in the vapor phase, the sample pressure in the gas cell was maintained at one Torr for maximum intensity.[10] The chlorine-$L_{II,III}$ spectra of CCl_4 in the solid and vapor phases were measured under the same excitation and are presented in Fig. 1. As seen from Fig. 1, there are no substantial differences between the gas phase and solid phase spectra. Since the fluorescent intensity from the solid phase was about ten times higher than in the gas phase, the spectra from the solid samples were used in the detailed analysis presented here.

Reagent grade CCl_4 was obtained commerically with better than 99% purity. All of the spectra presented in this work are the sum of at least three repeated runs and the individual runs reproduced within statistical deviations. Over 10^4 counts were collected at the peak in all spectra and the spectrometer was calibrated using Rh, Mo and Nb Mζ lines.[7,8] In all of the spectra, the peak intensities were normalized and background was not subtracted from the data because it was negligibly small.

A step-scanned spectrum thus obtained was

*In partial fulfillment of PhD, University of Hawaii, May 1978.

**Present address: Department of Physics, University of Sri Lanka, Peradeniya, Sri Lanka.

Reprinted from Applied Optics, Vol. 19, p. 749, March 1, 1980

Evaluation of high efficiency CsI and CuI photocathodes for soft x-ray diagnostics

E. B. Saloman, J. S Pearlman, and B. L. Henke

The photoefficiency of CsI and CuI photocathodes was measured for photons in the 22–240-eV (50–560-Å) energy range. The within-batch and batch-to-batch variation in photoefficiency were studied as was the sensitivity of the samples to storage under dry nitrogen. The effect of exposure to air was investigated. The shape of the photoefficiency curves was found to agree quite well with that expected from the photoabsorption cross sections of the materials. CsI in particular appears useful as a detector in soft x-ray diagnostics, especially as a narrowband detector in the 100-eV photon energy range where peak measured efficiencies can exceed 300%.

There has been increased interest recently in time-resolved measurements of UV and soft x-ray emission for the study of picosecond processes in fusion plasmas, biological systems, atomic collisions, and photochemical reactions. High sensitivity x-ray photocathodes for use in diodes or streak cameras could enhance the capability of existing diagnostic equipment used in these research areas. Two high-sensitivity photocathode surfaces, CsI and CuI,[1] were evaluated and compared with an evaporated aluminum surface. Their efficiences are substantially higher than aluminum (factors of 5–50 near 100-eV photon energy).

Several characteristics are important for a photocathode surface to be useful for ultrafast temporal diagnostics. These include good efficiency, reproducibility from batch to batch or good exposure and shelf-life characteristics, and a narrow secondary electron emission spectrum. In the results reported here, these characteristics are evaluated for CuI and CsI.

The electron emission of a photocathode involves several processes. Absorption of incident radiation leads to the generation of primary electrons. If the material thickness is larger than the primary electron range, a number of lower energy secondary electrons are created by each primary. In addition, the atoms excited by the incident radiation decay through fluorescence and Auger processes creating additional electrons. A certain number of the secondary electrons reach the photocathode surface with enough energy to escape. These electrons are measurable as a photoemission current.

The photoemission is proportional to the incident photon energy, the photon absorption characteristics, and the material's electron properties. From a simple phenomenological model, the photoemission is proportional to[2] $I\rho E\mu(E)f(E)$, where I is the incident x-ray intensity (photons/cm^2 sec), ρ is the mass density, E is the photon energy, $\mu(E)$ is the mass photoionization cross section, and $f(E)$ is the fraction of total energy deposited that is effective in secondary electron emission. This efficiency factor $f(E)$ is strongly material dependent. In metals, the predominant secondary electron generation mechanism is electron-electron collisions, while for semiconductors and insulators, where the number of free conduction electrons is lower, processes other than electron-electron collisions can be important. For example, in semiconductors (CuI), hole-pair formation plays an important role in creating low-energy electrons, while in insulators (CsI), electron-phonon processes (lattice vibration) can be significant. The dominance of different generation processes leads to widely varying values of secondary electron production efficiency, as will be seen.

The secondary electron generation process not only affects the emission efficiency but also the photoelectron energy distribution. Presented in Fig. 1 are the photoelectron energy distributions for the gold, aluminum (effectively Al_2O_3), copper iodide, and cesium

E. B. Saloman is with U.S. National Bureau of Standards, Center for Radiation Research, Synchrotron UV Radiation Facility, Washington, D.C. 20234. J. S Pearlman was with U.S. Department of Energy's Office of Laser Fusion; he is now with Maxwell Laboratories, Inc., San Diego, California 92123. B. L. Henke is with University of Hawaii, Department of Physics & Astronomy, Honolulu, Hawaii 96822.

Received 9 October 1979.
0003 6935/80/050749-05$00.50/0.

X-Ray Spectrometry (April 1980), 10 pages

Multilayer X-Ray Spectrometry in the 20—80 Region: A Molecular Orbital Analysis of CO and CO_2 in the Gas and Solid States

R.C.C. Perera† and B.L. Henke
University of Hawaii, Honolulu, Hawaii 96822, USA

Optimized multilayer X-ray spectrometry, using lead myristate and lead stearate analyzers (2*d* values of 80 and 100 Å) has been applied to the measurement of the O–Kα and the C–Kα spectral bands from CO and CO_2 in the gas and solid phases. The $L_{II,III}$ spectra were also measured for argon in the gas and solid states under similar conditions in order to identify and to minimize any non-molecular components in the CO and CO_2 spectra. These molecular orbital data have been related to those obtained with X-ray and ultraviolet photoelectron spectroscopy and grating X-ray spectroscopy. The consistency of the results of these complementary measurements is excellent. The ionization energies for the C and O 1s levels have been determined to be 295.4 and 542.0 eV for CO and 296.8 and 540.3 eV for CO_2. The MO data have also been compared with that predicted from the symmetry, strength and binding energy of the molecular orbital spectral components as calculated using the currently available computational models, CNDO/2, MINDO/3, MNDO, extended Hückel and *ab initio*. The molecular orbital calculated results for these organic compounds, CO and CO_2, are not in as good agreement with the experimental data as previously demonstrated for molecular orbital spectra measured for C–Kα and the $L_{II,III}$ bands of Cl, S and P for both organic and inorganic compounds.

INTRODUCTION

A molecular group of atoms is chemically characterized by the symmetries, strengths and binding energies of the molecular orbitals that are generated from the valence electrons of the atoms involved. In recent years, with the increased availability of large computers, more accurate programs have been developed for calculating these molecular orbital characteristics.[1] Because the more efficient of these programs are semi-empirical at this time, it is of considerable value to have precise experimental molecular orbital data on a selected series of molecular systems as can be obtained with photoelectron and X-ray spectroscopy. The molecular orbital binding energies can usually be measured within 1 eV or better by ultraviolet (UPS) or X-ray (XPS) photoelectron spectroscopy. The X-ray spectrometry of the fluorescent radiation resulting from single electron transitions from the molecular orbitals into single ionization vacancies in the nearby, relatively sharp core levels can provide data on the symmetries and the relative strengths of the molecular orbital components as well. For example, the Kα bands of the first-row elements reflect the p-character of the orbitals that are most strongly associated with the particular atom with the initial 1s vacancy. For the second-row elements, in a similar way, the Kβ bands and the $L_{II,III}$ bands measure the p-character and the s- and d-character, respectively, of the associated molecular orbitals. These Kβ and $L_{II,III}$ radiations are mostly in the 20–100 Å wavelength region. X-ray spectrometry in this long wavelength region requires either grazing incidence diffraction gratings or large *d*-spacing multilayer analyzers.

† Present address: Department of Physics, University of Sri Lanka, Peradeniya Campus, Peradeniya, Sri Lanka.

In order to generate the 'cleanest' spectra possible that are characteristic of the simple, single-electron transitions (and therefore which can be directly and quantitatively related to the calculated molecular orbital symmetries, populations and binding energies), it is necessary to minimize and to identify extraneous spectral features. For example, effects resulting from multiple ionization, high-order diffraction and radiation damage must be minimized. This can be accomplished by using photon excitation so as to selectively excite the desired initial core level vacancy. But even with such selective deposition of the excitation energy, the total spectral energy that is allowed for measurement is often seriously limited by the requirement that the excitation dosage should not cause significant radiation-induced changes in the sample. In order to meet the requirement for 'fast' X-ray spectroscopy, an optimized, high-efficiency spectroscopy has been developed[2,3] which utilizes multilayer analyzers such as the lead myristate, lead stearate and lead lignocerate systems with 2*d*-spacings of about 80, 100 and 130 Å, respectively. Because the transmission functions of the multilayer spectrograph can be accurately measured, the attainable energy resolution can be in the sub-electron-volt region through simple spectral devolution procedures.

Multilayer measurements of the $L_{II,III}$ spectral bands for the second-row elements, Cl, S and P, have been reported from this laboratory[4–6] as applied to the molecular orbital analyses of a selected series of chlorine, sulfur and phosphorus compounds. The samples were polycrystalline and it was established that the molecular orbital spectra for the central atoms of the anions were not affected significantly by crystal field effects (different cations). More recently, C–Kα and Cl–$L_{II,III}$ spectral band measurements by multilayer X-ray spectrometry have been applied to the

Nuclear Instruments and Methods 000 (1980) 000–000

X-RAY SPECTROSCOPY IN THE 100–1000 eV REGION

Burton L. HENKE
University of Hawaii, Department of Physics and Astronomy, 2505 Correa Road, Watanabe Hall, Honolulu, Hawaii 96822, USA

Some current methods for achieving low energy X-ray spectroscopy in the 10–100 Å region are reviewed. Gratings, crystals and multilayers can be used as monochromators or dispersive analyzers. Some of the important characteristics are noted here which can help to determine their applicability to a given spectroscopic analysis situation. The "trade-off" between resolution and spectrographic speed (gratings versus multilayers) may be an important consideration when the number of photons available for measurement is limited, as, for example, by the excitation dosage allowed for a given sample. For pulsed X-ray sources and for time-resolved spectroscopy, special fixed-crystal spectrographs have been developed. These may be applied with X-ray diodes and fast oscilloscopes or with X-ray streak cameras for detection. The optimum design and characterization of the photocathode systems for such detection have been studied in detail and some of the results of this work are briefly reviewed.

1. Introduction

The new synchrotron radiation and laser-produced plasma sources can provide pulsed, broad-band radiation in the UV and X-ray region of such high intensity as to present a new dimension for spectroscopic analysis. This may be of particular importance for low energy X-ray spectroscopy in the 10–100 Å region for which high intensity, selective excitation has generally not been available.

X-ray absorption and emission spectroscopy in this low energy region is of considerable interest for the measurement of the spectra that originate from transitions between the outermost electronic levels and the relatively sharp, first core levels. Such valence band spectroscopy can sensitively reflect the chemical, optical and electronic properties of matter.

The importance of having continuous selectivity of the excitation for absorption spectrometry is well known, particularly for extended absorption fine structure measurements. Selective, narrow-band excitation can also present a critical advantage in emission spectrometry by providing "clean" meaningful spectra with a minimum of background radiation, and by minimizing possible effects of radiation-induced changes in the sample.

An illustration of the critical role of radiation damage in molecular orbital spectroscopy is presented in fig. 1. The chlorine $L_{II,III}$ spectra in the 150–250 eV region were measured in order to determine the relative molecular orbital strengths of s and d symmetries for various oxidation states in chlorine

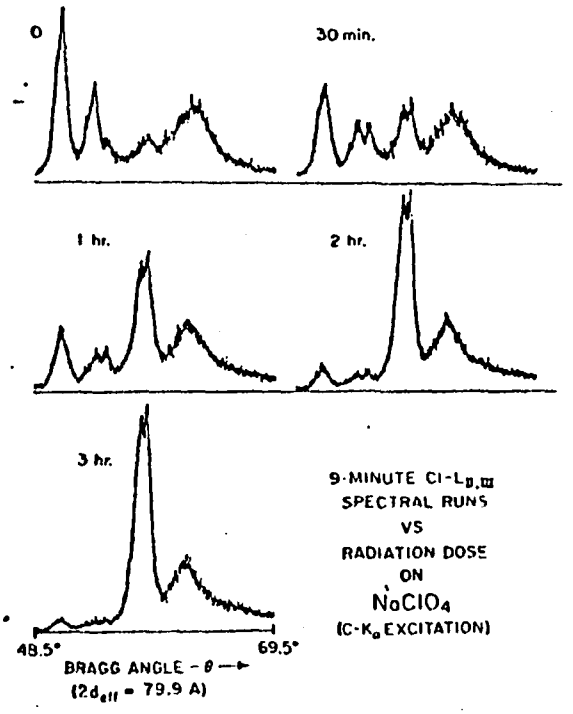

Fig. 1. Radiation-induced decomposition of polycrystalline $NaClO_4$. The excitation intensity was similar to that employed for the Cl-$L_{II,III}$ spectroscopy [1.75×10^{13} C-Kα (277 eV) photons/s cm^2 at the sample surface]. The quick scans reveal spectral changes corresponding to the appearance of reduction products such as $NaClO_3$ and $NaClO_2$. After three hours, the spectra correspond to that for NaCl.

Abstract Submitted
for the 1980 Annual Meeting of the
Division of Plasma Physics
American Physical Society

10-14 November 1980
San Diego, California

Some Recent Developments in Low Energy X-Ray Spectroscopy. B.L. Henke, U. of Hawaii--Briefly reviewed are the results of some recent collaborative efforts of this laboratory: 1) A new compilation has been completed of the photoionization cross sections for all elements and for the 30 eV to 10 keV region. These have been applied with the Kramers-Kronig dispersion relations to obtain the atomic scattering factor, $f_1 + if_2$, for all elements and for the 100-2000 eV region where anomalous dispersion effects are particularly strong. 2) The application of the new atomic scattering data to the characterization of low energy x-ray analyzers such as the acid phthalates, the molecular multilayers (Langmuir-Blodgett type) and the relatively new sputtered/evaporated multilayers, and the comparison of the theoretical with the experimental reflection data. 3) Detailed experimental measurements of the quantum yields for the 0.1-10 keV photon energy region of front-surface and transmission photocathode for the absolute calibration of time-resolved spectroscopy with x-ray diodes and x-ray streak cameras. The results are well described by a simple model for x-ray photoemission. And, 4) the development of a new, efficient x-ray spectrograph system for calibrated, pulsed source spectroscopy in the 100-1000 eV region utilizing "stacked" elliptically curved crystal/multilayer analyzers. This program is supported by AFOSR Grant 79-0027 and by a supplemental DOE/LLL Subcontract No. 9072209.

APPENDIX IV

THE LOW ENERGY X-RAY AND ELECTRON SPECTROGRAPHIC SYSTEMS DEVELOPED UNDER THIS PROGRAM

Figure I. Ultrasoft X-Ray Vacuum Spectrograph. A 2-to-4 kilowatt, demountable x-ray source of characteristic radiation directly, or be used to excite a fluorescent line source of slightly lower photon energy than the exciting line. Langmuir-Blodgett type multilayer analyzers specially developed in this laboratory with 2d-values in the 80-160 A range are employed for spectral analysis in the 20 to 150 A region (100-500 eV region). Pulse-height discriminating proportional counter detection is utilized to effectively reduce hard and soft background with better than 60% photon counting efficiency. Appropriate filter-windows in the tenth micron thickness range are used with a vacuum isolation window-gate on the x-ray source and for the proportional counter that is "pressure-tuned" for a given photon energy at subatmospheric pressures, typically 50-to-100 mm of propane counter gas. Spectral data is step-scanned, recorded on paper tape which is then processed on a small laboratory computer. This system is also used for the absolute calibration of x-ray detectors (XRD's) as shown here.

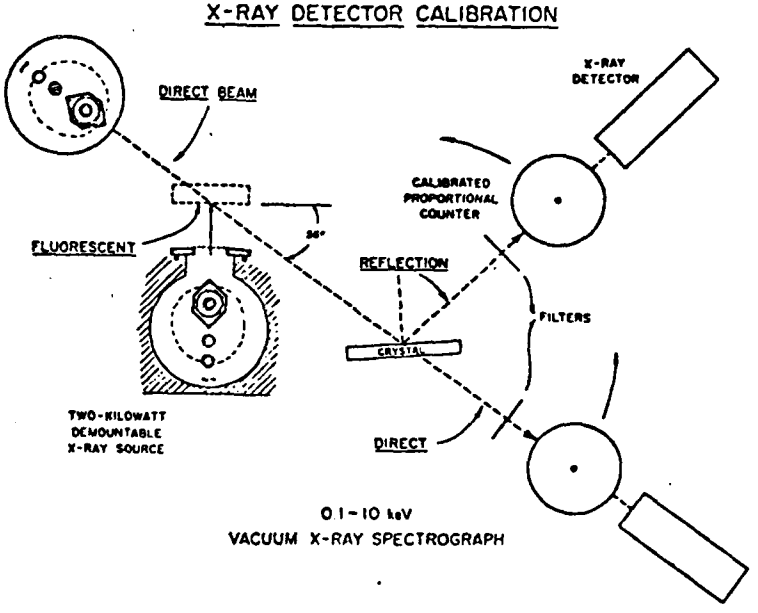

Figure 2. High Resolution, Low-Energy Electron Spectrograph. A filtered, characteristic line source of low-energy x-radiation is used to excite the photoelectron and subsequent Auger electron and secondary electron spectra from one of eight samples in a rotating holder. The emitted electrons are analyzed with a relative energy resolution of better than 0.3% by a hemispherical lens electrostatic analyzer of mean diameter of 20 inches. The electron counting is with a 16-stage electron multiplier tube. For the measurement of the secondary electron energy distributions of x-ray photocathode materials, the acceptance energy is typically fixed at 15 eV and the accelerating voltage applied to the sample is step-scanned and the spectra are recorded on paper tape and subsequently processed and plotted with a small laboratory computer system. The measured resolution of the secondary electron energy distributions is better than .05 eV.

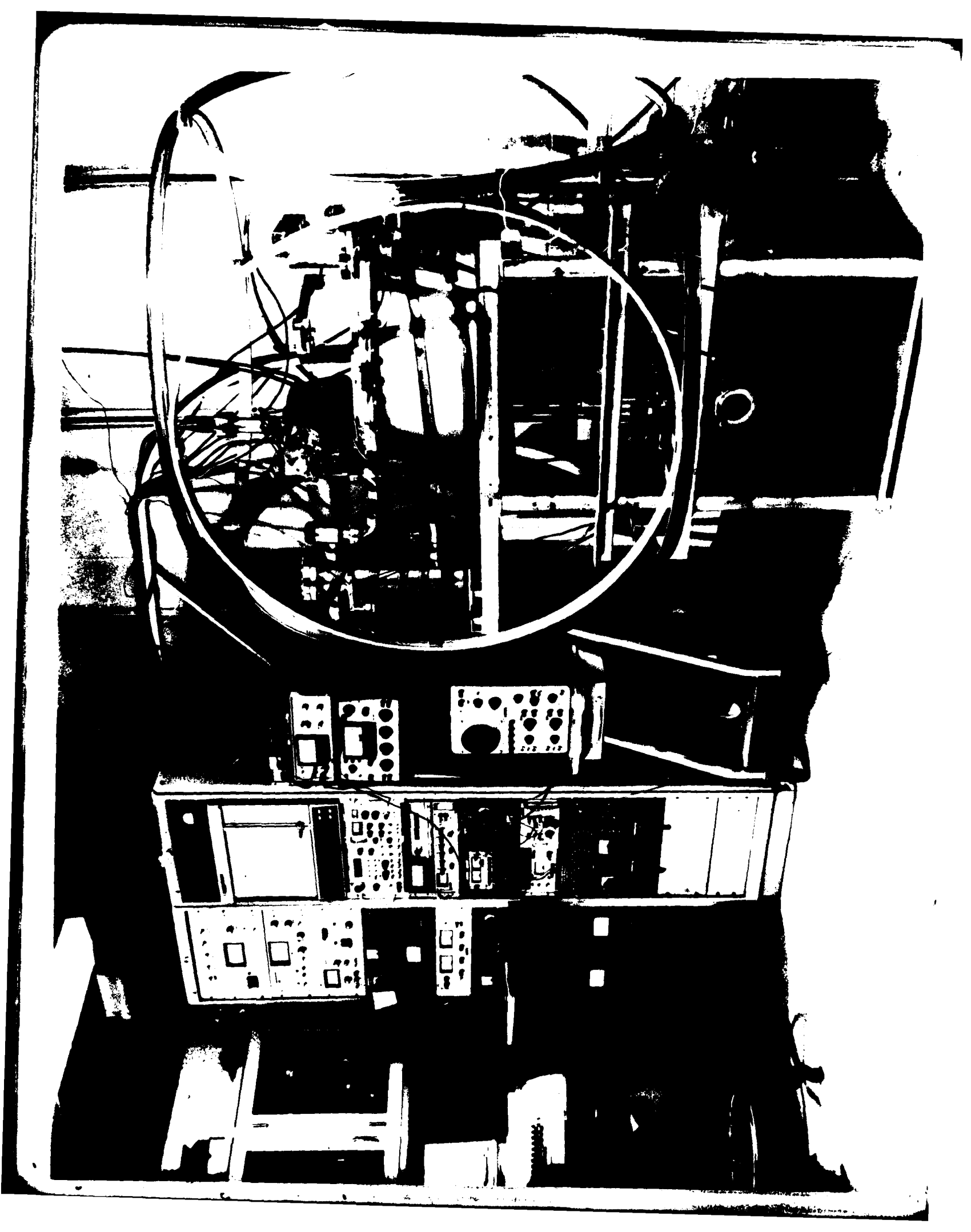

Figure 3. Facility for the Measurement of the Absolute Quantum Efficiency (for Total and Secondary Emission) of X-Ray Photocathode Materials.

A 2-to-4 kilowatt, filtered characteristic line source of x-radiation in the 0.1 to 10 keV region is closely coupled for the excitation of fluorescent line sources of energy just below that of the excitation source. Six fluorescent radiators are mounted on a rotating holder, permitting precise relative measurements. The sample in the radiated position is directly connected to a Carey 401 electrometer system and the photoelectric currents are monitored on an x-ray plotter. Cylindrical electrode systems are used to apply plus-minus 30 volt accelerating potentials to permit a differential measurement for the total and secondary electron yields for either thick or thin (transmission) photocathodes. The photons/steradian flux from the fluorescent source is measured by a calibrated flow proportional counter with the same filter-window as also introduced between the fluorescent source and the photocathode sample. Because of the relatively high photon intensity that is required for precise yield measurements, the absolute photon counter must be on an extended vacuum-pipe path and with an accurately calibrated "pinhole" window. For transmission photocathode studies, a second x-ray detector is used to measure the transmission of the photocathode system to permit a measurement of both the electron yield per incident photon and per transmitted photon.

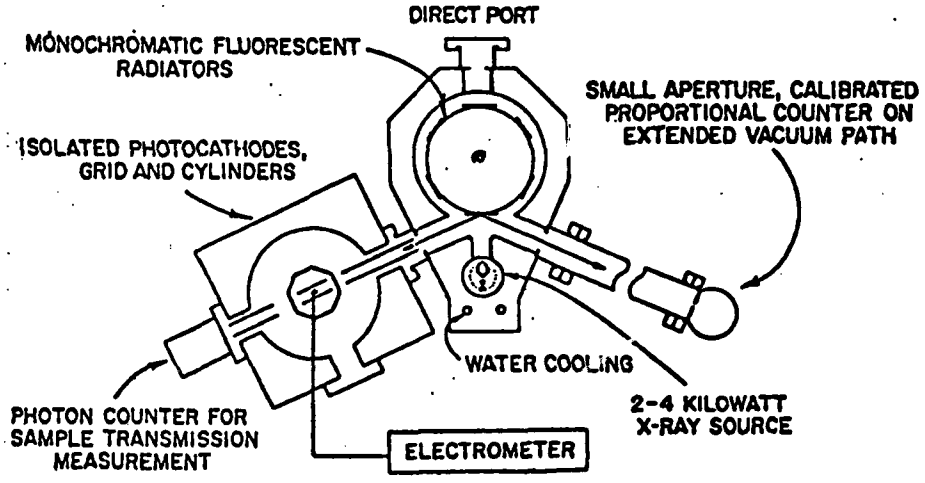

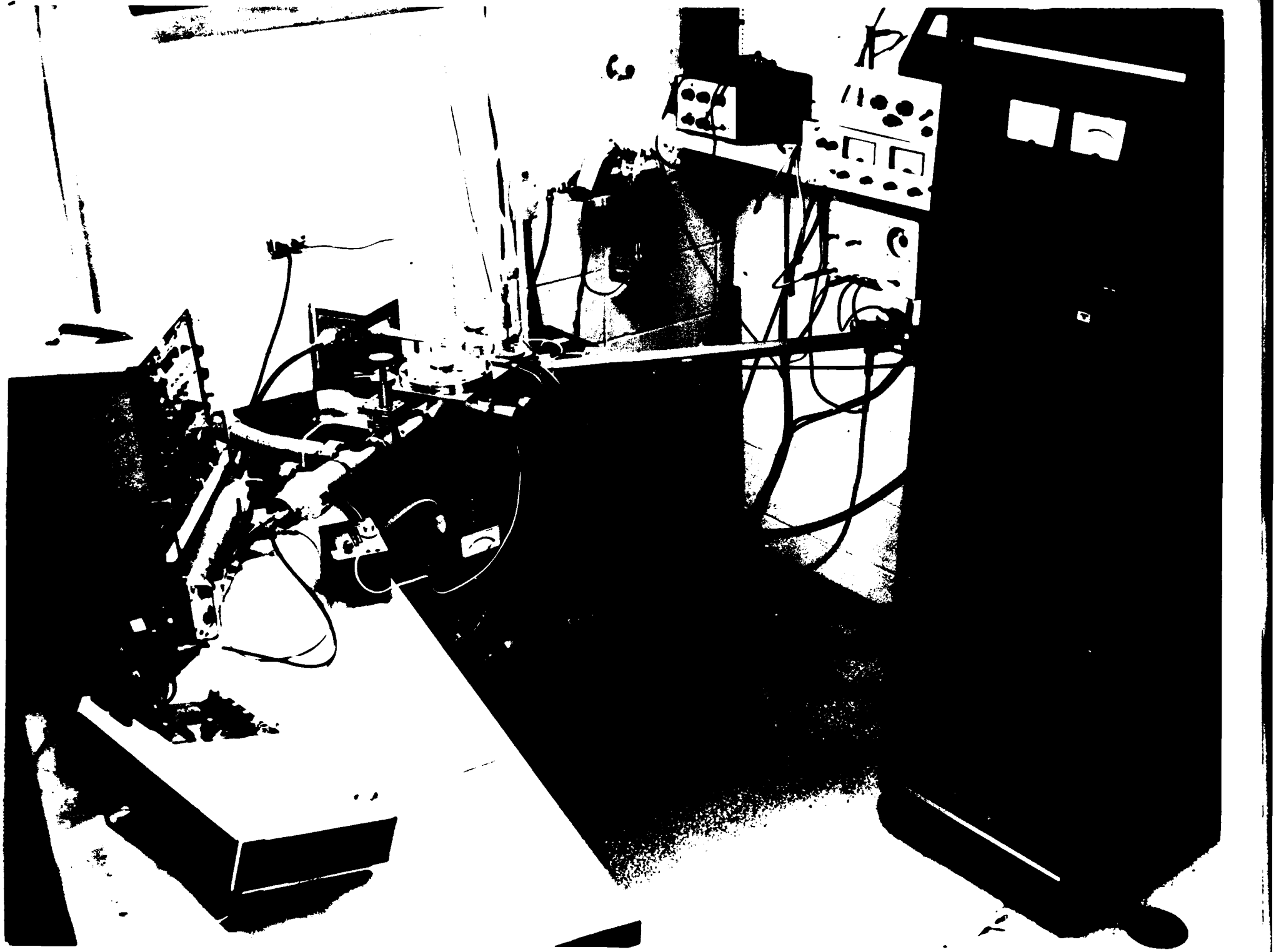

Figure 4. The high intensity excitation source that is used in this low energy x-ray and electron spectroscopy. Typical interchangeable anodes are of copper, aluminum and graphited copper for the Cu-K, Al-K, Cu-L and C-K characteristic radiations of 8050, 1487, 930 and 277 eV, respectively. Some useful fluorescent radiation line sources that are applied in this work in the low energy region are listed here.

Some Useful Characteristic Line Sources
for Ultrasoft X-Ray Spectroscopy

Line Source	Energy (KeV)	Wavelength (Angstroms)	Line Source	Energy (KeV)	Wavelength (Angstroms)
Al-K$\alpha_{1,2}$	1.487	8.34	Ti-L$\alpha_{1,2}$	.452	27.4
Mg-K$\alpha_{1,2}$	1.254	9.89	Ti-Lℓ	.395	31.4
Na-K$\alpha_{1,2}$	1.041	11.9	N-Kα	.392	31.6
Zn-L$\alpha_{1,2}$	1.012	12.3	C-Kα	.277	44.7
Cu-L$\alpha_{1,2}$	.930	13.3	W-N$_{V,VII}$	.212	58.4
Ni-L$\alpha_{1,2}$	.852	14.6	Mo-Mζ	.193	64.4
Co-L$\alpha_{1,2}$	.776	16.0	B-Kα	.183	67.6
Fe-L$\alpha_{1,2}$	.705	17.6	Nb-Mζ	.172	72.2
F-Kα	.677	18.3	Zr-Mζ	.151	81.9
Mn-L$\alpha_{1,2}$	.637	19.4	S-Lℓ	.149	83.4
Cr-L$\alpha_{1,2}$	.573	21.6	Y-Mζ	.133	93.4
Mn-Lℓ	.556	22.3	Sr-Mζ_1	.114	109.
O-Kα	.525	23.6	Be-Kα	.109	114.

TWO-KILOWATT ULTRASOFT X-RAY SOURCE

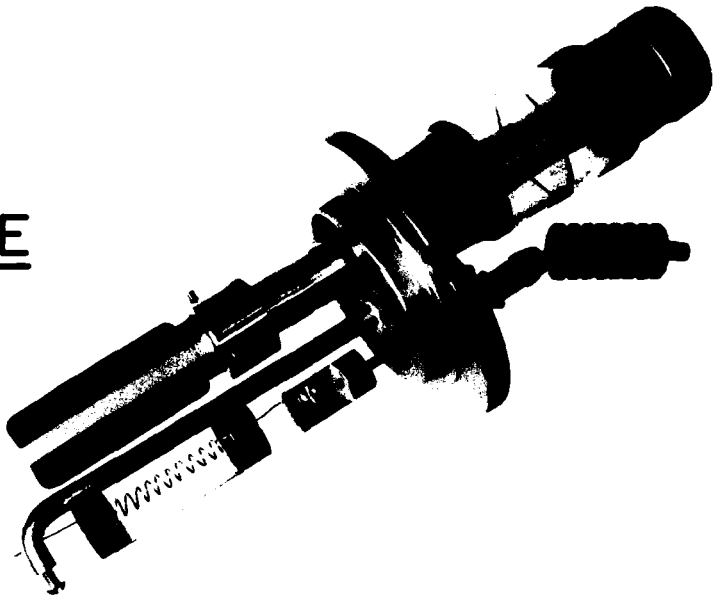

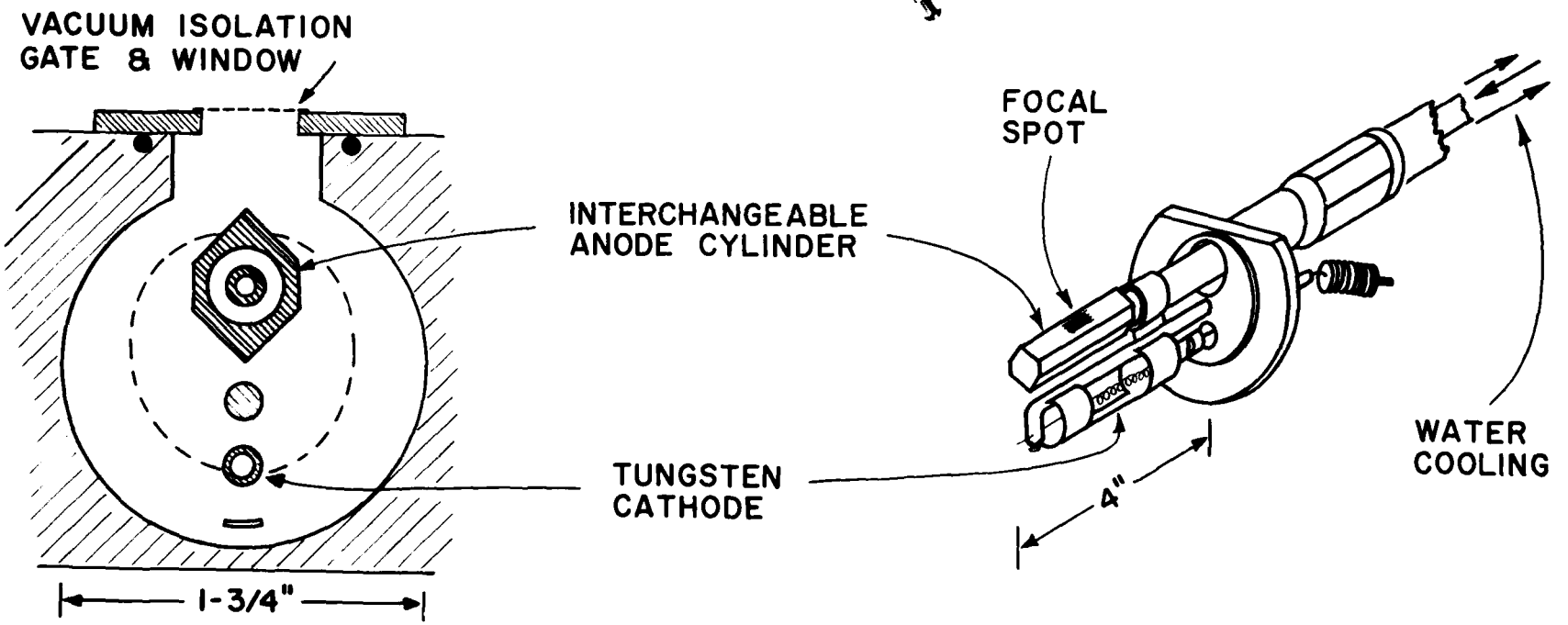

LOW ENERGY X-RAY AND ELECTRON ANALYSIS LABORATORY

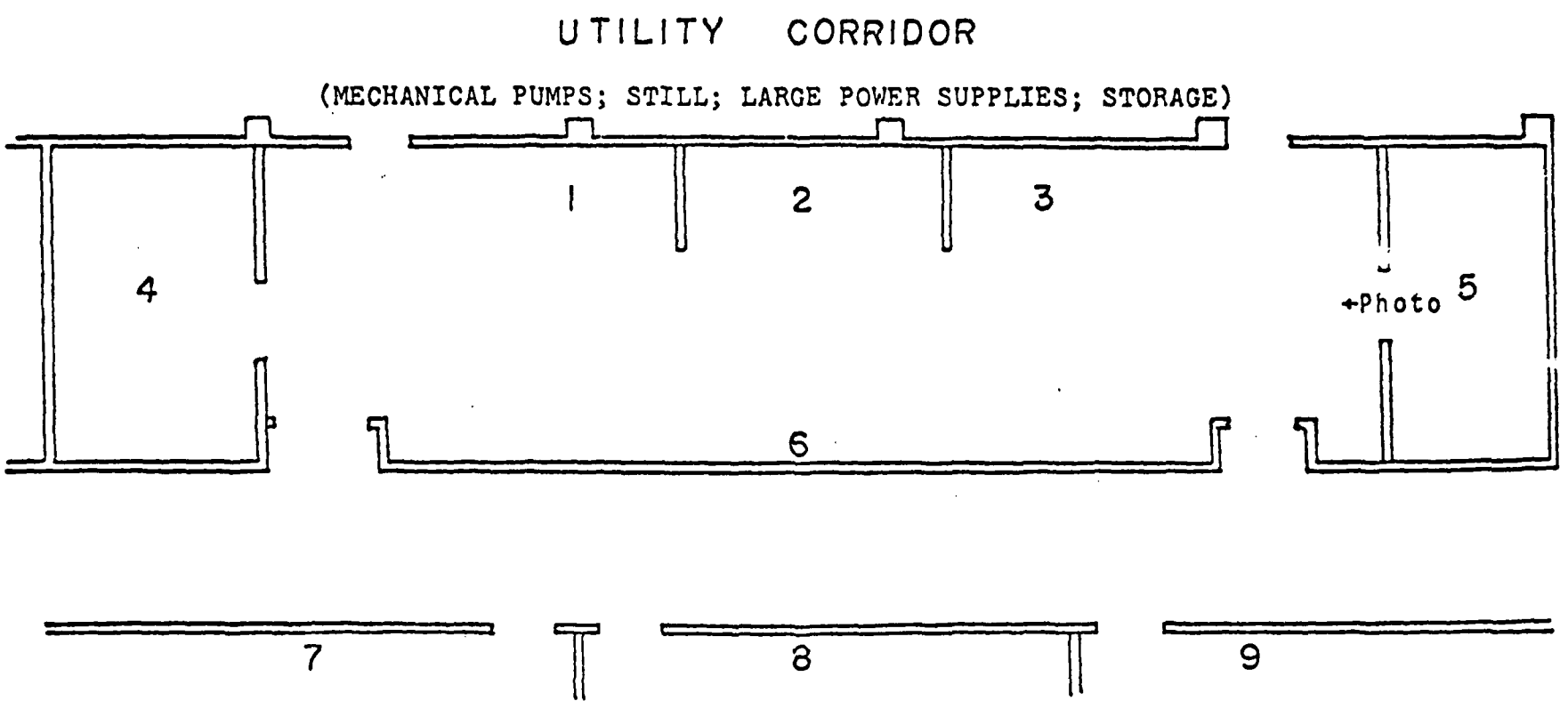

SCALE = 1/10" = 1'0"

1,2,3 - Low energy x-ray and electron spectroscopic systems

4 - Sample preparation lab and clean-bench for crystal research

5 - Data analysis lab and library

6 - Work benches and active storage

7,8,9 - Offices (Research associates, principal investigator, drafting room)

Figure 5. This low energy x-ray and electron spectroscopy laboratory (of more than 2000 square feet). Included are rooms at each end of the laboratory for sample preparation and crystal analyzer construction, and for a small computer and data analysis. Available to this laboratory are such facilities as a large IBM-370 computer system and a large, complete experimental machine shop.


DATE
ILME